British Geological Survey
NATURAL ENVIRONMENT RESEARCH COUNCIL

Arsenic dispersal and bioaccessibility in mine contaminated soils: a case study from an abandoned arsenic mine in Devon, UK

Environment Protection Programme
Research Report RR/04/003

BRITISH GEOLOGICAL SURVEY

RESEARCH REPORT RR/04/003

Arsenic dispersal and bioaccessibility in mine contaminated soils: a case study from an abandoned arsenic mine in Devon, UK

B A Klinck, B Palumbo, M Cave and J Wragg

Keywords

Arsenic, mining, bioaccessibility

Front cover

Remains of the Labyrinth Condenser, Devon Great Consols. Watercolour by Ben Klinck.

Bibliographical reference

KLINCK, B, PALUMBO, B, CAVE, M and WRAGG, J. 2005. Arsenic dispersal and bioaccessibility in mine contaminated soils: a case study from an abandoned arsenic mine in Devon, UK. *British Geological Survey Research Report* RR/04/003 52pp.

ISBN 0 85272 483 7

Keyworth, Nottingham British Geological Survey 2005

BRITISH GEOLOGICAL SURVEY

The full range of Survey publications is available from the BGS Sales Desks at Nottingham, Edinburgh and London; see contact details below or shop online at www.geologyshop.com

The London Information Office also maintains a reference collection of BGS publications including maps for consultation.

The Survey publishes an annual catalogue of its maps and other publications; this catalogue is available from any of the BGS Sales Desks.

The British Geological Survey carries out the geological survey of Great Britain and Northern Ireland (the latter is an agency service for the government of Northern Ireland), and of the surrounding continental shelf, as well as its basic research projects. It also undertakes programmes of British technical aid in geology in developing countries as arranged by the Department for International Development and other agencies.

The British Geological Survey is a component body of the Natural Environment Research Council.

British Geological Survey offices

Keyworth, Nottingham NG12 5GG
☎ 0115–936 3100 Fax 0115–936 3200
e-mail: sales @bgs.ac.uk
www.bgs.ac.uk
Online shop: www.geologyshop.com

Murchison House, West Mains Road, Edinburgh EH9 3LA
☎ 0131–667 1000 Fax 0131–668 2683
e-mail: scotsales@bgs.ac.uk

London Information Office at the Natural History Museum (Earth Galleries), Exhibition Road, South Kensington, London SW7 2DE
☎ 020–7589 4090 Fax 020–7584 8270
☎ 020–7942 5344/45 e-mail: bgslondon@bgs.ac.uk

Forde House, Park Five Business Centre, Harrier Way, Sowton, Exeter, Devon EX2 7HU
☎ 01392–445271 Fax 01392–445371

Geological Survey of Northern Ireland, Colby House, Stranmillis Court, Belfast BT9 5BF
☎ 028–9038 8462 Fax 028–9038 8461

Maclean Building, Crowmarsh Gifford, Wallingford, Oxfordshire OX10 8BB
☎ 01491–838800 Fax 01491–692345

Columbus House, Greenmeadow Springs, Tongwynlais, Cardiff, CF15 7NE
☎ 029–2052 1962 Fax 029–2052 1963

Parent Body

Natural Environment Research Council, Polaris House, North Star Avenue, Swindon, Wiltshire SN2 1EU
☎ 01793–411500 Fax 01793–411501

Foreword

This report is the published product of a study by the British Geological Survey (BGS) under one of its Core Strategic Programmes administered by the Environment and Hazards Directorate. The study belongs to the 'Tools for mapping and characterising abandoned mining related environmental risks' Project under the Environmental Protection Programme. The general aim of the study was to investigate the dispersal and bioaccessibility of arsenic in the environment as result of past mining activities.

Acknowledgements

A large number of individuals in BGS have contributed to the project. Tim Colman, Mike Lelliot and Kirsten O'Donnell are thanked for their contribution to the field work. Appreciation is extended to various members of the laboratory staff who provided mineralogical and chemical data. Antoni Miladoswki is especially acknowledged for the SEM work and Louise Ander for providing Eh-pH stability diagrams. Special thanks to colleague Helen Taylor for collecting XAS data at CLRC Daresbury Synchrotron Radiation Source. Gratefully acknowledgements are due to Fariba Bahrami (Daresbury) for the provision of beam time and John Charnock (Daresbury) for the interpretation of XAS spectra.

The authors would like to extend particular thanks to Mr J Berrange for giving access to his garden and vegetable plots, to Mr M Snelgrove, Tavistoch Woodland manager, for allowing access to Devon Great Consols Mine and Dr Richard Scrivener from the Exeter office for assistance during the field work.

We would also like to thank Professor Barry Smith who edited the report.

Contents

1 Introduction 1
1.1 Scope of the report 1

2 Geological setting and mineralisation 2
2.1 Cornubian Batholith 2

3 Devon Great Consols Mine 3
3.1 General 3
3.2 Methods of arsenic production 3

4 Sample collection 7

5 Analytical methods 9
5.1 Soil/vegetables chemical analysis 9
5.2 Water analysis 9
5.3 Arsenic speciation analysis by atomic fluorescence spectroscopy (AFS) 9
5.4 X-ray diffraction analysis 9
5.5 Scanning electron microscopy analysis 9
5.6 Sequential extraction test 9
5.7 X-ray absorption spectroscopy (XAS) analysis 10
5.8 Physiologically based extraction test (PBET) analysis 10

6 Mine waste and soil geochemistry 12
6.1 Tailings and waste material 12
6.2 Soils within the mine area 12
6.3 Soils outside the mine and background soils 13

7 Mine waste and soil mineralogy and petrography 14
7.1 Mineralogical composition of selected mine wastes 14
7.2 Petrographic observations 14

8 Vegetables 25

9 Surface water geochemistry 26

10 Acid mine drainage precipitates 28
10.1 Modelling arsenic sorption on iron precipitates 28

11 Arsenic bioaccessibility 29
11.1 Relationship of total arsenic and bioaccessible arsenic with other physico-chemical soil parameters 29

12 Arsenic speciation in solids by chemical extraction techniques 35
12.1 Iron sulphide and hematite reference material 35
12.2 The acid mine drainage (AMD) precipitate and soil affected by AMD pollution 35
12.3 Mine wastes: black furnace ash and sandy tailings and ore crusher ground 36
12.4 Mine site soils — medium arsenic content 36
12.5 Mine site soils — high arsenic content 36

13 Arsenic speciation in solids by EXAFS spectroscopy 45

14 Arsenic speciation in waters and leachates 47

15 Exposure assessment 49

16 Conclusions 50

References 51

FIGURES

1 Mineralisation (red lines) at Devon Great Consols 2
2 Location of study area and sampling areas 4
3 Site plan of 20th century arsenic works 5
4 The Brunton Calciner at Devon Great Consols 5
5 Arsenic condenser at Devon Great Consols. Chimney in the background 5
6 The floor of the arsenic mill 6
7 Tailings heap 7
8 Adit discharge from tailings heap 7
9 Sampling locations for soils (full circles), tailings (open circles), waters (triangles) at Devon Great Consols 8
10 Box-plots of arsenic data for tailings, DGC soils, background soils and Higher Todsworthy Farm soils 13
11 Spatial distribution of As in topsoils and wastes of DGC mine 13
12 SEM micrograph of $CaSO_4$ crystals in efflorescent masses at the furnace site and EDXA spectrum showing the presence of a large amount of arsenic 16
13 SEM micrographs and relative EDXA spectra of arsenic-iron-calcium coatings rimming sulphide grains 16
14 SEM micrograph of white flakes from the ore chrusher ground and EDXA spectrum showing the presence of a large amount of arsenic associated to calcium and iron 17
15 SEM micrograph of possible arsenolite crystal found at the ore crusher site and relative EDXA spectrum 17
16 BSEM image showing loose packed fragments of quartz (mid-grey) and microporous ash and slag impregnated by fine iron oxyhydroxide (bright). Sample MPS 90 17
17 BSEM image showing loose-packed fragments of quartz (dull grey), microporous ash or slag and partially altered cassiterite (bright) coated by thin fringe of iron oxyhydroxides. Sample MPS 90 18
18 BSEM image showing detail of a microporous altered vesicular glassy slag fragment, with thin bright fringes of iron oxyhydroxide lining vesicular cavities. A very bright relict of cassiterite can be seen within the ash fragment. A thin later layer of gel-like or colloform iron oxyhydroxide coats the outer edge of the grain. Sample MPS 90 18
19 BSEM image showing fragments of spoil cemented by arsenic-rich iron oxide, and very delicate skeletal structures outlined in iron oxyhydroxide that have formed by in situ dissolution of original constituents in the spoil. Sample MPS 90 19
20 BSEM image showing detail of arsenic-rich iron oxyhydroxide cement coating the surfaces of altered waste fragments. It shows banded colloform oxyhydroxide gel material displaying shrinkage (desiccation) cracks. This is encrusted by more crystalline acicular oxyhydroxide. Sample MPS 90 19
21 EDXA spectrum of arsenic-rich iron oxyhydroxide, showing high concentration of arsenic, major aluminium and silica, and minor sulphur (probably present as sulphate). Sample MPS 90 20
22 BSEM image showing a fragment of hydrothermal mineralisation consisting of an intergrowth of quartz

(dull grey), arsenopyrite (white) and siderite (mid-grey). Sample MPS 91 20
23 BSEM image showing fragments of illitic rock (fibrous grey material), quartz (dark grey) and altered fractured arsenopyrite (white) coated by a thin film of arsenic-rich iron oxyhydroxide. Sample MPS 91 21
24 BSEM image showing fragments of illitic rock (fibrous grey material), quartz (dark grey) and altered fractured arsenopyrite (white) coated by a thin film of arsenic-rich iron oxyhydroxide. The iron oxyhydroxide forms delicate meniscus cements that bridge between adjacent grains. Sample MPS 91 21
25 BSEM image showing detail of the edge of an altered arsenopyrite grain. Relict arsenopyrite (white) is directly enclosed by a matrix of gel-like As-rich iron oxyhydroxide (light grey) displaying irregular shrinkage cracks 22
26 BSEM image showing colloform banding within meniscus iron oxyhydroxide cement coating ferruginous micaceous and quartz grains (dark grey). Sample MPS 91 22
27 EDXA spectrum of low arsenic iron oxide coating on grain surfaces. Sample MPS 91 23
28 EDXA spectrum of arsenic rich iron oxyhydroxide alteration product directly replacing altered arsenopyrite grains . Sample MPS 91 23
29 EDXA spectrum of very arsenic rich iron oxyhydroxide forming thin grain coatings on pore surfaces immediately adjacent to altered arsenopyrite grains. Sample MPS 91 23
30 BSEM image showing pedified soil fabric, comprising rounded sand-sized peds of aggregated silt and clay grade quartz, chlorite, quartz, kaolinite, with scattered coarser quartz and rock fragments. MPS 96 Soil, B Horizon 24
31 BSEM image showing rare fragment of hematite-replaced illitic rock. MPS 96 Soil B Horizon 24
32 Computer model simulation showing the percentage of As, Cu and Zn adsorption onto hydrous ferric oxide as a function of pH for DC7 and DC13 at atmospheric P_{CO2} and P_{O2}. Solid line: DC7, dashed line: DC13 28
33 Box plot of bioaccessible As data (mg kg^{-1}) 32
34 Box plot of relative As bioaccessibility (% As_{tot}) 32
35 Calculated centroids for the physico-chemical variables around which each observation clusters 33
36 Map showing the spatial distribution of the clusters of soils identified by k-mean clustering 33
37 Relationship between the relative bioaccessibility of As and the total As in the four identified clusters in DGC soils 34
38 Triangular diagram showing composition of the CISED identified Fe-As-S geochemical components in the samples 36
39 Extraction profiles of the 9 identified components of the reference iron sulphide (X axis: extraction steps; Y axis: total extracted solid in mg kg^{-1}) 37
40 Extraction profiles of the 6 identified components of the reference hematite (X axis: extraction steps; Y axis: total extracted solid in mg kg^{-1}) 37
41 Extraction profiles of the 7 identified components of the AMD precipitate (MPS 71) (X axis: extraction steps; Y axis: total extracted solid in mg kg^{-1}) 38
42 Relative distribution of arsenic in the extracted physico-chemical components for the AMD precipitate sample (MPS 71) 38
43 Comparison of total, bioaccessible and CISED extracted As in the AMD precipitate sample (MPS 71) 38
44 Extraction profiles of the 9 identified components of the soil sample MPS 70 (X axis: extraction steps; Y axis: total extracted solid in mg kg^{-1}) 39
45 Relative distribution of arsenic in the extracted physico-chemical components for the soil sample MPS 70 39
46 Comparison of total, bioaccessible and CISED extracted As in the soil sample MPS 70 39
47 Extraction profiles of the 6 identified components of the sample MPS 90 (X axis: extraction steps; Y axis: total extracted solid in mg kg^{-1}) 40
48 Relative distribution of arsenic in the extracted physico-chemical components for the sample MPS 90 40
49 Comparison of total, bioaccessible and CISED extracted arsenic in the sample MPS 90 40
50 Extraction profiles of the 5 identified components of the sample MPS 91 (X axis: extraction steps; Y axis: total extracted solid in mg kg^{-1}) 41
51 Relative distribution of arsenic in the extracted physico-chemical components for the sample MPS 91 41
52 Comparison of total, bioaccessible and CISED extracted arsenic in sample MPS 91 41
53 Extraction profiles of the 6 identified components of the sample MPS 97 (X axis: extraction steps; Y axis: total extracted solid in mg kg^{-1}) 42
54 Relative distribution of arsenic in the extracted physico-chemical components for the sample MPS 97 42
55 Comparison of total, bioaccessible and CISED extracted arsenic in sample MPS 97 42
56 Extraction profiles of the 7 identified components of the soil sample MPS 20 (X axis: extraction steps; Y axis: total extracted solid in mg kg^{-1}) 43
57 Relative distribution of arsenic in the extracted physico-chemical components for the soil sample MPS 20 43
58 Comparison of total, bioaccessible and CISED extracted arsenic in soil sample MPS 20 43
59 Extraction profiles of the 6 identified components of the soil sample MPS 8 (X axis: extraction steps; Y axis: total extracted solid in mg kg^{-1}) 44
60 Relative distribution of arsenic in the extracted physico-chemical components for the soil sample MPS 8 44
61 Comparison of total, bioaccessible and CISED extracted As in the soil sample MPS 8 44
62 X-ray absorption near edge structure (XANES) spectra of mine waste and soil samples. A model compound $PbFe_3(SO_4)(AsO_4)(OH)_6$ is included. The dashed vertical lines show the theoretical absorption edge position for As(0) (11865 eV) and As(V) (11870 eV) 46
63 Normalised, K^3 — weighted EXAFS spectra for mine waste and soil samples. Solid line: experimental data, dashed line: least squares fit using parameters shown in Table 14 46
64 Radial structure functions (RSF) for mine waste and soil samples. Solid line: experimental data, dashed line: least squares fit using parameters shown in Table 14 46
65 Eh-pH arsenic stability diagram for arsenic species 48

TABLES

1 History of mining at Devon Great Consols 3
2 Summary statistics for As, Fe and S data 12
3 XRD analysis of selected tailings and waste material 14
4 As concentrations in vegetables from soils at Devon Great Consols 25
5 Chemical analysis of waters 26
6 Summary statistics for bioaccessible As data (mg kg^{-1}) 30

7 Summary Statistics for relative arsenic bioaccessibility data (% Astot) 30
8 Clusters of DGC soils obtained by k-means clustering of the soil physico-chemical variables 30
9 Correlation matrix for Cluster 1 of DGC soil samples 31
10 Correlation matrix for Cluster 2 of DGC soil samples 31
11 Multiple linear regression parameters for the Cluster 1 31
12 Multiple linear regression parameters for the Cluster 2 32
13 Arsenic (mg kg^{-1}) leached by de-ionised water in the first two steps of the sequential extraction 36
14 Best fit parameters for the As K-edge EXAFS spectra 45
15 Arsenic speciation in waters 47
16 As speciation in water leachates 47

Executive summary

South-west England has a legacy of metalliferous mining going back to Roman times. Intensive exploitation of metalliferous ore deposits, combined with the natural geochemical dispersion from the Cu-Sn-As mineralisation, has resulted in the creation of a significant area of arsenic-contaminated wastes and soils. Knowledge of the evolution of mine wastes and dispersion patterns is required for reducing concern on the health hazard associated to mining activities.

This study reports on As contamination in soils and waters in the vicinity of Devon Great Consols Mine, one of the largest and richest mines of the 19th century in the Tamar Valley of south-west England. The object of the study was to examine the distribution and speciation of As on the site and assess As soil bioaccessibility in order to estimate the significance of the soil ingestion pathway on human exposure to As in this area.

The Devon Great Consols Mine lies on the east bank of the River Tamar in the Tavistock district of Devon. Originally the mine raised copper ores from lodes consisting of chalcopyrite, pyrite, arsenopyrite and minor cassitierite with a gangue of quartz, fluorspar and brecciated mud rocks cemented by chlorite or siderite. In the mid 1800s at about the same time as copper ore production declined the use of As as a pesticide was developed and the mine had a new lease of life as an As producer. In 1869 the mine supplied half of the world's As production with activity continuing until about 1925.

The spatial distribution of As at Devon Great Consols defines widespread contamination of soils. The As median concentration in mine soils is 2105 mg kg^{-1}, but ranges from 249 mg kg^{-1} to 68 924 mg kg^{-1}. Soil samples that were taken from agricultural fields near to the village of Bere Alston, in order to provide background samples not affected by mineralisation or mining disturbance, have a median As value of 71 mg kg^{-1} and a range from 17 mg kg^{-1} to 172 mg kg^{-1}. A further set of soil samples collected from a farm about 2.5 km to the south-west of the Devon Great Consol, with underlying, unworked mineralisation, shows higher As concentrations than the Bere Alston background soils (As median concentration: 163 mg kg^{-1}).

The As bioaccessibility has been investigated using an *in vitro* test, the physiologically based extraction test (PBET), developed by Ruby et al. (1996), to simulate the leaching of a solid matrix in the human stomach and gastrointestinal tract. The term bioaccessibility is here used to describe the fraction of the total As concentration that is soluble in the stomach and gut and as a result is available for systemic uptake. The amount of As that is actually adsorbed systemically, the bioavailable fraction, is less than or equal to the amount that is bioaccessible. Therefore by using bioaccessibility data, a conservative dose estimate results which has clear implications for site specific risk assessments. It is less conservative than using total concentration data and hence may provide some down the line risk management benefits. The median value of bioaccessible As for the soils on the mine site is 408 mg kg^{-1}. Much lower concentrations are measured for the agricultural soils over mineralisation (PBET As median value of 14 mg kg^{-1}) and for the Bere Alston background soils (PBET As median: 7 mg kg^{-1}).

By using k-means clustering of the physico-chemical variables, the soils on the mine have been grouped into clusters with distinctive features and tentative assignments in terms of As source characterisation have been given. Clusters 1 and 2 group the soils that are characterised by low As concentration but with different As bioaccessibility. Correlation coefficients complemented by multiple linear regression analysis indicate that As is present in different chemical forms in the two groups of soils. The presence of As held in an iron sulphide phase is likely to be the factor responsible for the lower relative bioaccessibility of As in cluster 1 compared to cluster 2, where the element is possibly bound to an iron oxyhydroxide phase. The spatial plotting of the clusters identifies clearly cluster 4 as the area of major pollution, characterised by very high concentrations of As, Fe and S, around the As works area.

Chemical sequential extraction data have been used to help elucidate the nature of the physico-chemical forms of As in the soils and mine waste material. Data processing using the CISED method of analysis developed by Cave et al. (2004) allows characterisation of the matrix by resolving the number and composition of the physico-chemical components present. In all samples the most significant physico-chemical component percentage wise contains mainly Fe, As and traces of S and is extracted in the last stages of the extraction test.

Further evidence of the Fe-As association comes from scanning electron microscopy (SEM) equipped with an energy dispersive spectrometer (EDXA), which shows As-rich, iron oxyhydroxides coating the surface of altered waste fragments and clastic grains. The coatings show various microfabrics from colloform iron oxyhydroxide to more crystalline coatings (fine-needle-like crystals).

X-ray absorption near edge structure (XANES) analysis indicates that As(V) is the dominant oxidation state in the mine waste materials and soils (using a selection of soils from cluster 2). Quantitative fits of EXAFS spectra using theoretical standards indicate As(V) in tetrahedral coordination with O and second and third neighbour Fe atoms. Second and third neighbour As-Fe EXAFS distances imply either adsorption of the As onto an iron oxyhydroxide substrate or incorporation of the As into a mixed metal oxide phase.

Most of the waters flowing within the mine area and from tailings ponds contain elevated concentrations of As. Natural run-off collected from the calciner ashes near the works contains 6577 As µg l^{-1}. The As distribution pattern in the waters of Devon Great Consols Mine demonstrates the self mitigating capacity of mine drainage due to adsorption on iron-rich precipitates. This hypothesis is validated by chemical modelling.

Water leaching data indicates high solubility of As from the waste material surrounding the As works, in particular the As crusher area and the calciner ash spoil. Arsenic is barely leached by water in the iron oxy-hydroxides precipitated from the acid mine drainage waters on the mine site.

Arsenic(III) was determined to be the main species in surface waters and soils and tailings water leachates. This result contrasts with the findings of EXAFS

spectroscopy analysis. The low As(V)/As(III) ratio could be explained on the basis of preferential leaching of As(III) compared to As(V) as a result of a much weaker interaction of As(III) compared to As(V) and hydrous ferric oxides.

Using bioaccessible As concentrations an assessment of risk to human health arising from exposure to soil As contamination has been carried out using the CLEA model developed by DEFRA and the Environment Agency (2002). An average daily human exposure (ADE) that is 11 times the index dose of 0.0003 mg kg^{-1} body weight day^{-1} has been calculated for the soils surrounding the mine site. The implication is that there is a toxic risk associated with these soils.

1 Introduction

The south-western part of England is extensively contaminated with heavy metals and metalloids arising from centuries of mining activity in the region. Mineral exploitation can be traced back as far to the Phoenicians, who traded in tin ore, but it was not until the early 1800s that the main period of tin, copper and manganese, with subsidiary amounts of iron, lead, zinc, arsenic and uranium ore exploitation took place (Hamilton, 2000). From about 1860 to 1900, this region was the world's major producer of As, and the principal mineral of economic importance was arsenopyrite (FeAsS).

Mining and smelting activities have left a legacy of contaminated land, with As and Cu-rich mine tailings and other wastes abundant. Extensive areas of land were contaminated with fall out from smelting and ore roasting and some 700 km^2 of both agricultural and urban land are affected (Abrahams and Thornton, 1987). Today, many of the old mining and smelting sites are derelict, contaminated land, with large areas of mine spoil and the ruins of stacks, crushers and calciners.

The basis of any contaminated land risk assessment is a conceptual model that is created from knowledge of the evolution of mine wastes and dispersion patterns of contaminants. While the concentration of As in soils and rivers in south-west England is well documented (Abrahams and Thornton, 1987; Aston et al., 1975; Colbourn et al., 1975), less attention has been devoted to elucidating the partitioning and speciation of As occurring in contaminated soils and mine tailings.

The significance of soil ingestion and plant-uptake as major pathways to human exposure to As requires further research to gain an adequate understanding of the risk associated with mine pollution in this region.

1.1 SCOPE OF THE REPORT

This report focuses on As partitioning, mobility and bioaccessibility in soils contaminated by mining and ore processing at Devon Great Consols, an abandoned As mine in Devon. For comparison purposes the study also includes a mineralised site that has not been mined as well as a background, non-mineralised area.

Various approaches have been used to examine the geochemistry of As from mine-polluted soils. The investigative methods have included:

- measuring the spatial distribution of As in soils and mine wastes
- water sampling
- modelling water chemistry to determine potential for attenuation with changes in physico-chemical parameters
- examining the bioaccessibility of As in soil in order to estimate the significance of the soil ingestion pathway in relation to human exposure to As
- some preliminary data on vegetable uptake from contaminated garden soils are also introduced
- use of chemical extractions to identify geochemical phases/minerals controlling As sorption or solubility
- direct observations using electron microscopy techniques
- spectroscopic techniques (EXAFS analysis) for investigation of As oxidation state and coordination
- exposure assessment.

2 Geological setting and mineralisation

2.1 CORNUBIAN BATHOLITH

2.1.1 Introduction

The igneous body influencing mineralisation at Devon Great Consols is known as the Hingston Down Granite, one of eleven satellite intrusions and six major plutons comprising the Cornubian Batholith of south-west England. The batholith underlies the counties of Cornwall and Devon, and runs down the axis of the peninsula for a length in excess of 200 km. It includes a succession of deformed, low-grade, regionally metamorphosed sediments and igneous rocks of Devonian and lower Carboniferous age. The rocks of the batholith are granitic in nature and their origin is related to the later stages of the Variscan Orogeny (late Carboniferous) that had previously deformed and metamorphosed the sedimentary pile (Le Boutillier, 2001).

2.1.2 Age of emplacement

Geochronological data shows that the emplacement of the batholith spans some 20 million years, beginning in the Early Permian, during a period of orogenic extension, with the Carnmenellis pluton some 293 million years ago, and terminating with the Land's End pluton at 274 Ma. The Hingston Down pluton was intruded at 283 Ma. (Willis-Richards and Jackson, 1989). Halliday (1980) determined the first onset of mineralisation to be some three million years after the intrusion of the earliest granites in Carnmenellis. There is a similar hiatus prior to the onset of mineralisation on Dartmoor and in the Land's End granite (Le Boutillier, 2001).

2.1.3 Composition of the granites

The granites making up the batholith were rich in water, boron and other volatiles (Charoy, 1986) enabling them to transport large quantities of metal as halogen complexes (principally chlorine) and as complex silicic acids. With continued crystallisation leading to the concentration of incompatible elements, a series of residual volatile reservoirs formed in the apical sections of the various plutons (Dines, 1956). Subsequent vapour pressure increase led to hydraulic fracturing and the formation of high temperature griessen veins, breccia pipes and eventually, in conjunction with extensional and strike-slip faulting the formation of the main-stage lodes of the region (Le Boutillier, 2001). The initiation of large convection cells around the granite and the influx of meteoric fluids into the hydrothermal system allowed metals leached from the surrounding slates and metabasic rocks (principally copper and zinc) to be incorporated into the lode system and, later, allowed significant remobilisation and concentration of ores in some of the lodes (Dines, 1956).

Reactivation of north-north-west trending faults in the Late Permian–Early Triassic allowed basinal brines, to enter the Cornubian Massif and contribute a second phase of mineralisation to the orefield (Scrivener et al., 1994). This resulted in the mineralisation of some of the fault structures (cross courses) with lead, silver and a variety of minor metals (Le Boutillier, 2001).

Although the Hingston Down granite outcrops mainly on the Cornish bank of the River Tamar, mineral lodes occur on both sides of the river, covering an area roughly 12 miles wide by four miles north to south. The lodes are mainly east–west in trend and the ones within the metamorphic aureole were more productive than those in the granite. Copper, and its associated As, was, however, the most rewarding product of the area. In Devon Great Consols the Great Cross course heaves the main lode some 225 m in a right lateral sense. Most of the cross courses dip westwards at moderate to steep angles, and some carry a little galena and sphalerite mineralisation (Durrance and Laming, 1982). The mineralisation at Devon Great Consols is shown in Figure 1.

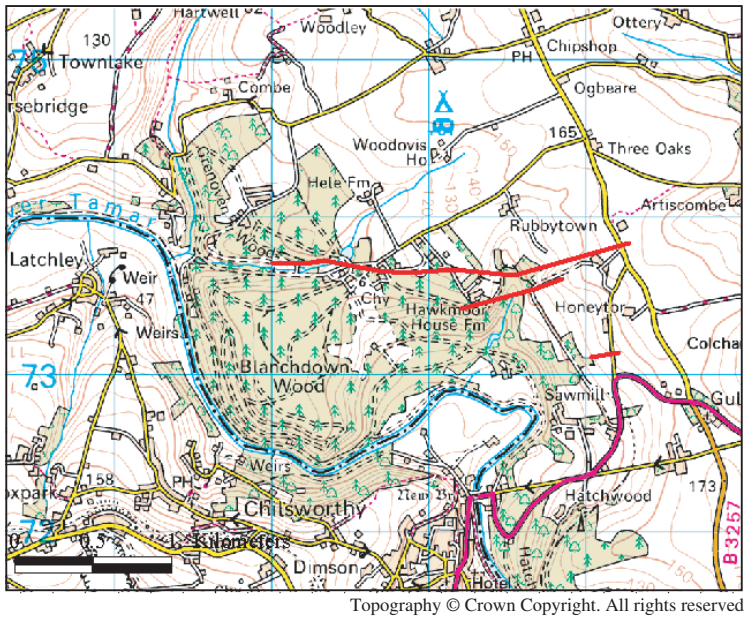

Figure 1 Mineralisation (red lines) at Devon Great Consols.

3 Devon Great Consols mine

3.1 GENERAL

The Devon Great Consols mine lies on the east bank of the River Tamar in the Tavistock district of Devon, UK [NGR SX 426 735] (Figure 2). The mine derived from the consolidation of five adjacent mines. It worked on lodes mainly consisting of chalcopyrite, pyrite, arsenopyrite and cassitierite. A summary of the history of mining at Devon Great Consols is outlined in Table 1.

In the 19th century Devon Great Consols was the richest and largest mine in the Tamar valley. The main product in the early years of operation was copper ore. Later attention was switched to arsenic and between 1848 and 1909 an output of over 70 000 tons is recorded (Dines, 1956). In the 1870s fifty percent of the world's production was estimated to come from half a dozen mines in the Callington and Tavistock area, including Devon Great Consols. Mining activity at Devon Great Consols ended in 1930 due to declining prices and loss of markets.

3.2 METHODS OF ARSENIC PRODUCTION

A comprehensive review of the method of arsenic production at Devon Great Consols can be found in Pye and Dixon (1989). The following is a brief summary that outlines the main stages that resulted in the output of refined arsenic. The site of the arsenic works was approximately 100 m in length and from 1921 to 1925 was involved in the processing, calcining, refining and milling of the ores collected on site. Figure 3 shows a plan of the works.

The ore was brought to the arsenic works from the various working mines and waste dumps, where it was reduced to small pieces by a crusher. The wooden and granite bases of the crusher still remain. It was then washed and sorted by large mechanical sieves powered by waterwheels. The processed ore was roasted in a pre-heated furnace (Figure 4), usually approximately 538–593°C, when the most efficient sublimation of arsenic occurs. Sulphur gases were also given off at this stage. After calcining the fumes passed into the labyrinth condenser (Figure 5) consisting of two separate sets of interconnecting

Table 1 History of mining at Devon Great Consols.

1844	– Extensive exploration of Blanchdown Wood–copper rich ore found
1845	– Entire complex becomes known as Devon Great Consols
1849	– River Tamar becomes harnessed for power and transport uses
1856	– After first 12 years of working, ore sales realised £1 400 000
1858	– Development of railway to Morwellham quay and major dock excavation
1865	– 420 000 tonnes of copper ore raised and sold since excavation began
1866	– Agreement signed to construct As works near Wheal Anna Maria
1868	– First As sales made
1869	– Arsenic production of 160 tonnes of refined As per month (50% of world's supply)
1871	– Arsenic reduction works completed at Wheal Maria capable of dealing with 2 500 t/yr early 1870s — copper becomes less plentiful and more difficult to extract and price falls considerably. Failed attempt to find tin at Wheal Josiah
1883	– Second failed attempt to find tin, this time at Wheal Emma - total value of tin found between both explorations was £170
1888	– About 240 tonnes of arsenic produced per month
1890	– Mine selling three times as much arsenic as copper
1891	– Total 'make' of arsenic was 5883 cwt barrels
1899	– Arsenic production declined to 150 tonnes per month
1901	– Price of arsenic slumped heavily; pumping and production ceased
1903	– Mine finally abandoned in the month of May
1915	– Upper levels of Wheal Fanny are reopened for arsenic extraction and Wheal Frementor for tin and wolfram (on a very small scale)
1919	– Railway re-laid between Wheal Anna Maria and Bedford United Mine to the south
1921	– Mining continued at Wheal Maria, Wheal Fanny and Frementor
1922	– Operation of two new calciners as supply and quality of ore deteriorates
1925	– Owing to a price slump, mining is suspended and only Frementor reopened later that year
1930	– Mining activity at Devon Great Consols effectively ended with the closure of Wheal Frementor

chambers built back to back to enhance the area of condensation. Here the temperature fell below 171ºC, and the grey 'crude' arsenic soot precipitated. The arsenic soot was removed by workmen, who gained access through a series of doors in the sidewalls of the condenser. This door arrangement allowed one set of chambers to be cleared out while precipitation was occurring in the other set and enabling the calciners to be worked continuously.

After collection the crude As (approximately 10% of which was soot, sulphur and other impurities) was recalcined in a circular, flat bed reverberatory furnace. This had a tiled floor and was fired using a smokeless fuel such as coke or anthracite to reduce the proportion of impurities in the final product. The crude As was spread over the floor, and 99.5% pure As was then precipitated as white crystals in the flues and condenser. Initially at Devon Great Consols, use was made of the same set of condensing chambers as were used for calcining. However, a new condenser with a tiled floor was added to the works solely for the precipitation of refined As. Such separate provision of condensing chambers avoided residues of lower-grade crude As being mixed in with the refined product during precipitation and clearance.

The white As crystals were milled to a fine powder, and packed into barrels. The remains of the grinding mill floor are still visible at the site (Figure 6).

After passing through the condensers, the remaining unprecipitated As and sulphur fumes had to be removed prior to emission from the stack in order to reduce pollution. For this purpose a 'waterfall' chamber was constructed between the condenser and the stack. Here the fumes passed through a water shower and amongst sodden wooden beams, and in the process most of the remaining As, the sulphur dioxide and sulphur trioxide was removed. Addition of limestone within the flue helped reduce the sulphur dioxide content. A 36 m high stack was constructed on top of a hill to facilitate the dispersal of the remaining fumes, as well as providing a draught for the calcining furnaces.

Figure 2 Location of study area and sampling areas.

Figure 3 Site plan of 20th century arsenic works.
1: Stack; 2: Flues; 3: Arsenic condenser; 4: Calciner; 5: Arsenic mill.

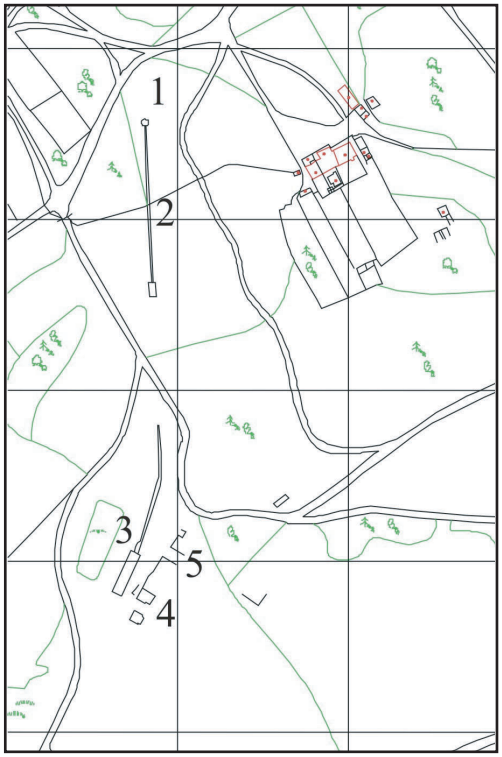

Figure 4 The Brunton Calciner at Devon Great Consols.

Figure 5 Arsenic condenser at Devon Great Consols. Chimney in the background.

Figure 6 The floor of the arsenic mill.

4 Sample collection

The Devon Great Consols Mine [SX 426 735] includes the arsenic processing plant and associated tailings tips and tailings lagoons (Figures 7 and 8). The soil and water sampling was mostly carried out in December 2000 in a period of heavy rainfall. Further sampling was carried out in October 2001. A third soil sampling was carried out in September 2003 with the aim of comparing field X-ray fluorescence to laboratory analysis of As. The complete set of samples is represented in Figure 9. Soils in the surroundings of the mine were also sampled. A further sampling exercise included a site on agricultural land located at Higher Todsworthy Farm, Drakewalls [SX 418 706], containing a mineral lode that has not been worked. Soils around Bere Alston village (outside of the mineralised area, approximately 7 km to the south-east of DGC) were also collected (Figure 2).

Each sample (0–15 cm depth) was made up of a composite of material from auger flights taken from five holes distributed within an area of approximately one metre square. At the processing plant, samples were collected from the ore crusher and the furnace slag heaps. Efflorescent masses of As-bearing salts on the brickwork at the furnace site were also sampled. The bed sediment was sampled from tailings ponds.

Water samples were collected from the tailings ponds, leats, adit discharges and seepages from tailings. Water samples were also collected from the main stream running in the eastern part of the site and from a borehole at Wheal Josiah Cottage on the northern border of the study site. Water pH, temperature, Eh, conductivity and alkalinity were measured in the field and samples preserved for chemical analysis.

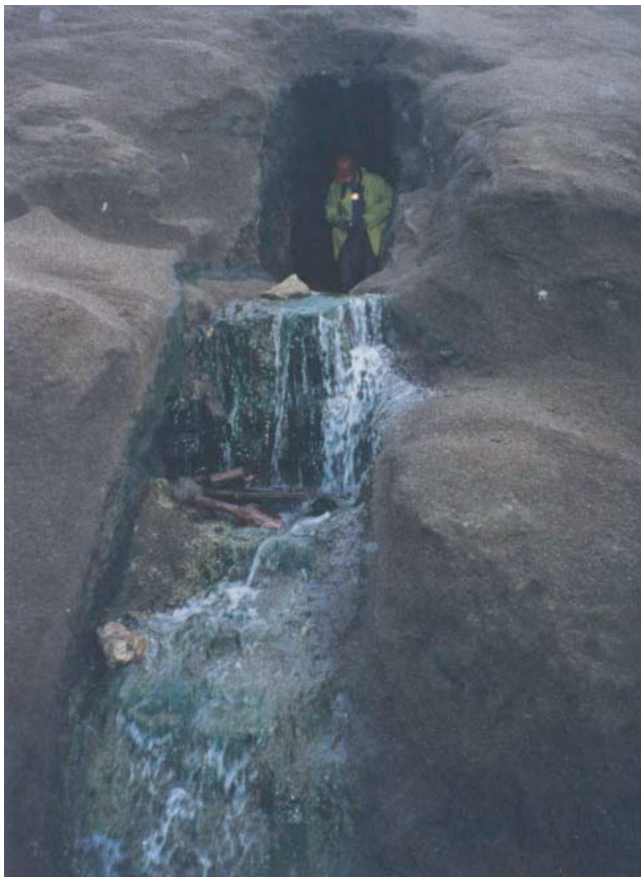

Figure 8 Adit discharge from tailings heap.

Figure 7 Tailings heap.

Figure 9 Sampling locations for soils (full circles), tailings (open circles), waters (triangles) at Devon Great Consols.

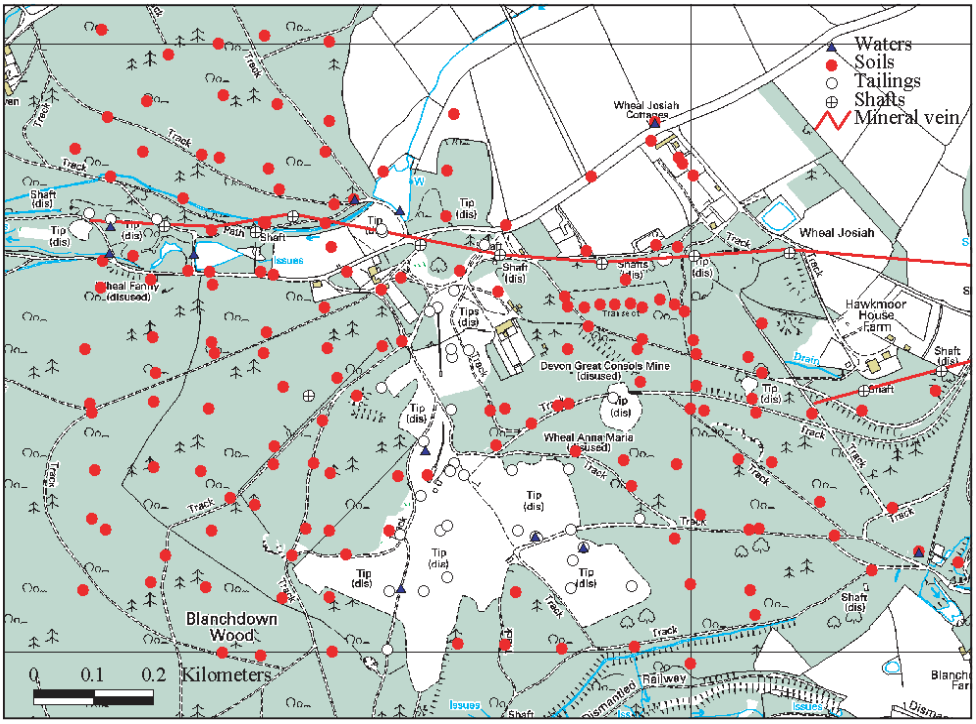

5 Analytical methods

5.1 SOIL/VEGETABLE CHEMICAL ANALYSIS

All soil samples were air-dried and sieved to <250 μm. Total element content of <250 μm fraction was obtained by inductively coupled plasma atomic emission spectroscopy (ICP-AES) subsequent to digestion of the samples with a mixture of hydrofluoric, perchloric and nitric acids. Organic matter content was estimated on the basis of loss on ignition (LOI) at 450°C, pH was measured in 0.01M $CaCl_2$ solution and cation exchange capacity (CEC) by titration.

Samples of vegetables from Wheal Josiah Cottage were washed to remove any residual soil, freeze dried and Tema milled prior to digestion in warm nitric acid and were analysed by inductively coupled plasma mass spectroscopy (ICP-MS).

5.2 WATER ANALYSIS

Water for inorganic analysis was filtered in the field using a disposable 0.45 μm cellulose-acetate cartridge filter. Determinations of major and trace elements were made by ICP-AES on 1% HNO_3 preserved filtered samples. Total As concentrations were determined by hydride generation AFS using 0.1% HCl-acidified samples. Fe(II) was determined by colorimetric analysis of 2–2 dipiridyl-spiked samples. The major anions NO_3, SO_4, Cl were determined by ion chromatography.

5.3 ARSENIC SPECIATION ANALYSIS BY ATOMIC FLUORESCENCE SPECTROSCOPY (AFS)

As III is determined by on-line mixing with pumped flows of acidified sample and alkaline sodium borohydride which react to form hydrogen and gaseous As hydride. A gas-liquid separator is used to separate these gases from solution which are then transported by argon gas to a hydrogen diffusion flame where As hydride is broken down to As atoms which are then excited with light from an As boosted hollow cathode lamp. The atomic fluorescence from the excited atoms is measured with a photomultiplier tube and the intensity is directly proportional to the concentration of As(III) in solution. As(V) does not react to form gaseous hydride and so in order to determine total arsenic, As(V) is reduced to As(III) by the addition of potassium iodide and ascorbic acid prior to analysis. To determine just As(III), potassium iodide and ascorbic acid are not added to the solution prior to analysis.

5.4 X-RAY DIFFRACTION ANALYSIS

A sample subset of tailings and soils were analysed by X-ray diffraction (XRD) using a Philips PW1700 series diffractometer fitted with a cobalt-target tube and operated at 45 kV and 40 mA. The samples were scanned from 3 to 65°2 Θ at a scanning speed of 0.7°2 Θ/minute. Diffraction data were analysed using Philips X'Pert software coupled to an International Centre for Diffraction Data (ICDD) database.

5.5 SCANNING ELECTRON MICROSCOPY ANALYSIS

Three samples of soil and tailings pond waste were collected in situ in 50 x 100 mm aluminium boxes ('Kubiena soil tins') to minimise sampling disturbance and preserve any delicate authigenic secondary mineral fabrics. The samples were air dried in the aluminium boxes and impregnated, under vacuum, with epoxy resin to stabilise the 'soils' for thin section preparation. A blue dye was added to the epoxy resin in order to highlight natural porosity during optical petrographic observation. The samples were then cut and prepared as uncovered polished thin sections.

The thin sections were briefly examined with an optical petrographic microscope (in transmitted and reflected light) prior to detailed petrographic characterisation using backscattered scanning electron microscopy (BSEM). BSEM observations were made using a LEO 435VP variable pressure digital scanning electron microscope (SEM) instrument. This was equipped with a KE Developments four-element solid-state backscattered electron detector, and an Oxford Instruments ISIS 300 digital energy-dispersive X-ray microanalysis system. The SEM instrument was operated in the low vacuum mode, at a vacuum of 0.3 to 0.4 torr, enabling the polished thin sections to be observed without the need for coating the samples with an electrically-conductive film (e.g. gold or carbon which would have been required for conventional high vacuum scanning electron microscopy). This allowed the sections to be re-examined by transmitted light optical microscopy without the surface being obscured by any surface coating. Observations were recorded using a beam accelerating potential of 10 to 20 kV; probe currents of 100 to 700 pA, and a working distance of 18 to 25 mm.

Mineral identifications were based on the evaluation of semi-qualitative microchemical information obtained from EDXA spectra recorded simultaneously during BSEM observation.

In addition, SEM observations were made on individual grains loosely dispersed onto a carbon adhesive tab and sputter coated with a conductive layer of gold metal. The efflorescent masses of As-bearing salts on the brickwork at the furnace site were also analysed.

5.6 SEQUENTIAL EXTRACTION TEST

A subset of 17 soils and tailings were selected for a non-specific chemical sequential extraction (Cave et al., 2004) in order to characterise element solid partitioning. An arsenical pyrite-enriched sample derived from the heavy mineral fractionation of a waste rock was also analysed. The extraction vessels employed were Schleicher and

Schuell® 'Centrex MF-25' polypropylene centrifuge tubes with filter inserts consisting of a regenerated cellulose membrane (pore size 0.45 μm). Two grams of each sample were accurately weighed into the filter tube insert and the first 10 ml aliquot of solvent added to the tube. The vessel was then centrifuged for 10 minutes at 3000 rpm, and the extract removed for analysis. This processes was repeated sequentially until 14 extracts, each of volume 10 ml, had been processed.

The solvents used for this technique were: de-ionised water (extracts 1 and 2), 0.01 M HNO_3 (extracts 3 and 4), 0.05 M HNO_3 (extracts 5 and 6), 0.1 M HNO_3 (extracts 7 and 8), 0.5 M HNO_3 (extracts 9 and 10), 1 M HNO_3 (extracts 11 and 12) and 5 M HNO_3 (extracts 13 and 14). For the 0.1, 0.5, 1 and 5 M HNO_3 extracts, 0.25, 0.50, 0.75 and 1 ml, respectively, of hydrogen peroxide were also added to each extract before making up to 10 ml volume. The extracted solutions were analysed by ICP-AES.

A data-processising alogorithm was used to identify the number of physico-chemical components extracted, their composition and the proportion of each in each extract according to the method called Chemometric Identification of Substrates and Element Distributions (CISED) described in Cave et al. (2004). The chemometric data-processing methodology is based on the assumption that the material is made of a mixture of discrete physico-chemical components characterised by distinct element composition. Under increasing acid concentration each physico-chemical component will dissolve accordingly to its degree of solubility. The non-specific extraction approach has already been shown to have a number of analytical advantages over a specific extraction scheme and the CISED method has also shown the ability to clearly identify physico-chemical components in the soil that have been validated independently by mineralogical analysis (Cave et al., 2004).

5.7 X-RAY ABSORPTION SPECTROSCOPY (XAS) ANALYSIS

X-ray absorption spectra at the As K-edge were collected on Station 16.5 at the CLRC Daresbury SRS operating at 2 GeV with an average current of 140 mA, using a vertically focusing mirror and a sagitally bent focussing Si(220) double crystal monochromator detuned to 80% transmission to minimise harmonic rejection. Data were collected with the station operating in fluorescence mode using an Ortec 30 element solid state Ge detector. Experiments were performed at ambient temperature. Single scans were sufficient for most samples, but for two dilute samples multiple scans were collected and averaged to improve the signal to noise ratio.

Background subtracted extended X-ray absorption fine structure spectroscopy (EXAFS) spectra were analysed in EXCURV98 using full curved wave theory (Binsted, 1998; Gurman et al., 1984). Phase shifts were derived in the program from *ab initio* calculations using Hedin-Lundqvist potentials and von Barth ground states (Hedin and Lundqvist, 1969). Fourier transforms of the EXAFS spectra were used to obtain an approximate radial distribution function around the central As atom (the absorber atom); the peaks of the Fourier transform can be related to 'shells' of surrounding back scattering atoms characterised by atom type, number of atoms in the shell, the absorber-scatterer distance, and the Debye-Waller factor, $2\sigma^2$ (a measure of both the thermal motion between the absorber and scatterer and of the static disorder or range of absorber-scatterer distances). The data were fitted for each sample by defining a theoretical model and comparing the calculated EXAFS spectrum with the experimental data. Shells of backscatterers were added around the As and by refining an energy correction Ef (the Fermi energy), the absorber-scatterer distance, and Debye-Waller factor for each shell, a least squares residual, the *R*-factor (Binsted et al., 1992), was minimised. For the first shell of scatterers around the As, the number of atoms in the shell was chosen as the integer that gave the best fit but was not further refined. Arbitrary numbers of atoms were chosen for the outer shells.

5.8 PHYSIOLOGICALLY BASED EXTRACTION TEST (PBET) ANALYSIS

In this study the physiologically based extraction test (PBET) has been carried out to address the bioaccessibility of As in soils and mine wastes. The term bioaccessibility is used here to describe the fraction of the total concentration of a metal that is soluble in the stomach and gut and is available for adsorption (Ruby et al., 1999). The bioaccessible fraction is not necessarily equal to the bioavailable fraction, but defines the maximum amount of a metal that is available for systemic adsorption. The adsorption of a particular element from a soil or dust after oral exposure is dependent on a number of factors, including the proportion of less soluble species present as well as interactions between the element and other soil constituents. Such factors limit the dissolution of the element during transit through the gastrointestinal tract and hence reduce adsorption. In order to account for limited dissolution of contaminants from ingested soil an *in vitro* test, the physiologically based extraction test (PBET), has been developed by Ruby et al. (1996) to simulate the leaching of a solid matrix in the human gastrointestinal tract.

Each air-dried and sieved (<250 μm) sample was homogenised prior to obtaining a 1.0 g sub-sample. In addition to a sample blank and a certified reference material, NIST, Butte Montana 2710, at least one sample was extracted in duplicate per extraction run of ten.

The simulated gastric solution for the PBET was prepared by diluting with deionised (DI) water to 1l volume: 1.25 g of pepsin (activity of 800–2500 units/mg), 0.50 g of citrate, 0.50 g of malate, 420 μL of lactic acid (synthetic syrup) and 500 μL of acetic acid. The pH of the simulated gastric solution is adjusted with 12 N HCl to a value of pH 2.5.

One hundred ± 5 ml of gastric solution was added to each 1.0 g sub-sample. The extraction took place in a specifically designed rotating water bath (based on a modified Toxicity Leaching Protocol Extractor) which was maintained at 37°C + 2°C using an immersion circulator to simulate gastrointestinal conditions. The extractor was capable of holding ten, 125-ml wide mouth high-density polyethylene (HDPE) bottles.

The PBET was divided into three stages, defined by three sets of sampling. Stage 1 corresponds to the period spent in the stomach environment and stage 2 and 3 those spent in the small intestine environment:

Stage 1: An aliquot (5-ml) was removed from each flask one hour from the beginning of the experiment and filtered to 0.45 μm using cellulose acetate syringe filters. The aliquots were placed into plastic test tubes.

Stage 2: All solutions were neutralised by introducing into each flask a solution containing a calculated amount of $NaHCO_3$ and 5 ml DI water. When pH 7.0 was achieved, bile salt (175 mg) and pancreatine (50 mg) were added to each flask. Each flask was then replaced in the rotating water bath. A 5 ml aliquot was taken from each flask 2 hours after the pH was set at 7.0.

Stage 3: 5 ml aliquots were taken four hours after the pH was set at 7.0.

In order to maintain the 100 ml volume in the reaction flask throughout the experiment, each time aliquots were taken, their volume was replaced immediately with the same amount of stomach solution.

The samples simulating time spent in the stomach environment and the small intestine environment were analysed by ICP-AES.

Relative bioaccessibility (%) was calculated as the fraction of the element present in the fluid phase divided by the total element concentration in the reaction vessel.

6 Mine waste and soil geochemistry

6.1 TAILINGS AND WASTE MATERIAL

Low pH and low organic matter content are characteristic of the tailings and waste materials. All samples exhibit elevated As values with the median value of 19 170 mg kg^{-1}, an upper quartile value, Q (0.75), of 26 921 mg kg^{-1} and a lower quartile value, Q (0.25), of 10 929 mg kg^{-1} (Figure 10). Samples are also typically enriched in iron and in many samples high sulphur content, up to 2.2%, is present. The summary statistics table describes the distribution of the data for As, Fe and S (Table 2).

6.2 SOILS WITHIN THE MINE AREA

Soils at the mine generally show acid-sulphate characteristics with extreme acidity (pH_{CaCl_2} mean value 3.88) and high sulphur content. According to Bloomfield and Coulter (1973) acid sulphate soils are those that have developed low pH as a result of oxidation of sulphides with segregation of iron and aluminium sulphates (particularly jarosite) in the form of yellow mottles or coatings.

The lower quartile value of As, Q (0.25), and the upper quartile value, Q (0.75), are respectively of 867 mg kg^{-1} and 8449 mg kg^{-1} and the median value is 2105 mg kg^{-1} (Table 2).

Figure 11 shows the spatial distribution of As throughout the study area. It is evident that the highest As values occur as clusters around the As works, in proximity to the main tailings heaps (south of the As works) and along the tailings ponds and leat crossing the north-west of the mine. The concentrations of As in the woodland covering a large part of the mine are relatively lower, ranging between 250 and 1000 mg kg^{-1}.

A west to east 200 m transect was located east of the chimney in the woodland and nine samples were collected along the transect to estimate the role played by wind dispersion from the stack in the contamination of the site.

Table 2 Summary statistics for As, Fe and S data (mg kg^{-1}).

Summary statistics for As data

	Tailings	DGC soils	Outside DGC soils	Background soils	Todsworthy Farm soils
Min:	1279	249	252	17	123
1st Qu.:	10929	867	798	59	147
Mean:	30842	8081	2019	82	166
Median:	19170	2105	1695	71	163
3rd Qu.:	26921	8449	3352	93	191
Max:	204478	68924	4482	172	205
Total N:	20	73	10	5	20
Std Dev.:	44685	12753	1481	57	27
Skewness:	3.44	2.58	0.53	0.94	-0.08

Summary statistics for Fe data

	Tailings	DGC soils	Outside DGC soils	Background soils	Todsworthy Farm soils
Min:	39564	28705	34054	47264	26339
1st Qu.:	69917	43192	40810	48517	31344
Mean:	124660	65654	42955	48927	33153
Median:	127124	49545	43131	48656	32664
3rd Qu.:	158904	73233	44860	50000	33711
Max:	303555	191976	53014	50198	50642
Total N:	20	73	10	5	20
Std Dev.:	66222	38900	5160	1201	4957
Skewness:	0.85	1.86	0.16	-0.34	2.30

Summary statistics for S data

	Tailings	DGC soils	Outside DGC soils	Background soils	Todsworthy Farm soils
Min:	63	58	428	271	327
1st Qu.:	705	205	663	282	410
Mean:	4772	984	1386	341	447
Median:	3416	470	1299	339	434
3rd Qu.:	6283	1304	1771	403	475
Max:	22400	8282	3529	411	610
Total N:	20	73	10	5	20
Std Dev.:	5410	1399	935	65	75
Skewness:	2.03	3.08	1.39	0.03	0.66

Contamination by condensation from smelter fumes is often an extensive feature at mine sites with the effect usually confined to the top few centimetres of soil (Rose et al., 1979). The contamination generally takes the form of an ellipse with the major axis being along the direction of the prevailing wind (Davies, 1971). However, looking at the rather homogeneous As soil contents along the transect it is evident that dispersion from the stack by regional westerly prevailing winds have played a minor role in the present As soil distribution.

6.3 SOILS OUTSIDE THE MINE AND BACKGROUND SOILS

The soils sampled from fields surrounding the mine site have pH ranging from 4.36 to 6.86 and show high As concentrations between 252 and 4482 mg kg^{-1} (Figure 10, Table 2). In particular, the soils analysed from the garden of Wheal Josiah Cottage yield As concentrations from 805 mg kg^{-1} to 3684 mg kg^{-1}. A soil sampled in Gunnislake village has an As concentration of 252 mg kg^{-1}.

Soils from Higher Todsworthy Farm, Drakewalls, represent soils sampled over mineralisation not affected by mining activities. Arsenic concentrations range from 123 mg kg^{-1} to 205 mg kg^{-1} (mean 166 mg kg^{-1}) (Figure 10, Table 2) and the pH ranges from 4.34 to 5.37.

The soils collected in Bere Alston represent background concentrations. This area is not mineralised and removed from mining activity, and has values for As of 59–172 mg kg^{-1} (mean 82 mg kg^{-1}) and higher pH values (mean pH 5.24).

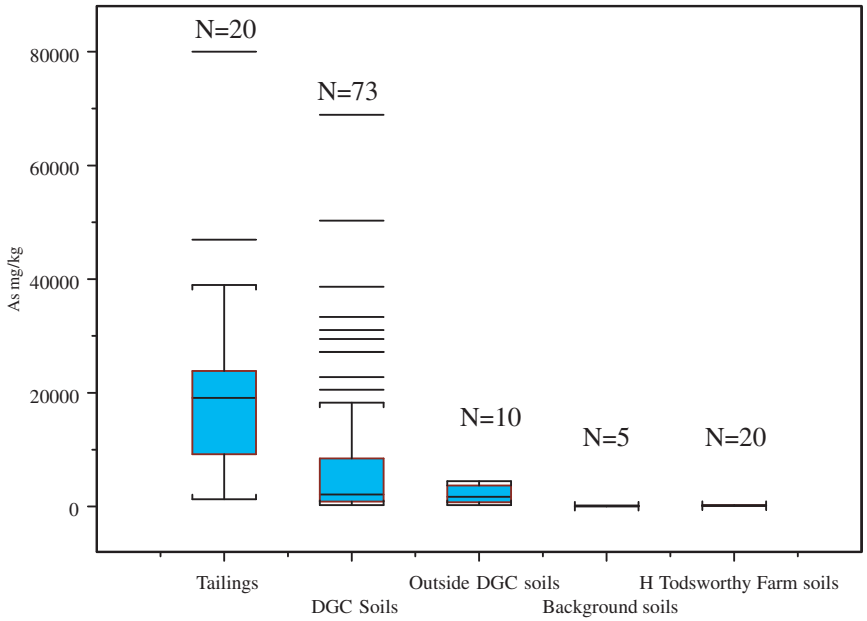

Figure 10 Box-plots of arsenic data for tailings, DGC soils, background soils and Higher Todsworthy Farm soils in which the limits of the boxes enclose the interquartile ranges and the whiskers extend to fences at the quartile plus and minus 1.5 times the interquartile range. The figure shows also the outliers (plain lines outside the fences) and the median (horizontal segment inside the box) for each group.

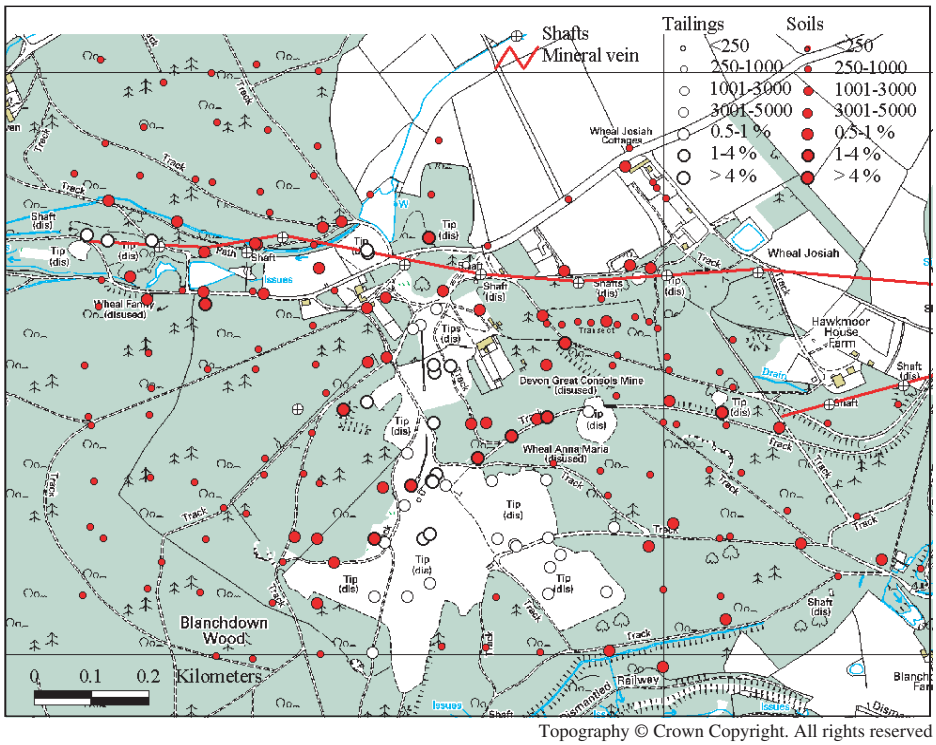

Topography © Crown Copyright. All rights reserved

Figure 11 Spatial distribution of As in topsoils and wastes of DGC mine.

7 Mine waste and soil mineralogy and petrography

7.1 MINERALOGICAL COMPOSITION OF SELECTED MINE WASTES

Samples MPM 4, sandy tailings material, MPS 90, black furnace slag, and MPS 92, bed sediment from a dried up tailings pond, were analysed by XRD. The results of qualitative XRD analysis are given in Table 3 where ranking (major, minor or trace) is on the basis of relative X-ray intensity ('?' was used when some evidence was found for the presence of the mineral but not enough for an identification).

XRD analysis of the tailings sample MPM 4 shows the presence of the gangue minerals (quartz, fluorite, mica and chlorite) and possibly traces of pyrite. The relatively high detection limit of XRD analysis (~5%) negates the detection of arsenic secondary minerals.

Cassiterite was found in MPS 90, the black furnace slag material. Evidence of jarosite are found in both the furnace slag and the tailings pond sediment.

7.2 PETROGRAPHIC OBSERVATIONS

7.2.1 As-rich efflorescence

The white-pink efflorescent masses found on the brickwork at the condenser site are made of microcrystalline gypsum (XRD analysis). Intimate association of gypsum ($CaSO_4 \cdot 2H_2O$) and As is evidenced by SEM-EDXA (Figure 12). Whether or not a calcium arsenate phase is present along with the calcium sulphate is difficult to confirm, although very soluble calcium arsenates such as weilite, haidingerite and pharmacolite have been identified on precipitates from As-rich waste leaching in industrial sites (Juillot et al., 1999).

7.2.2 Ore crusher ground

SEM analysis of the material adjacent to the ore crusher shows common chalcopyrite (FeCuS) and arsenopyrite (FeAsS) grains (Figure 13). A secondary phase composed of Fe, As and Ca is often rimming the sulphide grains. Semi-quantitative EDXA indicates that the grain-coating cement usually contains high As, typically between 24 and 45% As_2O_3, high iron, between 41 and 47% Fe_2O_3 and minor calcium, between 3 and 9% CaO. Discrete sandy-size white aggregates, commonly observed in the waste, show the same composition (Figure 14). Evidence of arsenolite presence is also found (Figure 15).

Black furnace ash, sample MPS 90

This material comprises of a poorly sorted gravel with sandy matrix (Figure 16). It is composed mainly of sand- to gravel-sized fragments of ash or slag, altered illite-quartz slate or pelite rock fragments, rock fragments heavily mineralised (or replaced) by hematite and/or iron oxyhydroxide, fragments of intergrown quartz and hematite/iron oxyhydroxide mineralisation (possibly gossan material), and simple quartz fragments (Figure 16). Minor amounts of altered tin mineralisation are also present. This is represented by grains of gel-like iron oxyhydroxide containing relict fractured cores of cassiterite (Figure 17). Small sand-sized grains of fresh cassiterite are common. Fragments containing sulphide mineralisation are very rare, and consist of fragments of gel-like iron oxyhydroxide replacing and enclosing relict corroded cores of micro-fractured pyrite.

The ash or slag fragments are composed of highly microporous glassy material with globular pores or vesicles, which are impregnated and lined by films of very fine iron oxyhydroxide (Figures 16 and 18). EDXA shows that the glassy matrix is composed of Si, Al, Fe, K, Ca and Na. Some clinker fragments contain disseminated grains of cassiterite (Figure 18).

BSEM observation shows that grains are coated by a thin layer of iron oxyhydroxide (Figure 17, Figure 19). This locally cements the fragments together with a patchily developed iron oxide cement (Figure 19). The iron oxide coatings often preserve very delicate skeletal fabrics (e.g. Figure 19) formed where the host grain has been dissolved away, leaving an internal mould preserved in iron oxyhydroxide. Such delicate fabrics would easily be destroyed by movement or transport, and must therefore have formed in situ within the tailings deposit. They represent the dissolution of very unstable components — perhaps carbonate grains or sulphide grains.

Detailed BSEM observations show that the iron oxide coatings have a complex microfabric (Figure 20). They consist mainly of an earlier layer of finely banded colloform iron oxyhydroxide, which rests directly on the

Table 3 XRD analysis of selected tailings and waste material.

Sample	Mineralogy
MPM4, < 63 mm	Major: quartz, ?amorphous silica. Minor: 'mica', fluorite, ?chlorite. Trace: ?pyrite
MPM4, -150 + 63 mm	Major: quartz. Minor: fluorite, 'mica', chlorite. Trace: ?pyrite, ?plagioclase, ?native arsenic
MPM4, -250 + 150 mm	Major: quartz. Minor: fluorite, chlorite, 'mica', ?kaolinite. Trace: ?pyrite
MPS90, < 2 mm	Quartz, hematite, magnetite, cassiterite, 'mica', ?albite, ?fluorite, ?jarosite ($KFe(SO_4)_2(OH)_6$)
MPS92, < 2 mm	Quartz, hematite, 'mica', chlorite, albite, ?magnetite, ?jarosite ($KFe(SO_4)_2(OH)_6$), ?fluorite, ?cassiterite

grain surfaces, or lines pores and dissolution cavities. It typically displays irregular shrinkage microfractures, indicating that it was originally very hydrous. This shrinkage may have taken place as a result of the sample drying out during collection and subsequent thin section preparation. A later generation of more crystalline iron oxyhydroxide forms an outer coating of fine needle-like crystals resting on the colloform iron oxyhydroxide (Figure 20).

EDXA observations indicate that the iron oxyhydroxide usually contains several percent of silica. It can also be As-rich (e.g. Figure 21), varying in composition from <0.5% As_2O_3 up to approximately 30% As_2O_3 (based on semi-quantitative EDXA observations). There appears to be no difference in composition between the different bands of colloform oxide, nor between the colloform oxyhydroxide and the more crystalline oxyhydroxide, within any particular region in the sample. However, the oxide compositions vary irregularly from point to point across the sample, indicating that it is inhomogeneous in composition.

Sandy tailings, sample MPS 91

This sample comprises largely angular fragments of quartz, rock fragments composed dominantly of illite, illite-quartz, or illite-quartz-chlorite-feldspar (possibly pelite or slate). Most of the illitic and chloritic rock fragments (which may also include sericitic fragments) are heavily impregnated or partially replaced by very fine iron oxide (goethite and or hematite).

Fragments of partially altered hydrothermal mineralisation containing arsenopyrite, often associated with quartz and siderite are common minor constituents (Figure 22). Some of the arsenopyrite is fresh (Figure 22) but it commonly displays partial alteration to iron oxyhydroxides (Figure 23). Altered pyrite (partially replaced by fine gel-like iron oxyhydroxide) and pyrite-quartz fragments are also present but are much less abundant than arsenopyrite. Small cassiterite grains are present in trace amounts.

All of the rock and mineral fragments are coated with a thin film of iron oxyhydroxide (Figures 22 to 24) that may be up to 50 μm thick. This oxide also forms delicate arcuate structures that bridge across pore throats between adjacent grains (Figures 23 to 25), weakly cementing the tailings particles and demonstrates that the oxide formed in situ since such delicate structures would not survive much physical disturbance or transport. It appears to have formed by precipitation of the iron oxyhydroxide within, or on, meniscus films of water between adjacent grains, indicating formation within the tailings under unsaturated groundwater conditions (i.e. capillary pore water).

The iron oxyhydroxide films have finely banded colloform texture (Figure 26), and it often displays shrinkage cracks indicating that it may have been a very hydrous gel originally. No difference in composition is observed between the EDXA spectra of the different colloform layers, suggesting that the variation in brightness of the colloform bands seen under BSEM simply reflects a variation in water content. Semi-quantitative EDXA also indicates that the iron oxyhydroxide grain-coating cement usually contains a small amount of As, typically between <0.5 to 3% As_2O_3 (Figure 27).

Iron oxyhydroxide replacing or altering directly from arsenopyrite (e.g. Figures 23 and 25) generally contains much higher As concentrations than most of the grain-coating iron oxyhydroxide cement, and is of the order of several tens of percent As_2O_3 (Figure 28). However, the iron oxyhydroxide cement which coats the surfaces of altered arsenopyrite grains is also highly enriched in As (Figure 29), and it appears to have a higher concentration of As than the underlying iron oxide that directly replaces the arsenopyrite. This may indicate different origins for the two iron oxyhydroxides. The oxide directly replacing arsenopyrite may represent hydrothermal or supergene mineralisation (e.g. gossan material) that was originally included within the tailings deposits, whereas the grain coating iron oxyhydroxide is later and clearly formed in situ within the tailings deposit. Consequently, any differences in As content between these two oxyhydroxide generations may reflect differences in the pore water As chemistry at the time of formation.

Soil sample MPS 96

This sample contrasts markedly with the waste materials having a well-pedified soil fabric comprising weakly to moderately compacted sand-sized ‘peds’ composed of dense-packed silt- and clay-grade quartz, illite, kaolinite and chlorite (Figure 30). The peds may contain traces of fine (sub-micron) hematite (or iron oxyhydroxide) and titanium oxide particles disseminated through the matrix of the ped. Angular rock fragments (pelitic) and quartz grains, and rare altered ilmenite or magnetite grains are scattered through the soil. Some root channels or burrows lined by clay are also apparent in this sample.

In marked contrast to the tailings, no iron oxide coatings or cements were observed on the surfaces of either grains or impregnating soil peds. Furthermore, mineralised rock fragments are relatively rare, and are limited to a few scattered grains of micaceous rock material replaced by hematite (Figure 31). The hematitisation of these rock fragments is clearly exogenic in origin.

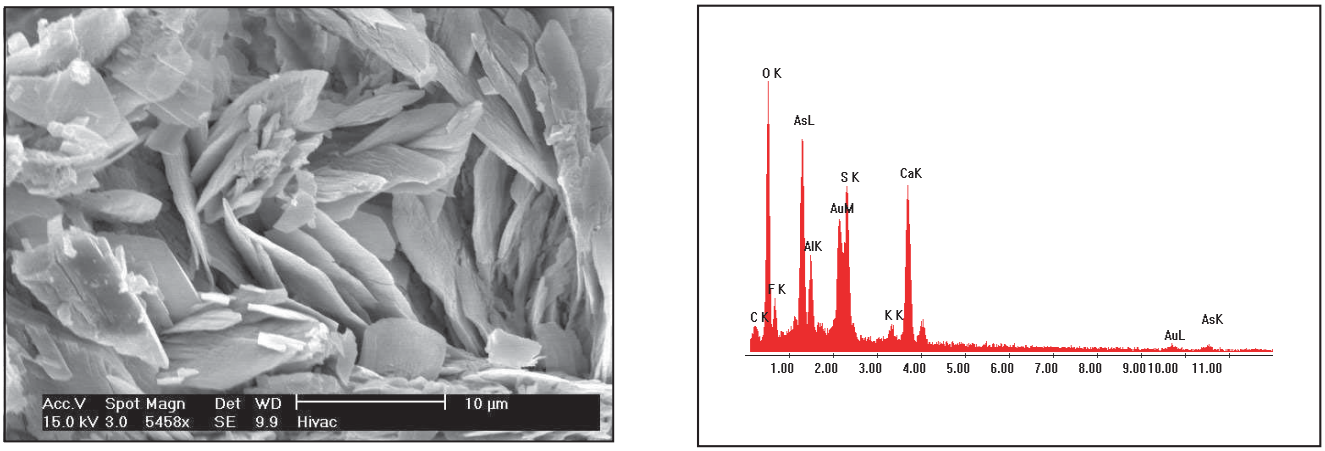

Figure 12 SEM micrograph of $CaSO_4$ crystals in efflorescent masses at the furnace site and EDXA spectrum showing the presence of a large amount of arsenic.

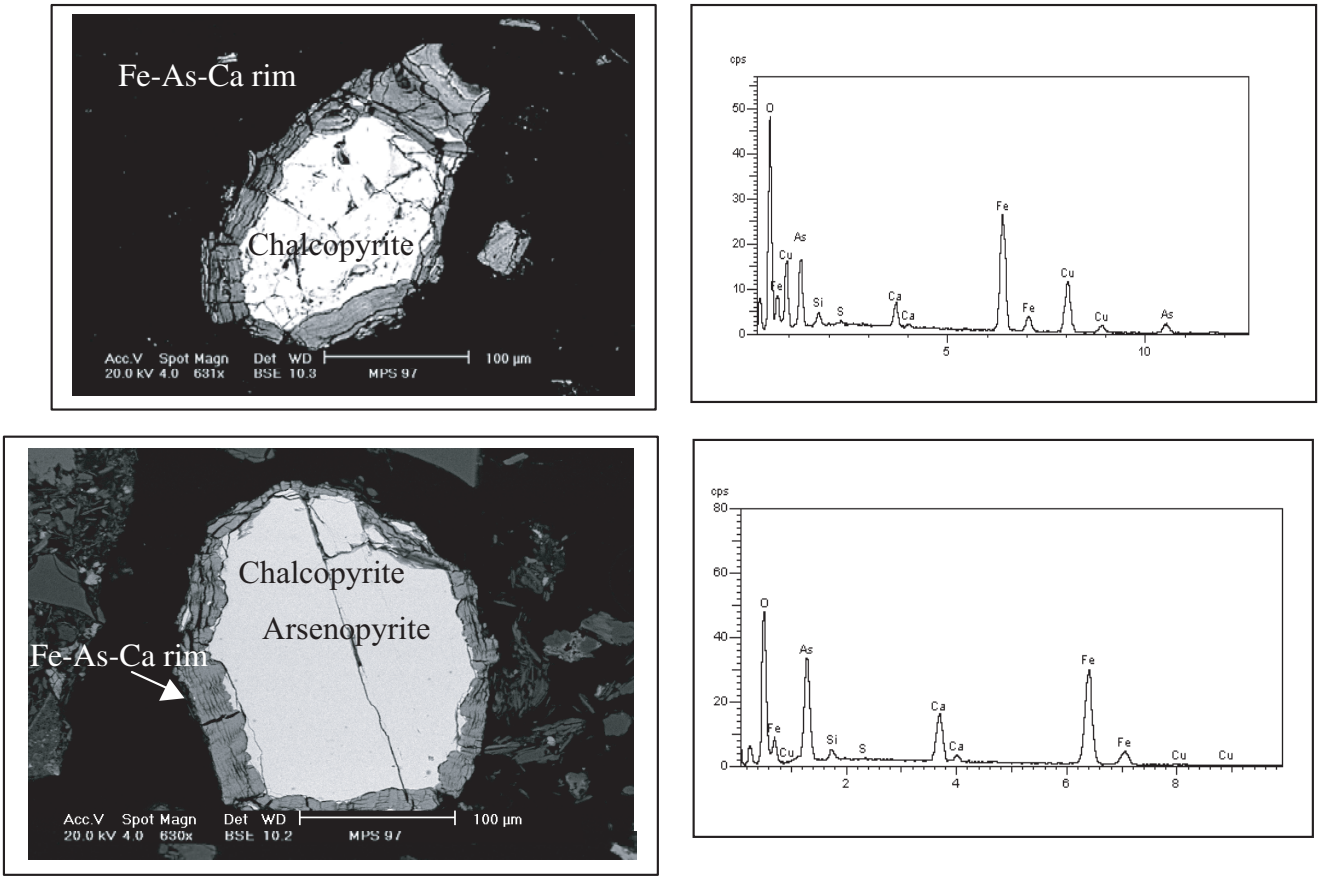

Figure 13 SEM micrographs and relative EDXA spectra of arsenic-iron-calcium coatings rimming sulphide grains.

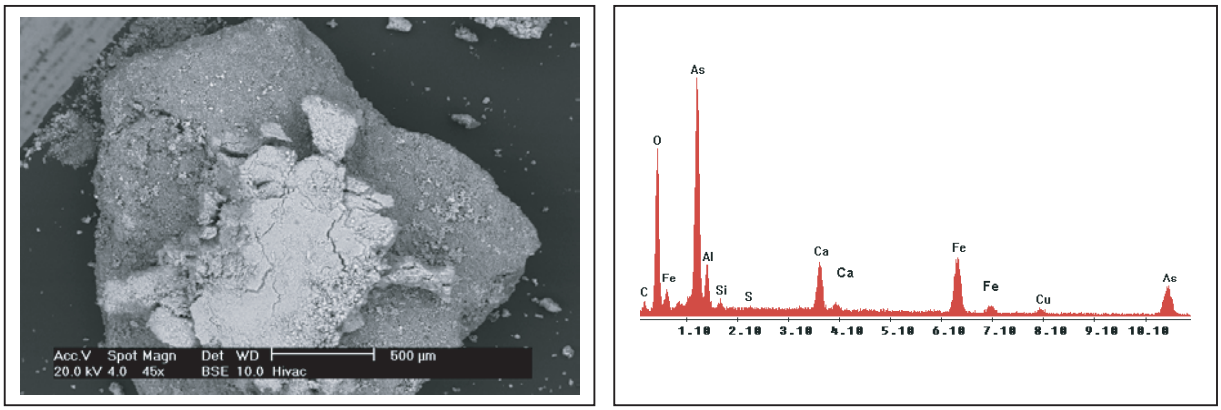

Figure 14 SEM micrograph of white flakes from the ore chrusher ground and EDXA spectrum showing the presence of a large amount of arsenic associated to calcium and iron.

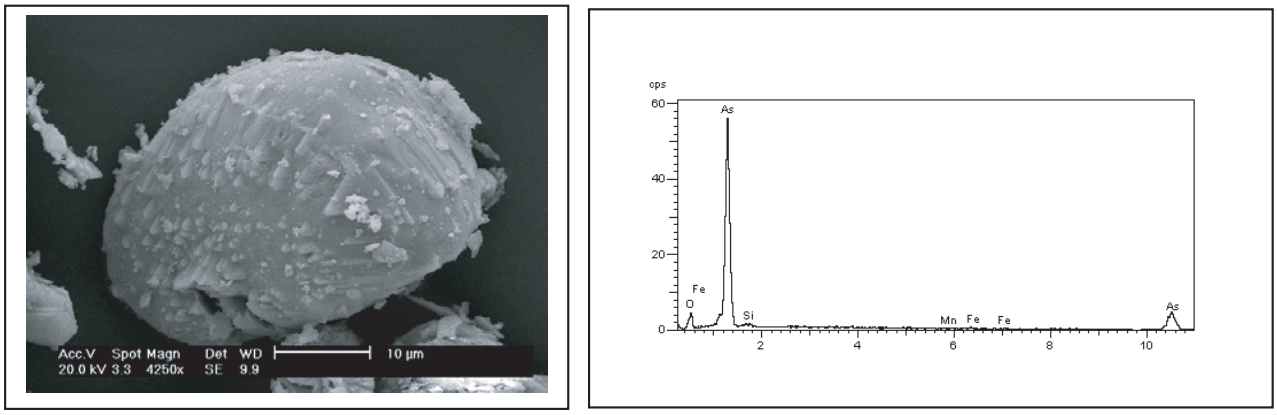

Figure 15 SEM micrograph of possible arsenolite crystal found at the ore crusher site and relative EDXA spectrum.

Figure 16 BSEM image showing loose packed fragments of quartz (mid-grey) and microporous ash and slag impregnated by fine iron oxyhydroxide (bright). Sample MPS 90.

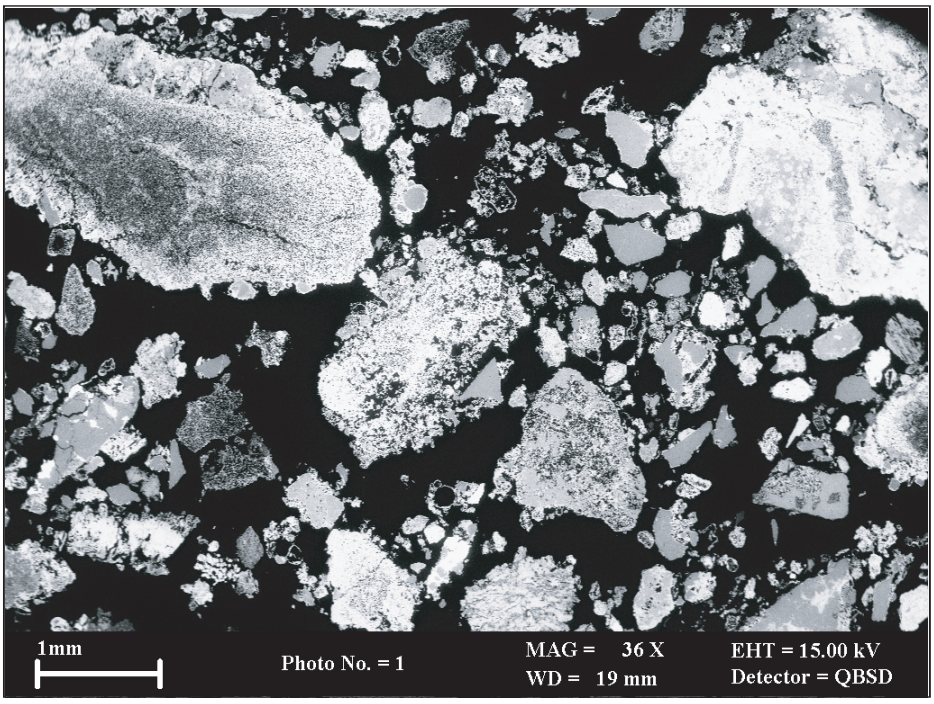

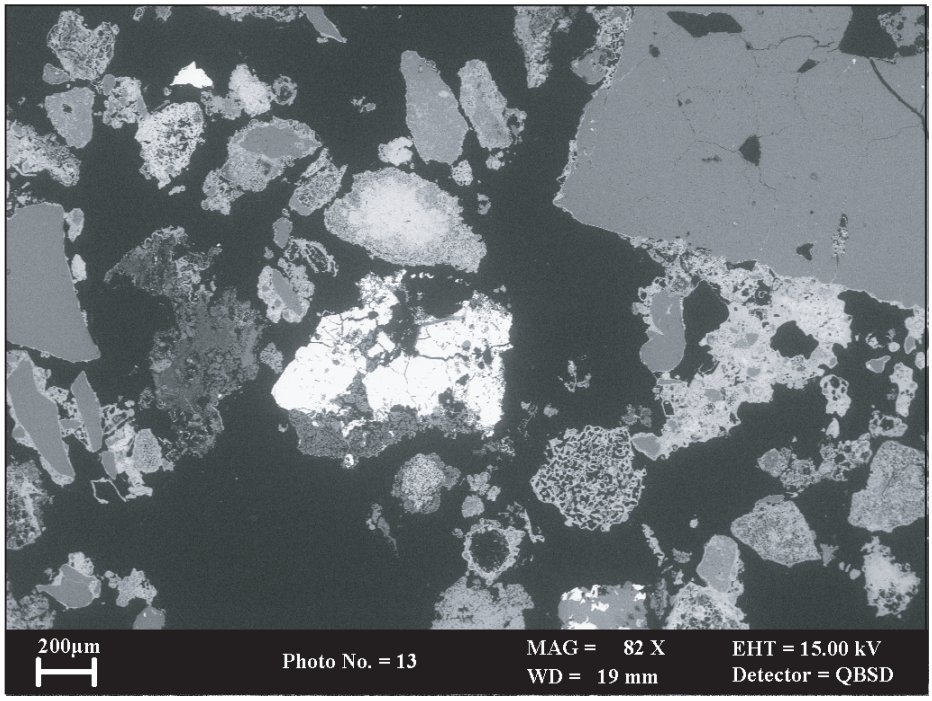

Figure 17 BSEM image showing loose-packed fragments of quartz (dull grey), microporous ash or slag and partially altered cassiterite (bright) coated by thin fringe of iron oxyhydroxides. Sample MPS 90.

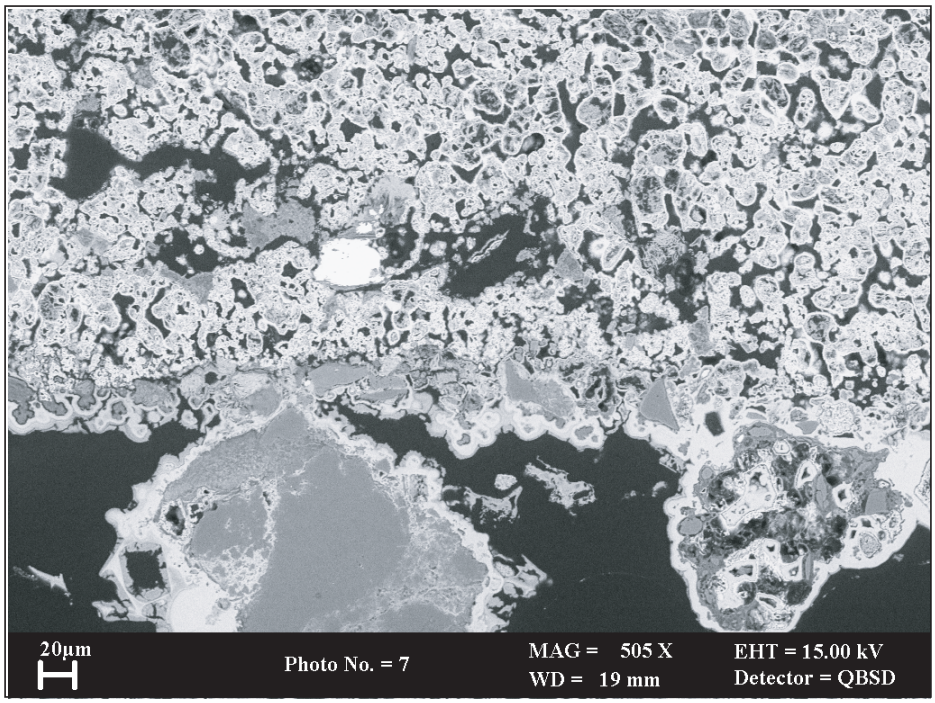

Figure 18 BSEM image showing detail of a microporous altered vesicular glassy slag fragment, with thin bright fringes of iron oxyhydroxide lining vesicular cavities. A very bright relict of cassiterite can be seen within the ash fragment. A thin later layer of gel-like or colloform iron oxyhydroxide coats the outer edge of the grain. Sample MPS 90.

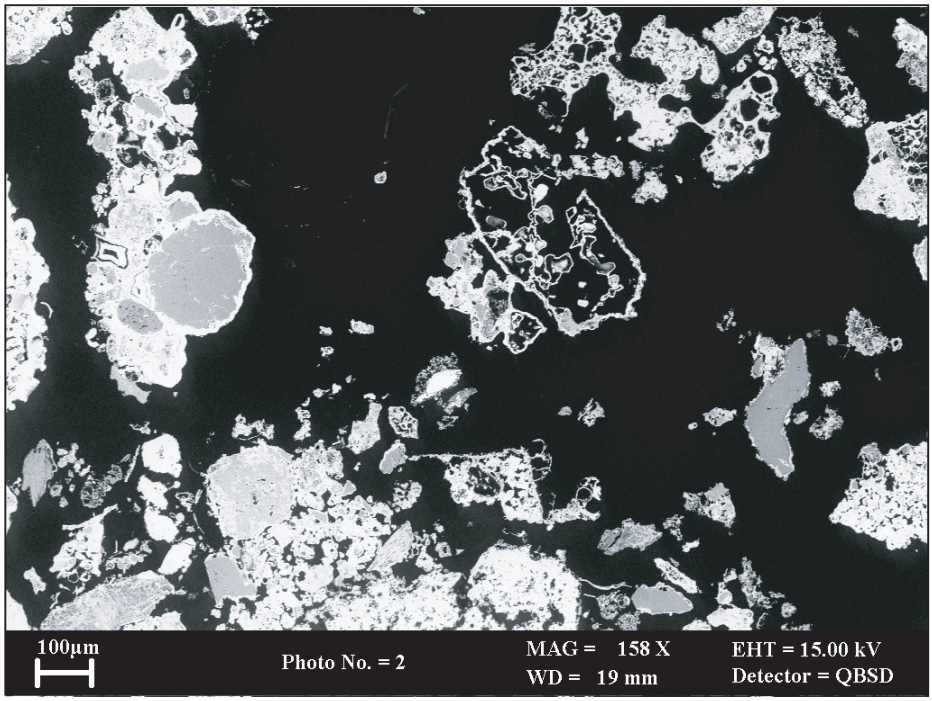

Figure 19 BSEM image showing fragments of spoil cemented by arsenic-rich iron oxide, and very delicate skeletal structures outlined in iron oxyhydroxide that have formed by in situ dissolution of original constituents in the spoil. Sample MPS 90.

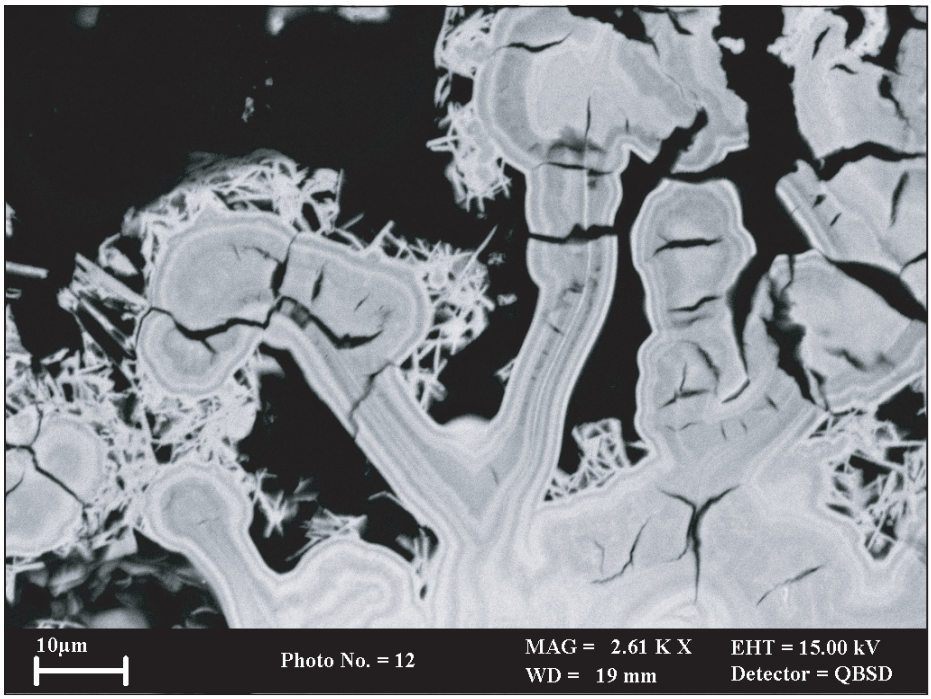

Figure 20 BSEM image showing detail of arsenic-rich iron oxyhydroxide cement coating the surfaces of altered waste fragments. It shows banded colloform oxyhydroxide gel material displaying shrinkage (desiccation) cracks. This is encrusted by more crystalline acicular oxyhydroxide. Sample MPS 90.

Figure 21 EDXA spectrum of arsenic-rich iron oxyhydroxide, showing high concentration of arsenic, major aluminium and silica, and minor sulphur (probably present as sulphate). Sample MPS 90.

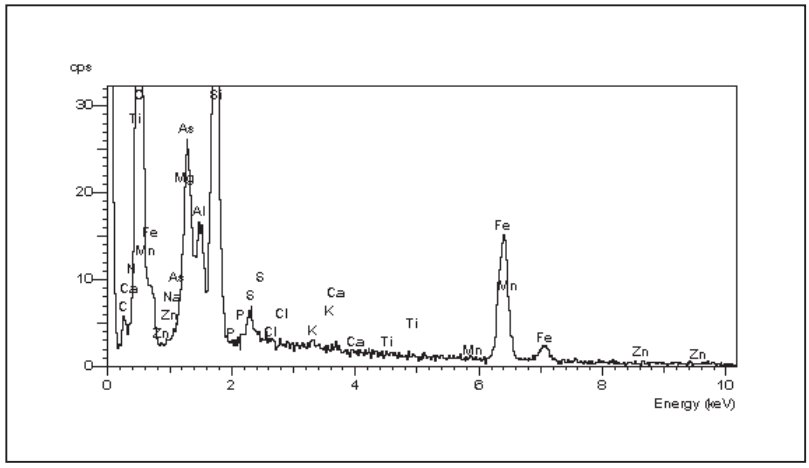

Figure 22 BSEM image showing a fragment of hydrothermal mineralisation consisting of an intergrowth of quartz (dull grey), arsenopyrite (white) and siderite (mid-grey). Sample MPS 91.

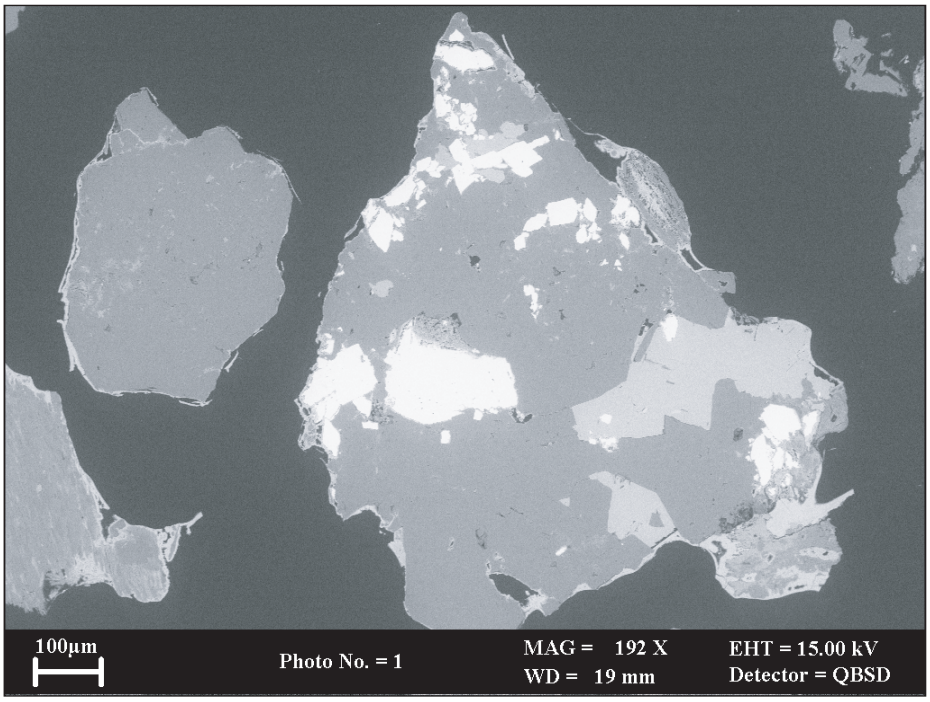

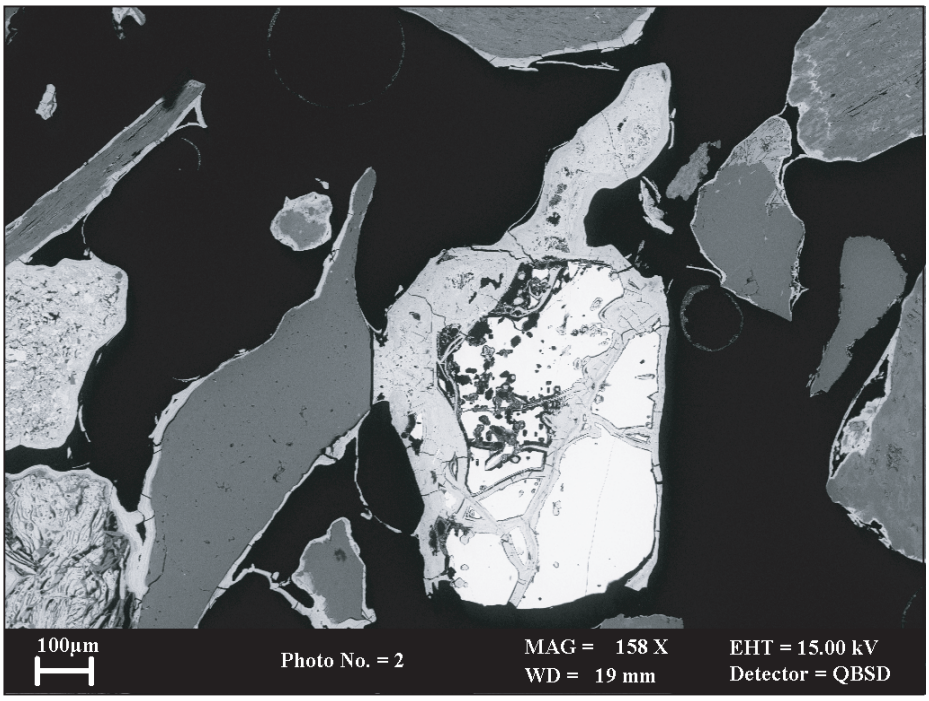

Figure 23 BSEM image showing fragments of illitic rock (fibrous grey material), quartz (dark grey) and altered fractured arsenopyrite (white) coated by a thin film of arsenic-rich iron oxyhydroxide. Sample MPS 91.

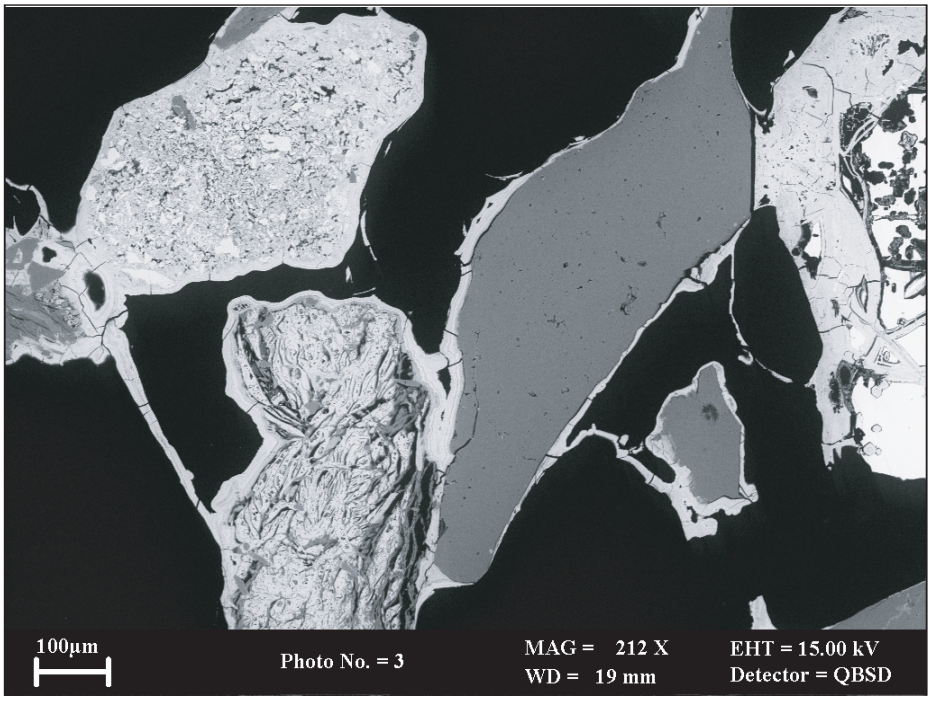

Figure 24 BSEM image showing fragments of illitic rock (fibrous grey material), quartz (dark grey) and altered fractured arsenopyrite (white) coated by a thin film of arsenic-rich iron oxyhydroxide. The iron oxyhydroxide forms delicate meniscus cements that bridge between adjacent grains. Sample MPS 91.

Figure 25 BSEM image showing detail of the edge of an altered arsenopyrite grain. Relict arsenopyrite (white) is directly enclosed by a matrix of gel-like As-rich iron oxyhydroxide (light grey) displaying irregular shrinkage cracks. A slightly brighter, and more As-rich, iron oxyhydroxide coats the margins of the grain and forms a colloform meniscus cement bridging to, and coating, the adjacent quartz grain (dark grey). Sample MPS 91.

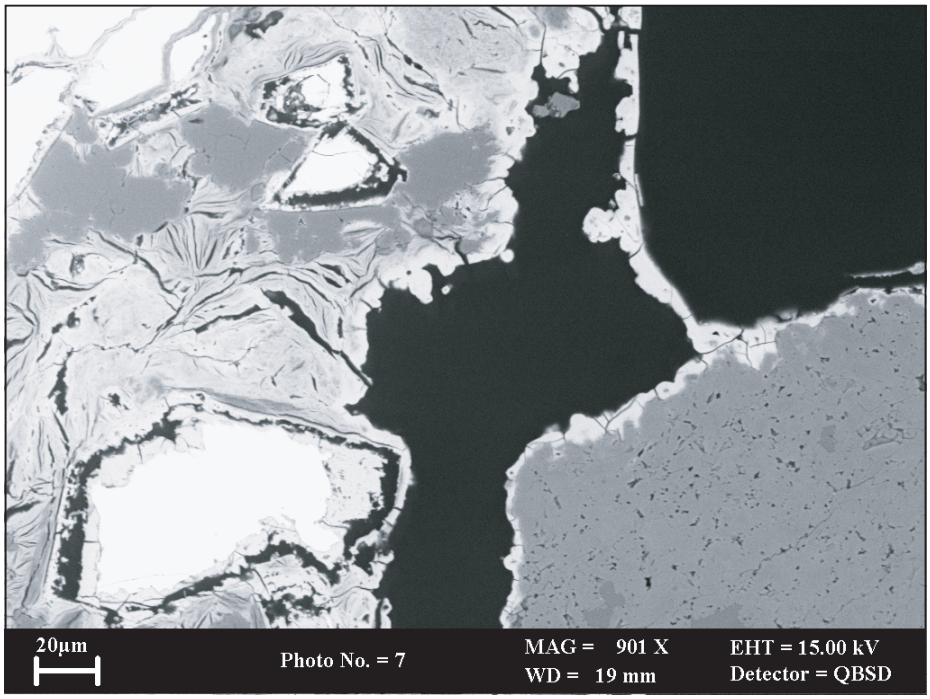

Figure 26 BSEM image showing colloform banding within meniscus iron oxyhydroxide cement coating ferruginous micaceous and quartz grains (dark grey). Sample MPS 91.

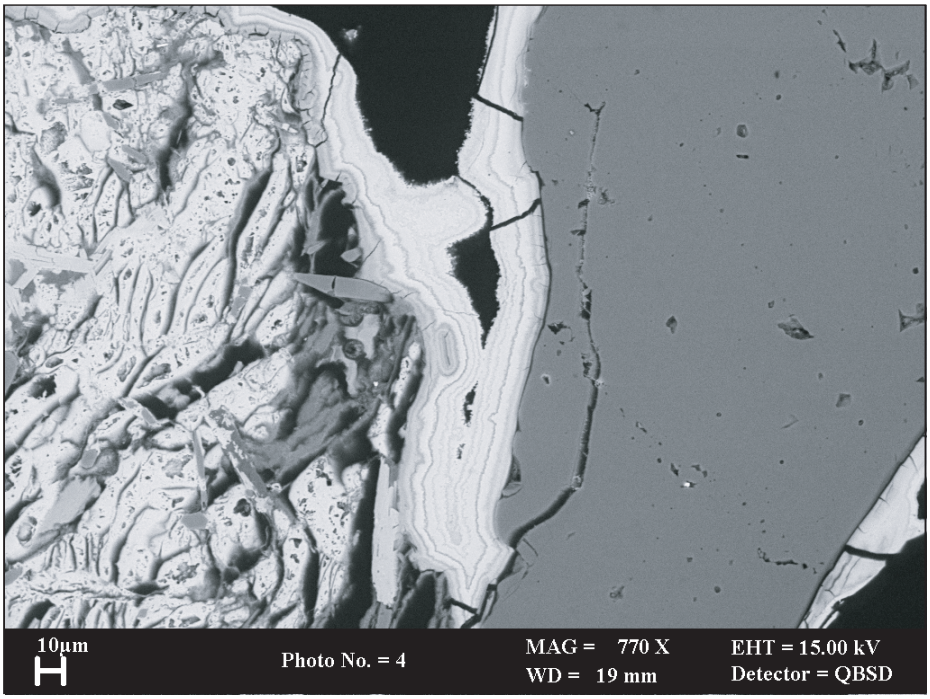

Figure 27 EDXA spectrum of low arsenic iron oxide coating on grain surfaces. Sample MPS 91.

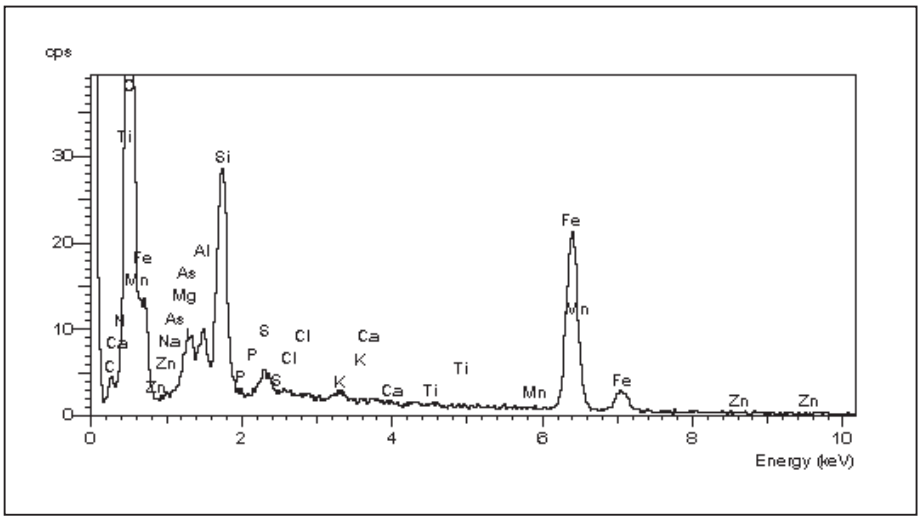

Figure 28 Figure 3. EDXA spectrum of arsenic rich iron oxyhydroxide alteration product directly replacing altered arsenopyrite grains. Sample MPS 91.

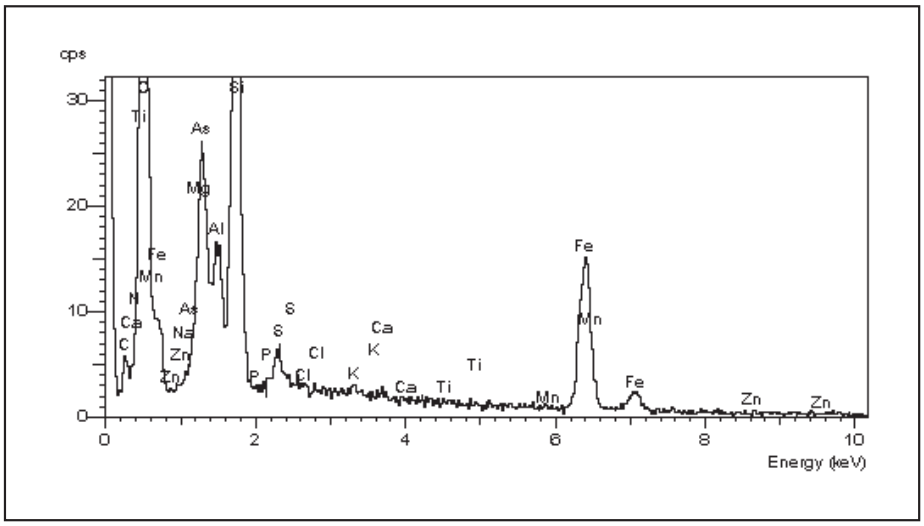

Figure 29 EDXA spectrum of very arsenic rich iron oxyhydroxide forming thin grain coatings on pore surfaces immediately adjacent to altered arsenopyrite grains. Sample MPS 91.

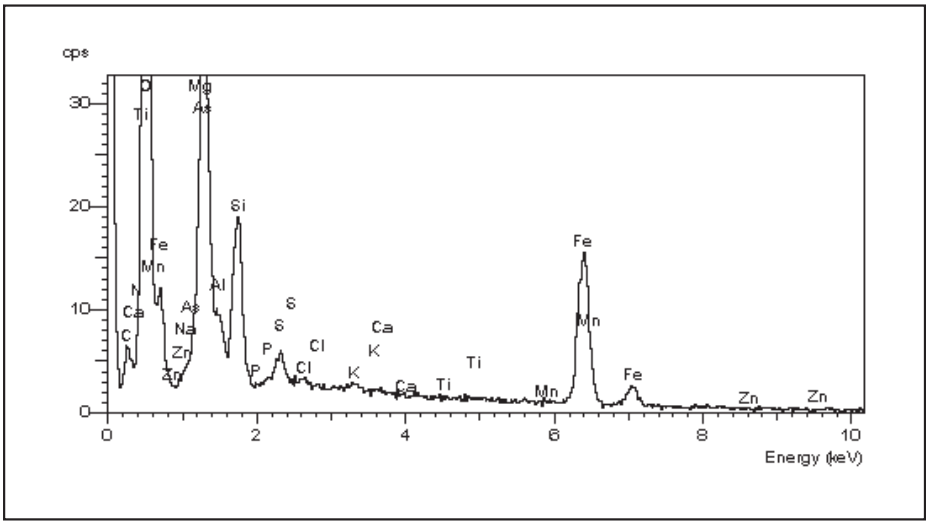

Figure 30 BSEM image showing pedified soil fabric, comprising rounded sand-sized peds of aggregated silt and clay grade quartz, chlorite, quartz, kaolinite, with scattered coarser quartz and rock fragments. MPS 96 Soil, B Horizon.

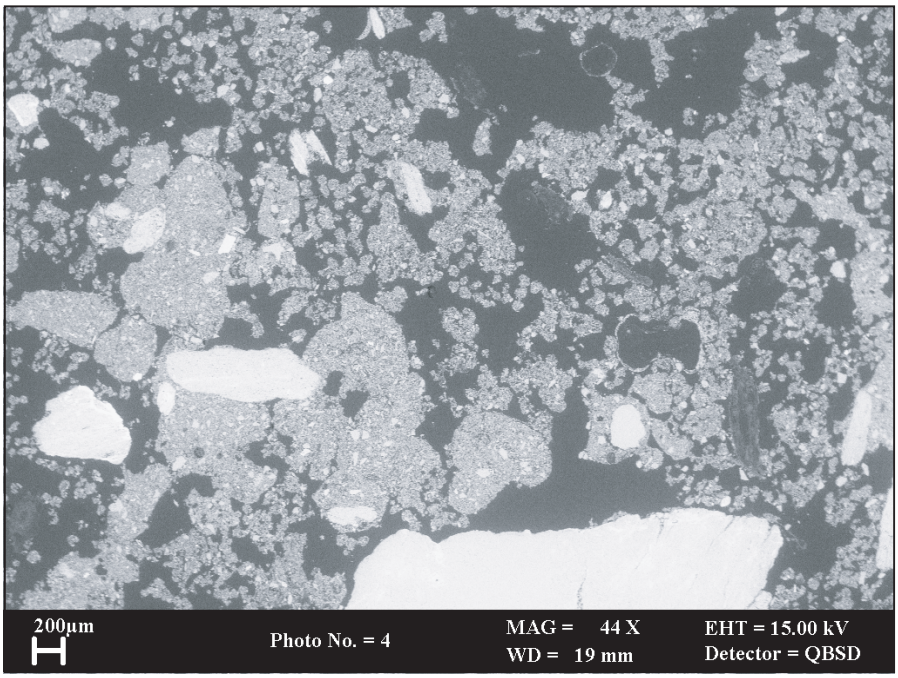

Figure 31 BSEM image showing rare fragment of hematite-replaced illitic rock. MPS 96 Soil B Horizon.

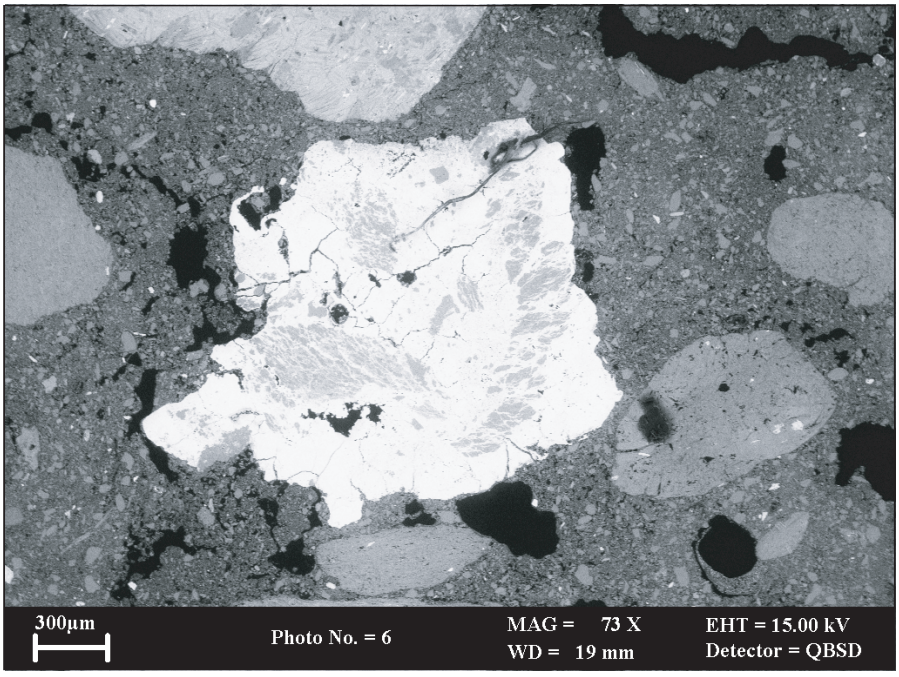

8 Vegetables

Arsenic concentrations from vegetables grown in the garden of a local dwelling, Wheal Josiah Cottage, are reported in Table 4. The UK statutory limit of 1 mg kg^{-1} (fresh weight) in food (MAFF, 1982) is exceeded in the beetroot, tomato, celery and lettuce samples. The results show how lettuce and celery tend to accumulate a higher concentration than fruits. This feature has previously been described by other authors, i.e. Farago et al. (1997), Kabata-Pendias (2000), Thoresby and Thornton (1979), Xu and Thornton (1985). Arsenic also appears to accumulate in rhubarb leaves. These results reaffirm and support the concern raised by Farago et al. (1997) over the possibility of high human intake of As due to consumption of locally grown food in south-west England.

Table 4 As concentrations in vegetables from soils at Devon Great Consols.

Sample	As mg kg^{-1} (fresh weight)
Beetroot	8.5
Tomatoes	7.18
Celery	15.5
Lettuce	22.3
Rhubarb	0.07
Rhubarb leaf	0.29

9 Surface water geochemistry

The chemical analyses of water samples are summarised in Table 5. Tailings pond waters (DC1-DC5-DC8) are generally acid with a pH range of 5.17–5.71. Water samples taken from the outlets of two tailings ponds at the western end of the mine site show more alkaline values of pH (7.3–7.4). Weakly acid to alkaline values of pH (6.5–7.5) are found in the settling pond (DC11) and stream (DC12) in the eastern part of the mine. Seepage samples (DC3–DC6) show a pH range 5.2–6.1. The most acid waters with a pH of 3.5 occur at an adit discharge (DC7) and in a leat (DC13) where ochre precipitates are particularly evident on the stream bed.

The redox potential (Eh) was measured in the range 209–718 mV (Table 5), the highest value recorded was in the leat with iron precipitates (DC13). High Eh values (400–600 mV) prevail in most waters. Lower redox potential (209 mV) characterises the seepage (DC6) over a clayey outcrop close to the As works.

Table 5 Chemical analysis of waters.

Sample	Description	T	Eh	HCO3	Cond.	pH	Ca	Mg	Na	K	Cl	SO4	NO3	Br	F
		°C	mV	mg l^{-1}	µScm^{-1}						mg l^{-1}				
DC1	Tailings pond	11.3	599	3.3	173	5.71	30.6	4.4	8.1	1.7	15.0	103.0	2.7	0.1	8.4
DC2	Tailings pond	11.1	573	26.4	133	7.33	17.2	3.1	9.3	3.2	35.6	28.8	31.9	0.1	0.6
DC3	Seepage	10.5	601	2.0	111	6.11	12.9	3.3	11.2	2.1	21.3	34.5	9.5	0.1	1.3
DC4	Tailings pond	11.2	557	22.8	132	7.40	16.5	3.0	9.6	4.1	18.9	15.8	15.2	0.1	0.7
DC5	Tailings pond	9.2	333	1.6	65	5.17	5.1	1.1	7.5	0.7	13.6	14.6	0.5	0.0	3.8
DC5R	Tailings pond	17.6	463	4.6	216	5.61	6.0	1.2	4.9	2.2	6.3	15.8	0.1	0.0	6.2
DC6	Seepage	9.5	209	0.8	76	5.20	9.3	1.1	6.7	1.2	12.5	18.8	1.1	0.0	3.6
DC7	Adit discharge	11.5	657	0.0	519	3.50	54.8	8.2	8.9	0.8	15.8	261.0	2.6	0.1	31.9
DC7R	Adit discharge	16.3	616	0.0	1058	3.82	114.6	15.9	8.6	1.1	14.8	516.0	0.8	0.0	67.4
DC8	Tailings pond	9.6	377	0.8	50.6	5.33	4.3	0.6	5.4	0.5	9.3	8.0	0.1	0.0	1.8
DC9	Borehole	10.8	380	6.9	138	5.87	6.8	8.0	12.0	1.6	20.9	34.2	11.1	0.1	0.2
DC11	Pond	11.0	428	6.9	178	6.56	15.9	4.3	8.3	3.8	16.4	41.1	18.1	0.1	0.2
DC12	Stream	11.2	370	34.2	156	7.48	19.8	3.6	9.8	6.9	18.1	16.5	21.9	0.1	0.1
DC13	Leat	17.1	718	0.0	440	3.52	18.4	10.4	15.9	2.6	22.5	135.0	3.6	0.1	3.2
DC14	Leat	13.2	437	92.5	209	7.30	19.6	3.2	10.9	2.8	19.2	10.2	14.6	0.1	0.1

Sample		TOC	TIC	Tot P	Tot S	Si	SiO2	Ba	Sr	Mn	Fe t	Fe(II)	Fe(III)	Al
								mg l -1						
DC1		<1.00	0.95	<0.04	33.4	5.06	10.82	0.006	0.04	0.37	0.01	0.02	<0.01	4.12
DC2		1.01	6.48	<0.04	5.18	1.41	3.02	0.003	0.03	0.04	0.02	<0.02	0.02	0.10
DC3		<1.00	1.59	<0.04	11.0	2.93	6.26	0.002	0.02	0.14	0.01	<0.02	0.01	0.79
DC4		1.28	6.16	<0.04	5.00	1.41	3.01	0.003	0.03	0.04	0.05	0.02	0.03	0.18
DC5		1.37	0.59	<0.04	4.91	1.35	2.88	0.002	0.01	0.20	0.09	0.06	0.03	1.49
DC5R		4.00	<0.50	<0.04	5.63	0.81	1.73	<0.002	0.01	0.36	0.09	0.07	0.02	2.01
DC6		<1.00	<0.50	<0.04	6.30	6.93	14.8	0.002	0.01	0.05	0.01	<0.02	0.01	1.49
DC7	as above	<1.00	0.56	<0.12	93.0	11.6	24.7	0.005	0.03	2.46	1.37	0.28	1.09	23.58
DC7R		4.20	<0.50	0.05	172	15.6	33.5	0.006	0.04	5.22	2.69	1.39	1.31	47.87
DC8		<1.00	<0.50	<0.04	2.74	0.70	1.51	<0.001	0.00	0.01	0.02	0.03	<0.01	0.32
DC9		<1.00	4.68	<0.04	10.69	2.31	4.93	0.004	0.03	0.01	0.02	<0.02	0.02	0.04
DC11		<1.00	3.07	<0.04	12.9	3.08	6.59	0.006	0.03	0.17	0.01	<0.02	0.01	0.60
DC12		2.16	7.35	0.22	5.40	1.80	3.84	0.005	0.04	0.06	0.17	0.02	0.15	0.23
DC13		<1.00	0.52	<0.04	43.45	10.17	21.76	<0.002	0.03	2.33	0.23	0.12	0.12	4.74
DC14		3.85	9.43	0.04	3.93	1.66	3.55	0.00	0.04	0.00	0.15	0.16	<0.01	<0.02

Sample		Co	Ni	Cu	Zn	Cr	Mo	Cd	Pb	V	Li	B	As	As III	As V
									mg l -1						
DC1		24	28	3306	474	<0.5	0	2	0	<0.1	43	41	40	24	15
DC2		2	3	167	24	<0.5	1	0	<0.1	0	3	20	12	7	4
DC3		8	7	683	41	<0.5	0	0	1	<0.1	20	<20	3	1	2
DC4		3	3	184	24	<0.5	0	0	0	0	4	<20	22	13	8
DC5		7	6	518	95	<0.5	<0.1	0	0	0	6	<20	163	142	21
DC5R		<14	<16	176	55	<13	<11	<6	<40	<8	19	21	613	480	133
DC6		2	4	53	24	<0.5	0	0	0	1	13	21	6577	5831	746
DC7	as above	119	82	22530	949	1	<0.1	3	1	<0.1	160	93	19	10	9
DC7R		263	204	26037	1824	14	25	10	90	<8	457	144	90	73	17
DC8		1	2	140	25	<0.5	0	0	<0.1	0	2	<20	360	316	45
DC9		1	10	5	73	<0.5	<0.1	0	0	<0.1	22	25	2	2	0
DC11		18	33	1068	1052	5	<0.1	1	0	<0.1	25	26	21	18	3
DC12		4	8	191	249	1	<0.1	0	0	0	5	<20	13	11	1
DC13		75	98	430	1357	<13	<11	<6	<40	<8	275	506	15	12	3
DC14		<14	<16	4	<2	<13	<11	<6	<40	<8	<3	22	22	18	4

R = October sampling

The principal anions in the surface waters, HCO_3, SO_4 and Cl were recorded at concentrations of 0.0–42 mg l^{-1}, 8–516 mg l^{-1} and 9.3–35.6 mg l^{-1}, respectively. The adit discharge (DC7), the tailings pond (DC1) and the leat with ochre precipitates (DC13) are SO_4-dominated.

Lower As contents in DC5R and DC7R in relation to DC5 and DC7 are associated with the wet season sampling (December sampling), likely because of the dilution effect of long periods of rainfall.

The dominant cation is Ca. The minor and trace element content is variable. Manganese concentration ranges from 0.004 to 5.22 mg l^{-1}, Fe 0.008–2.69 mg l^{-1}, Al 0.097–47.9 mg l^{-1}, Co 1–262 µg l^{-1}, Ni 2–203 µg l^{-1}, Cu 53–26037 µg l^{-1}, Zn 24–1823 µg l^{-1}, Cd 0.03–9.6 µg l^{-1}, Pb <0.10–90 µg l^{-1}, As 3–6577 µg l^{-1} and F 0.1–67 µg l^{-1}.

The highest As concentration of 6577 µg l^{-1} occurs in the seepage DC6 from the clayey outcrops consisting mainly of ash material (MPS 90). High As values are registered in the acid tailings ponds (DC1-DC5-DC8), while lower values are found in the more alkaline tailings ponds. The leat water with ochre precipitates (DC13) and the adit discharge (DC7), both acid waters with high Eh, are characterised by relatively low As values but are enriched in Cu and Zn (22 530 µg l^{-1} and 948 µg l^{-1}, respectively).

Sample DC9, which represents water from a deep borehole at a local residence, has a pH value of 5.9 and As at 2 µg l^{-1}.

No general correlation between pH and As concentrations in waters is observed.

10 Acid mine drainage precipitates

Iron rich ochre precipitates are often associated with mine drainage. Several studies have shown the importance of metal adsorption by iron oxyhydroxide ochres in limiting toxic element discharge from mine workings (Bowel and Bruce, 1995; Fuge et al., 1994; Rose and Ghazi, 1997; Singh et al., 1999; Webster et al., 1998). Mineral and trace element characterisation of an iron-rich precipitate, MPS 71, collected from the leat at [SX 433 731], was accomplished by XRD and ICP chemical analysis.

XRD analysis shows a broad peak at 2.54 Å in the diffraction spectrum (CoKa radiation), characteristic of poorly ordered iron hydroxides.

Chemical analyses indicate that these acid mine drainage precipitates are composed of 410 800 mg kg^{-1} of Fe, 62 700 mg kg^{-1} of As and 26 968 mg kg^{-1} of S and minor quantities of Al, P and Ca. Concentrations of Zn, Cu, Pb and Ni are very low. The pH is acid (2.97) and the CEC 73.5 meq 100 g^{-1}.

In order to define the distribution of elements between water and precipitates, the enrichment factor defined as $EF= (X)_s/(X)_l$, where $(X)_s$ is the concentration of the element in the precipitate and $(X)_l$ the concentration of the element in water, has been calculated. The EFs for As and Fe indicate that the concentration of these elements in the accumulated ochre precipitates is 6 to 7 orders of magnitude higher than those measured in water (DC13) at the same site.

Bigham et al. (1996) suggest that it is possible to use chemical analysis to estimate the mineralogical composition for ochre precipitates from acid mine drainage. Accordingly, the observed molar ratio Fe/S of 8.74 could indicate the presence of schwertmannite $Fe_8O_8(OH)_x(SO_4)_y$ (ratio typically ranges between 4.6 and 8). The relatively higher value could be a result of the presence of trace amounts of goethite with adsorbed sulphate. The pH of DC13 water of 3.52 is ideal for schwertmannite precipitation. Schwertmannite like ferrihydrite is metastable and ultimately converts to goethite via the overall reaction:

$$Fe_8O_8(OH)_{5.5}(SO_4)_{1.25} + 2.5\ H_2O = 8FeOOH + 2.5\ H^+ + 1.25\ SO_4^{-2}.$$

10.1 MODELLING ARSENIC SORPTION ON IRON PRECIPITATES

Arsenic concentrations in waters are not correlated to water pH. In particular DC7 and DC13 (pH 3.5) are relatively low in As. This seems to suggest that As presence in waters is not exclusively a function of sulphide mineral oxidation and generation of acid mine drainage, but also may depend on the removal of As by oxidation of Fe^{2+} to Fe^{3+} and subsequent precipitation of Fe and As in Fe oxy-hydroxides as ochre.

The geochemical model PHREEQC (Parkhurst, 1995) with the WATEQ4F (Ball and Nordstrom, 1991) thermodynamic database was used to evaluate adsorption to precipitated iron oxy-hydroxides as a control mechanism on dissolved As concentration. For modelling purposes the concentration of hydrous ferric oxides (HFO) present as the sorbing phase was arbitrarily fixed at 0.09 g. The hydrous ferric oxide properties are those described by Dzombak and Morel (1990) and HFO is the sole sorbing material in the computer-model simulation. The pH was set at incremental values from 3 to 6.5 and P_{CO2} and P_{O2} were fixed at atmospheric concentrations ($10^{-3.52}$ atm and $10^{-0.68}$ atm, respectively). Figure 32 shows adsorption of As, Cu and Zn on HFO modelled as a function of pH. Most of the As is predicted to be adsorbed over the studied pH range, less than 1% of Cu and Zn are predicted to be retained by HFO at pH 3.5 but sorption increases at pH>5. Hence, dissolved Cu and Zn would be expected to be mobile at these sites (DC7 and DC13) and dissolved As strongly attenuated if iron oxy-hydroxides are available in the bed sediments or as suspended particulates.

The modelling results could explain the different EF values for As and Cu and Zn of the analysed ochre precipitates and the observed relatively low As values in DC7 and DC13 waters.

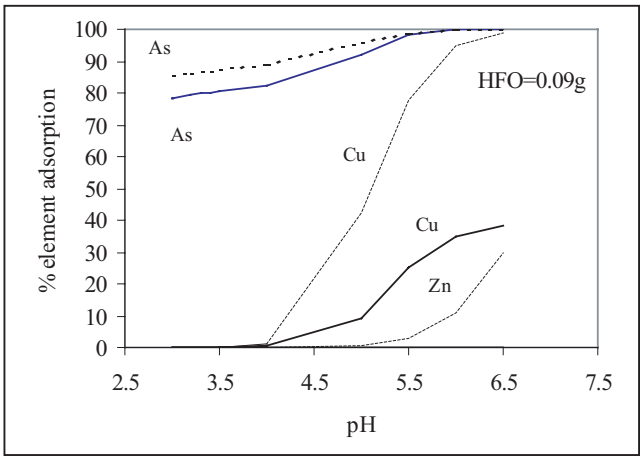

Figure 32 Computer model simulation showing the percentage of As, Cu and Zn adsorption onto hydrous ferric oxide as a function of pH for DC7 and DC13 at atmospheric P_{CO2} and P_{O2}. Solid line: DC7, dashed line: DC13.

11 Arsenic bioaccessibility

In Figure 33 the distribution of bioaccessible As (PBET As mg kg^{-1}) is summarised for tailings, soils from Devon Great Consols, soils surrounding the mine, background soils from Bere Alston and soils from Higher Todsworthy Farm. The median values of bioaccessible As for the tailings and the soils in the mine are 845 mg kg^{-1} and 408 mg kg^{-1}, respectively (Table 6). Bioaccessible As in the soils sampled from the fields surrounding DGC is 189 mg kg^{-1} (median). Much lower median values of bioaccessible As are measured for the background soils in Bere Alston and the soils over mineralisation from Higher Todsworthy Farm (PBET As: 7 mg kg^{-1} and 14 mg kg^{-1}, respectively).

Using the bioaccessible concentration of As in soils gives a more realistic indication of areas that are likely to pose an unacceptable risk to human health. Samples with bioaccessible concentrations above the soil guideline values (SGV) for a certain land use indicate areas of greatest potential risk. Accordingly, the soils from Bere Alston and Higher Todsworthy Farm are close to or above the 20 mg $kg^{(-1)}$ DEFRA-EA SGV (DEFRA, 2002) for residential gardens and allotments. The values for the soils in the mine area, the surroundings of the mine and the mine tailings are well above any threshold concentrations. In particular, high concentrations up to 624 mg kg^{-1} of bioaccessible As measured in residential gardens and farm fields around the mine highlight areas at highest risk in terms of source to receptor transfer.

The distribution of As relative bioaccessibility data (PBET As as % Astot) is shown in Figure 34 and the summary statistics reported in Table 7. Arsenic relative bioaccessibility data for tailings are spread, with a long upper tail and the median value of 5.05%. An outside value is indicated (PBET As of 61%) and identified as sample MPS 15, a soil mixed with waste rock in Devon Great Consols (DGC). The values for DGC soils are distributed more symmetrically and show a median value of 15% and a range from 0.54% to 42%. A relative As bioaccessibility of 13% is found in the soils surrounding the mine (median value). PBET data for the background soils and Todsworthy Farm soils show a distribution falling within the spread of data for DGC soils and have median values of 9.95% and 9.13%, respectively.

11.1 RELATIONSHIP OF TOTAL ARSENIC AND BIOACCESSIBLE ARSENIC WITH OTHER PHYSICO-CHEMICAL SOIL PARAMETERS

The chemical and physical data obtained from the soils within the mine area have been analysed using a combination of statistical methods and data processing to identify factors, clusters or patterns, which may be of interest for interpreting relationships and prediction.

Total As concentrations in DGC soils span two orders of magnitude, with a number of outliers suggesting that the As data are derived from more than one population of samples. By using k-means clustering of the soil physico-chemical variables the soils have been grouped into 4 clusters as summarised in Table 8. Figure 35 shows the calculated centroids of each observation cluster. Clusters 1 and 2 group the soils characterised by low As concentration. Cluster 4 contains soils with very high concentrations of As, Fe and S. Cluster 3 has intermediate As values.

The spatial plotting of the clusters locates cluster 4 around the As works area, identifying clearly the area of major pollution (Figure 36). Cluster 2 is distributed in the eastern part of the mine area, while cluster 1 occupies the western and south-eastern part of the mine area. Cluster 3 is slightly more concentrated in the north-western boundary of the mine.

Figure 37 shows how the relationship between total As and relative bioaccessibility of As varies for the four clusters. Cluster 1 and cluster 2 have similar total As but cluster 2 has higher relative bioaccessibility. Cluster 3 has similar bioaccessibility to cluster 1 but has a higher As content. Finally, cluster 4 has the highest As content and the lowest relative bioaccessibility. It is plausible to assume that these differences in relative bioaccessibility are related to the different structural states of the host mineral phases.

An attempt to discern the possible factors affecting the different bioaccessibility observed in cluster 1 and 2, total As content remaining similar, is done by analysing the correlation matrix for these clusters (Table 9 and Table 10). A correlation matrix could not be produced for clusters 3 and 4 since they contained insufficient sample numbers. For cluster 1 total As is correlated to Fe and S, suggesting a source such as arsenopyrite where one would expect the As to be less freely available and 'locked up' in the crystal structure. In cluster 2 As is more bioaccessible and correlated with Fe (with a level of significance $\alpha = 0.05$) but not with S, possibly implying sorption to an iron oxyhydroxide phase with weaker binding sites compared to arsenopyrite.

Multiple Linear Regression (MLR) is used to further analyse the relationship between the bioaccessible As content of the soil and other soil parameters for cluster 1 and cluster 2. The total element content, pH and organic matter were used as predictor variables and the two models' coefficients and related statistics are summarised in Table 11 and Table 12.

For cluster 1, 91.8% of the variance in the bioaccessible As is modelled using the total As and the total iron content. Total As has a positive coefficient and iron has a negative coefficient. This suggests that there is a portion of As bound to an iron-rich source that holds As in a non-bioaccessible form such as arsenopyrite. For cluster 2, 93.8% of the variance is modelled entirely by the total As content.

These findings complement the inferences made from the correlation matrices, suggesting the presence of at least two different sources of As in the clusters, an iron sulphide contribution in cluster 1 and an iron oxide source in cluster 2 affecting the observed differences in relative bioaccessibility of As. This is in agreement with Ruby et al. (1996) who found that for constant soil particle size As in Fe sulphides and As dispersed in slag have a lower relative bioavailability than Fe-As oxides and Mn-As oxides.

Table 6 Summary statistics for bioaccessible As data (mg kg^{-1}).

	Tailings	DGC soils	Outside DGC soils	Background soils	Todsworthy Farm soils
Min	91	12	25	7	11.1
1st Qu.	564	114	128	7	13.5
Mean	1947.5	783	300	8.4	15.7
Median	845	407.5	189	7	14.4
3rd Qu.	1314.5	1343	372	10	16.6
Max	13290	2744	934	11	26.6
Total N	20	73	10	5	20
Std Dev.	3156.73	808.73	287.46	1.95	3.54
Skewness	3.02	0.95	1.39	0.76	1.80

Table 7 Summary Statistics for relative arsenic bioaccessibility data (% Astot).

	Tailings	DGC soils	Outside DGC soils	Background soils	Todsworthy Farm soils
Min	0.89	0.54	3.8	6.01	7.37
1st Qu.	2.88	9.01	9.53	8.30	8.26
Mean	11.14	15.89	13.99	10.84	9.86
Median	5.06	15.09	13.00	9.95	9.14
3rd Qu.	15.79	21.01	19.23	13.59	10.57
Max	61.15	42.03	25	16.57	16.74
Total N	20	73	10	5	20
Std Dev.	14.61	8.83	6.96	4.04	2.40
Skewness	2.42	0.63	0.37	0.48	1.59

Table 8 Clusters of DGC soils obtained by k-means clustering of the soil physico-chemical variables.

	Cluster 1	Cluster 2	Cluster 3	Cluster 4
Size	**21**	**29**	**15**	**8**
	MPS3	MPS1	MPS2	MPS6
	MPS21	MPS4	MPS17	MPS8
	MPS29	MPS5	MPS32	MPS31
	MPS30	MPS7	MPS34	MPS56
	MPS39	MPS9	MPS35	MPS62
	MPS40	MPS10	MPS38	MPS63
	MPS41	MPS11	MPS42	MPS74
	MPS44	MPS12	MPS50	MPS75
	MPS45	MPS13	MPS66	
	MPS46	MPS18	MPS68	
	MPS47	MPS19	MPS70	
	MPS48	MPS20	MPS78	
	MPS49	MPS22	MPS79	
	MPS52	MPS26	MPS80	
	MPS53	MPS27	MPS81	
	MPS57	MPS28		
	MPS58	MPS33		
	MPS59	MPS51		
	MPS60	MPS65		
	MPS61	MPS67		
	MPS64	MPS69		
		MPS72		
		MPS76		
		MPS77		
		MPS82		
		MPS93		
		MPS94		
		MPS95		
		MPS96		

Table 9 Correlation matrix for Cluster 1 of DGC soil samples.

pbet	As	RBA	Al	As	Ba	Ca	Fe	K	Mn	Mg	Na	P	S	Sr	OM	CEC	pH
Pbet As	1.00																
RBA	0.02	1.00															
Al	**0.72**	-0.06	1.00														
As	**0.95**	-0.20	**0.75**	1.00													
Ba	**0.74**	-0.12	**0.84**	**0.78**	1.00												
Ca	**0.82**	-0.31	**0.64**	**0.89**	**0.67**	1.00											
Fe	**0.90**	-0.33	**0.76**	**0.98**	**0.77**	**0.89**	1.00										
K	**0.84**	-0.20	**0.86**	**0.91**	**0.92**	**0.80**	**0.92**	1.00									
Mn	-0.15	-0.32	-0.08	-0.09	0.11	-0.09	-0.05	0.02	1.00								
Mg	0.19	-0.49	0.43	0.27	0.33	0.41	0.40	0.41	0.19	1.00							
Na	0.27	0.13	0.28	0.23	0.24	0.23	0.23	0.23	-0.37	0.10	1.00						
P	0.25	-0.10	0.09	0.32	0.17	0.47	0.36	0.27	-0.03	0.28	0.50	1.00					
S	**0.85**	-0.34	**0.67**	**0.96**	**0.72**	**0.93**	**0.96**	**0.88**	-0.02	0.34	0.18	0.46	1.00				
Sr	**0.88**	-0.20	**0.66**	**0.91**	**0.67**	**0.90**	**0.90**	**0.83**	-0.11	0.35	0.40	0.46	**0.91**	1.00			
OM %	-0.24	0.08	-0.32	-0.18	-0.41	-0.30	-0.18	-0.27	0.15	-0.33	-0.30	0.16	-0.17	-0.26	1.00		
CEC	-0.33	0.11	-0.49	-0.30	-0.37	-0.09	-0.35	-0.34	0.08	-0.21	-0.29	0.31	-0.17	-0.22	0.50	1.00	
pH	-0.13	-0.37	-0.31	-0.10	-0.08	0.26	-0.09	-0.17	0.10	0.21	-0.15	0.14	0.03	-0.01	-0.36	0.28	1.00

In bold, significant values (except diagonal) at the level of significance alpha=0.010 (Two-tailed test)

Table 10 Correlation matrix for Cluster 2 of DGC soil samples.

pbet	As	RBA	Al	As	Ba	Ca	Fe	K	Mn	Mg	Na	P	S	Sr	OM	CEC	pH
Pbet As	1.00																
RBA	**0.70**	1.00															
Al	-0.24	-0.40	1.00														
As	**0.94**	0.45	-0.18	1.00													
Ba	0.11	-0.18	**0.75**	0.20	1.00												
Ca	0.43	0.05	-0.47	**0.57**	-0.15	1.00											
Fe	0.39	0.00	0.39	0.47	**0.67**	0.27	1.00										
K	-0.16	-0.41	**0.74**	-0.07	**0.90**	-0.23	0.46	1.00									
Mn	0.08	-0.18	0.35	0.20	0.21	0.25	0.26	0.09	1.00								
Mg	-0.15	-0.51	0.11	-0.01	-0.02	0.40	0.21	0.15	0.27	1.00							
Na	-0.05	-0.06	0.18	-0.07	-0.07	0.06	0.18	-0.13	0.29	0.50	1.00						
P	0.21	-0.11	-0.16	0.29	-0.05	**0.60**	0.26	-0.08	0.19	0.40	0.06	1.00					
S	-0.03	0.07	**-0.55**	-0.06	-0.51	0.33	-0.52	-0.37	-0.10	0.15	-0.08	0.36	1.00				
Sr	-0.13	0.04	0.19	-0.19	0.30	-0.16	0.20	0.42	-0.41	0.11	-0.14	0.07	-0.10	1.00			
OM %	0.06	0.31	**-0.63**	-0.02	**-0.63**	0.29	**-0.56**	**-0.61**	-0.21	-0.14	-0.24	0.38	**0.65**	0.05	1.00		
CEC	-0.14	0.16	**-0.60**	-0.25	**-0.73**	0.05	**-0.75**	**-0.58**	-0.33	-0.12	-0.18	0.24	**0.63**	0.03	**0.89**	1.00	
pH	0.29	-0.25	0.34	0.48	0.47	0.46	**0.79**	0.30	0.53	0.42	0.23	0.36	-0.44	-0.17	-0.53	**-0.73**	1.00

1.00In bold, significant values (except diagonal) at the level of significance alpha=0.010 (Two-tailed test)

Table 11 Multiple linear regression parameters for the Cluster 1.

Regression parameters and corresponding statistics:
Determination coefficient r2: 0.9176

	Value	**Std dev.**	**Student's t**	**Corresponding probability**	**Lower 95% bound**	**Upper 95% bound**
Intercept	457.0897	112.5492	4.0612	0.0008	219.6312	694.5481
As	0.142016	0.0122	11.6360	0.0001	0.1163	0.1678
Fe	-0.00957	0.0024	-3.9170	0.0011	-0.0147	-0.0044

The equation of the model is: Y = 457.089655859201 + 0.142015826141954*X1 -9.57258850987285E-03*X2

Table 12 Multiple linear regression parameters for the Cluster 2.

Regression parameters and corresponding statistics:
Determination coefficient r2: 0.9378

	Value	Std dev.	Student's t	Corresponding probability	Lower 95% bound	Upper 95% bound
Intercept	-135.736	39.6144	-3.4264	0.0020	-217.0176	-54.4537
As	0.349743	0.0173	20.1831	0.0001	0.3142	0.3853

The equation of the model is: Y = -135.735665125456 + 0.349743018650286*X1

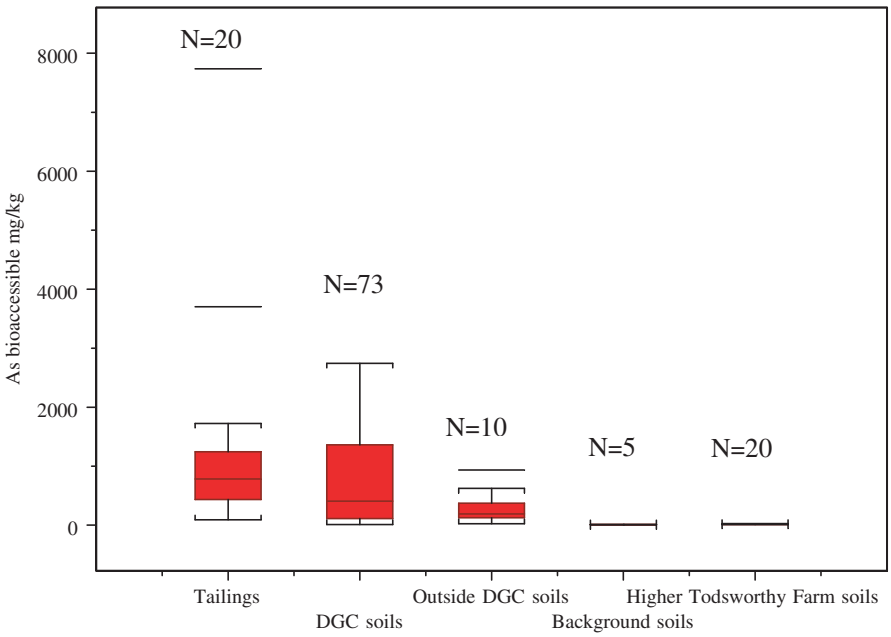

Figure 33 Box plot of bioaccessible As data (mg kg^{-1}).

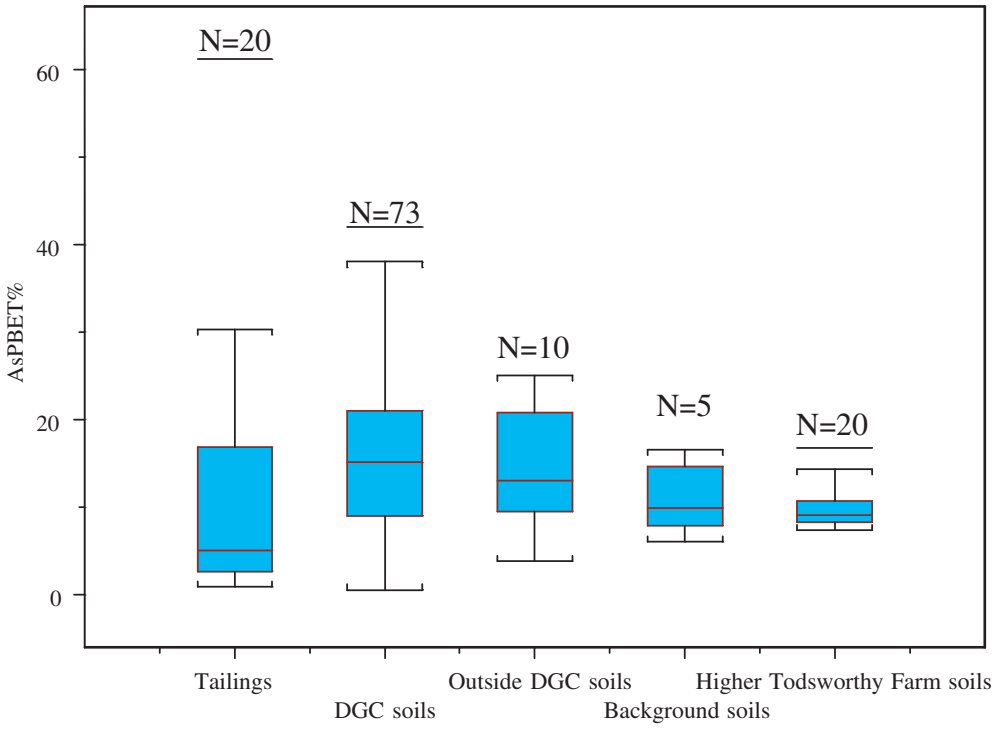

Figure 34 Box plot of relative As bioaccessibility (% Astot).

Figure 35 Calculated centroids for the physico-chemical variables around which each observation clusters.

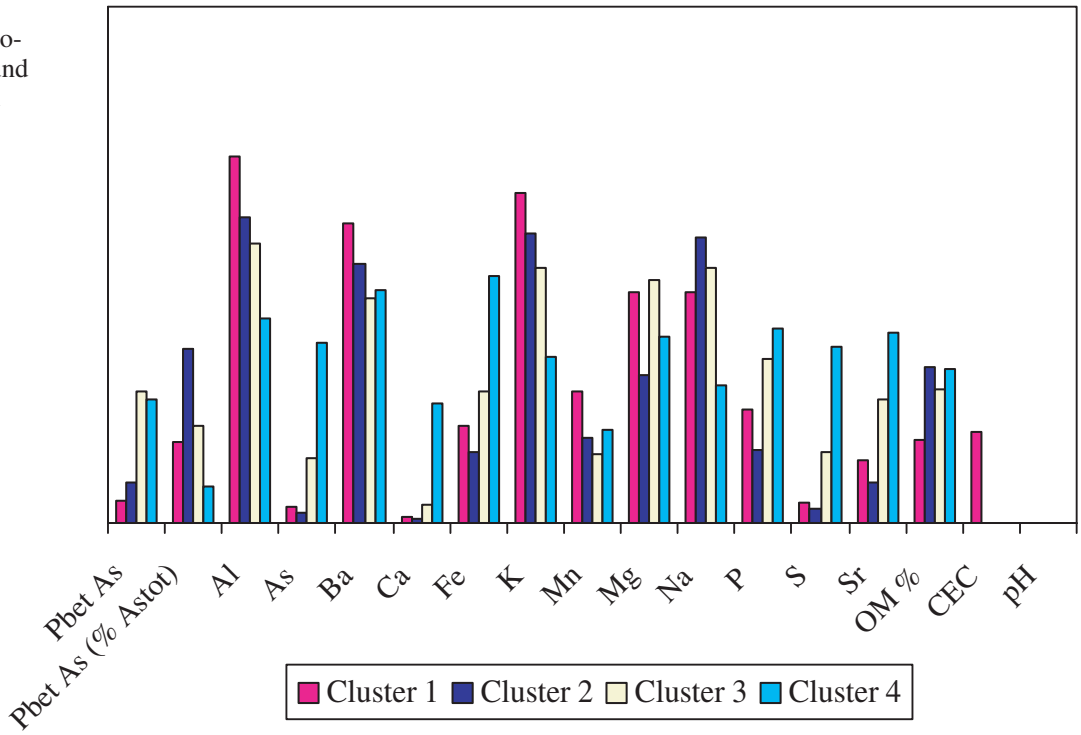

Figure 36 Map showing the spatial distribution of the clusters of soils identified by k-mean clustering.

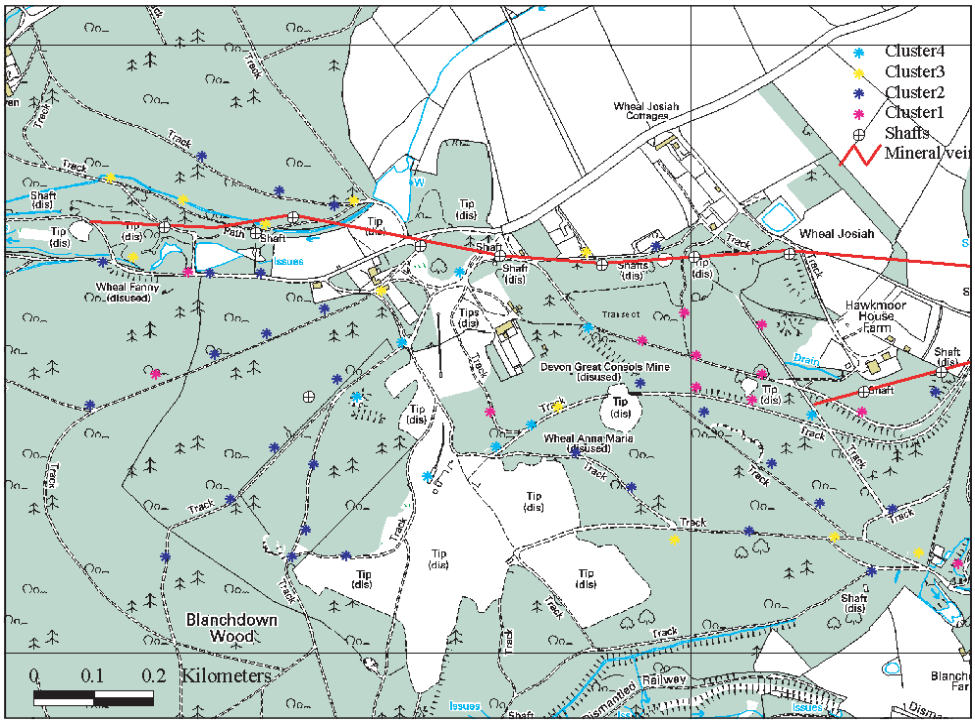

Figure 37 Relationship between the relative bioaccessibility of As and the total As in the four identified clusters in DGC soils.

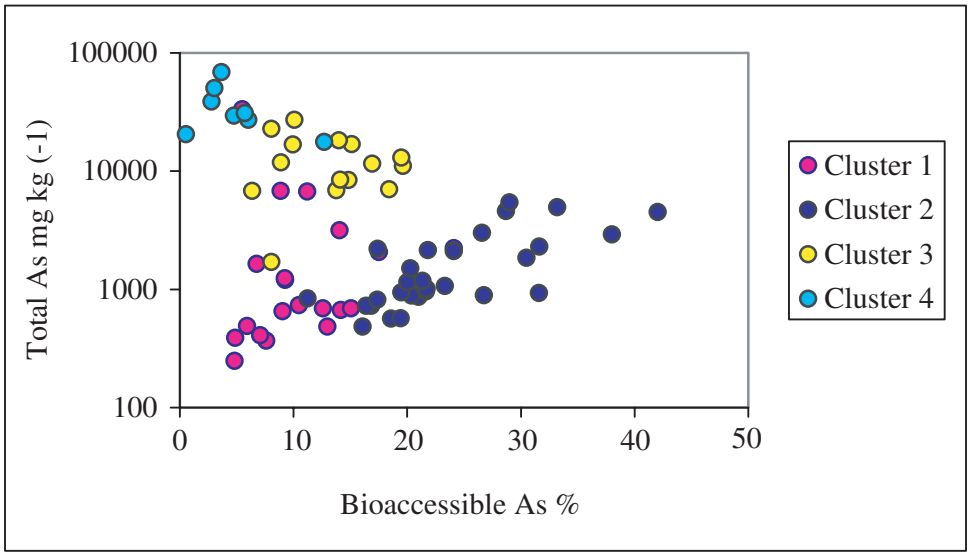

12 Arsenic speciation in solids by chemical extraction techniques

Sequential extraction data have been used to help elucidate the nature of the As hosts in the different soil types and mine spoil and to understand which of these is responsible for the mobile bioaccessible fraction. Arsenic recovery at the end of the sequential leaching was in the range of 39–92% of the total As content in soils and 32–96% of the total As content in tailings and waste rocks, with the lowest recovery in the ash materials (MPS 90 and MPS 73) and the ochre precipitates (e.g. MPS 71). Iron was extracted from 16% to 61% of the total Fe content in soils and from 12% to 100% in tailings and waste rocks. Most of the Al was not leachable (0.11–20% extracted) with the exception of MPS 73 (ash material), where 60% of the Al was extracted. Calcium was readily leached in both soils and tailings/wastes except for some tailings samples (MPS43-MPM1-MPM4) that are characterised by Ca extracted <30% total Ca.

In order to identify the solid phase partitioning of As the data were subjected to the chemometric data-processing procedure (Cave et al., 2004) as described in the analytical methods. The chemometric data-processing methodology is based on the assumption that the material is made of a mixture of discrete physico-chemical components characterised by distinct element composition. Tentative assignments are done based on their composition and order of extraction and aided by the mineralogical analysis and SEM observations.

The composition of each of the resolved components is reported in element % together with the extraction profile in mg kg^{-1} of each component for each extraction stage.

In all samples the physico-chemical component which makes up the most significant percentage of the total extract contains mainly Fe, As and S in variable proportion, but with iron always predominant (Figure 38). This component is extracted over the range 0.5M–5M HNO_3 (step 9 to 14) with more defined windows of extraction at 0.5M and 5M HNO_3.

Figure 38 also plots the composition of the Fe-As-S component resolved from the sequential leaching data relative to the arsenopyrite reference material. It is evident that the elements Fe, As and S in soils and tailings are associated in different proportion compared to the sulphide and the results suggest that As has been sequestered into secondary mineral phases, strongly depleted in sulphur. The Fe-As-S component of the acid mine drainage precipitates, consisting of a mixture of poorly crystalline components, identified by XRD possibly as a mixture of schwertmannite and goethite, has a composition similar to that of the soils and tailings samples.

The results for a selection of samples are discussed in the following paragraphs.

12.1 IRON SULPHIDE AND HEMATITE REFERENCE MATERIAL

The heavy mineral fraction of an arsenopyrite rich waste rock sample (MPR2 He), collected from the site, and a sample of synthetic hematite were processed with the soils and tailings to provide reference extraction profiles (Figure 39 and Figure 40). In the iron sulphide reference material (MPR2 He) two components, made up predominantly of iron and sulphur (45% Fe and 54% S), represent most of the total extracted solid and are leached at the last steps 13–14 with 5M HNO3. In these components 0.6% As is present. The element is more abundant in a component always dominated by iron and sulphur but with a more diffuse window of extraction from step 8 to 13, (0.5M–5M HNO_3), possibly deriving from the dissolution of weathering rims around the sulphide grains.

The reference hematite is mainly extracted at steps 11 (1M HNO_3) and 13 (5M HNO_3).

12.2 THE ACID MINE DRAINAGE (AMD) PRECIPITATE AND SOIL AFFECTED BY AMD POLLUTION

Figures 41, 42 and 43 summarise the results of the CISED extraction test carried out on the acid mine drainage precipitate (MPS 71) previously characterised by XRD and chemical analysis as poorly crystalline iron-rich material, possibly as a mixture of schwertmannite and goethite. Figure 41 shows the extraction profiles for the seven resolved physico-chemical components, in order of decreasing abundance (total extracted solid in mg kg^{-1}), characterising the sample. Each component has been named using a combination of the chemical elements that contribute more than 10% by weight to the composition of the components (elements in brackets between 5 and 10%). Various iron-rich components are identified, each removed at a different extraction step and in association with different elements, together with a subordinate water soluble calcium-sulphur component (likely representing gypsum). The majority of the As is associated with the Fe-As-(S) component mainly extracted at steps 9 to 10 of the sequential extraction corresponding to a nitric acid concentration of 0.5M (Figure 41), indicating a possible occurrence of As as bound or coprecipitated with iron oxyhydroxides. Figure 43 shows that only a small fraction of the total As is however removed during the sequential extraction (about 30%) and even a lower percentage (less than 1%) is bioaccessible.

The results of the sequential extraction on the soil sample MPS 70, flooded by AMD waters, indicate that the majority of As is associated with three components made up principally of Fe and As and dissolved mainly during the 1M–5M nitric acid extraction steps (step 11–14) (Figure 44 and 45). These components are however bioaccessible only in very small proportion (Figure 46). The presence of a Fe-(Al) components containing a small fraction of the total extracted As and dissolved earlier in the sequential leaching, may contribute to the bioaccessible fraction of As.

Comparison of the sequence of extraction of Fe and As in the sulphide reference material (MPR2 He) with the AMD precipitate sample (MPS 71) points to a higher leachability of As present as arsenate/As-bearing iron oxide phases rather than as As-Fe sulphide. The difference in leachability rate of the Fe-As components in the AMD precipitate (step 9–10) and in the soil polluted by AMD (later step 11–14)

may reflect differences in Fe oxyhydroxide degree of crystallinity. More ordered iron oxyhydroxides as result of aging during pedogenesis would in fact be more stable and dissolve later and could explain the lower As leachability in the soil compared to the AMD.

12.3 MINE WASTES: BLACK FURNACE ASH AND SANDY TAILINGS AND ORE CRUSHER GROUND

In the black slag (MPS 90) and the sandy tailings (MPS 91) two Fe-rich components are identified, one Fe-dominated and with high As content and another one richer in Ca along with Fe and much lower in As leached at an earlier stage in the extraction (Figures 47–48 and Figures 50–51). These results together with the previous ones related to the AMD and AMD polluted soil possibly suggests the existence of different As-bearing Fe phases (i.e. amorphous/crystalline, fine texture/coarse texture, Ca-rich/As-rich) that are being dissolved at different rates in the acid extracts. For these samples petrographic analysis was undertaken, which allows validation of the chemometric analysis. The main As-Fe association is recognized in As-Fe oxyhydroxide cements coating micaceous and quartz grains (MPS 91) or vesicular glassy slag fragments (MPS 90).

In the ore crusher ground (MPS 97) As is more evenly distributed among the identified components (Figures 53–54). Noteworthy it is a water soluble phase identifiable (step 1–2, H_2O extracts), which extracts more than 1000 mg kg^{-1} of As. A component made of 78% Ca and 12% As is also identified with a diffuse window of extraction in the steps 3–7 (0.01M–0.1M HNO_3).

The As-Ca-Fe association is recognised in the coatings rimming sulphide grains and in discrete Ca-As-Fe particles by SEM observation.

Figure 55 shows how the Ca-As components are the most important hosts of bioaccessible As.

Table 13 Arsenic (mg kg^{-1}) leached by de-ionised water in the first two steps of the sequential extraction.

DIW extract	Sample type	As (mg kg^{-1})
MPS8	Soil	3.80
MPS20	Soil	4.28
MPS23	Tailings	3.99
MPS38	Soil	17.65
MPS43	Tailings	0.65
MPS56	Tailings	5.73
MPM1	Tailings	0.09
MPM4	Soil	4.01
MPM9	Tailings	1.17
MPS90	Ash	1.03
MPS71	Fe-rich precipitates.	0.19
MPS92	Lagoon bed	6.46
MPS97	Ore crusher ground	1441.08
MPM4D	Tailings	8.55
MPS70	Soil	3.04
MPS73	Ash	499.81
MPS95	Soil	23.33
MPS91	Tailings	0.30
MPS87	Soil	0.01
MPS100	Soil	1.59
Arsenopyrite		6.6

12.4 MINE SITE SOILS — MEDIUM ARSENIC CONTENT

Figures 56 and 57 show that in MPS 20, a soil with ca. 1000 mg kg^{-1} As belonging to cluster 2, almost all of the As is associated with an Fe-oxide phase and that the bioaccessible fraction is probably derived from a partial dissolution of this component. A number of subordinate components rich in Al with a diffuse window of extraction from the early steps 3–5 of the extraction (0.01M–0.05M HNO_3) (Figure 56) are also present, but they do not contain As. These components probably represents Al-hydroxide polymers, which commonly occur in acid soils, adsorbed on humus and soil minerals.

12.5 MINE SITE SOILS — HIGH ARSENIC CONTENT

The results of the CISED processing of soil MPS8, an As-rich soil belonging to cluster 4, show that As is mainly associated with Fe-dominated components extracted at the last stages of the extraction test (Figures 59 and 60). The other resolved components are Ca-Fe dominated containing a few percent Cu (probably a carbonate phase) and sulphate salts; aluminium phases are subordinate.

Water leachates from sequential extractions

The first two steps of the sequential extraction method using de-ionised water (DIW) as the solvent represent a fraction subject to instantaneous dissolution/desorption upon wetting. The description of this fraction is important because it provides an indication of the potential mobility of As in the tested materials.

The DIW leaching, defined in terms of release of the element per gram of material ranges from 0.01 mg kg^{-1} to 23.33 mg kg^{-1} As in the soils and 0.09 to 1441 mg kg^{-1} As in the tailings (Table 13). In percentage terms values are in the range 0.0001 to 3.7%, with the highest leachability found in the material collected from around the site of the ore crusher (MPS 73–MPS 97). Up to 2.7% As dissolution is observed in some soils (e.g. MPS20-MPS38-MPS95). In contrast, in the ochre precipitates with more than 60 000 mg kg^{-1} total As only 0.19 mg kg^{-1} As was found to be water leachable.

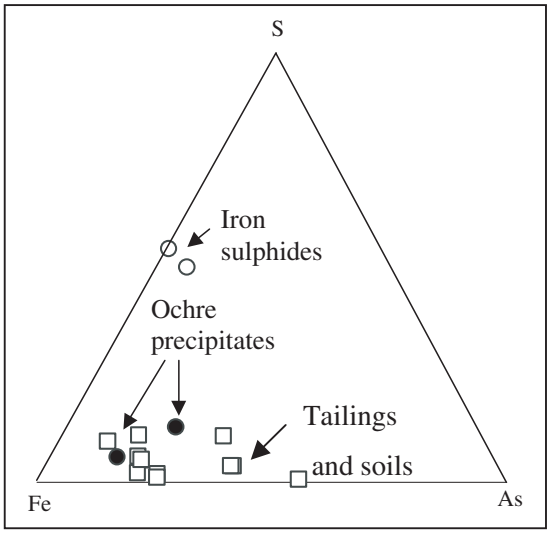

Figure 38 Triangular diagram showing composition of the CISED identified Fe-As-S geochemical components in the samples.

No significant correlations between elements are observed in the DIW-leached fraction, which would allow identification of possible mineralogical phases and hence solubility control. The high pH (7.1) of the ore crusher material (MPS97) might be responsible for the significantly higher percentage of DIW-extractable As, consistent with a decrease of As adsorption on Fe-oxides towards alkaline pH (Pierce and Moore, 1982). Any further pH-dependence of As leachability is impossible to verify as the pH of both DIW leached soils and tailings varies only slightly over a narrow range of pH 3 to 4. Occurrence of Ca-arsenates rimming ore particles in the crusher ground material as shown by SEM may contribute to the higher As mobility because of the higher solubility of Ca-arsenates than Fe-arsenates (Gaskova et al., 2001).

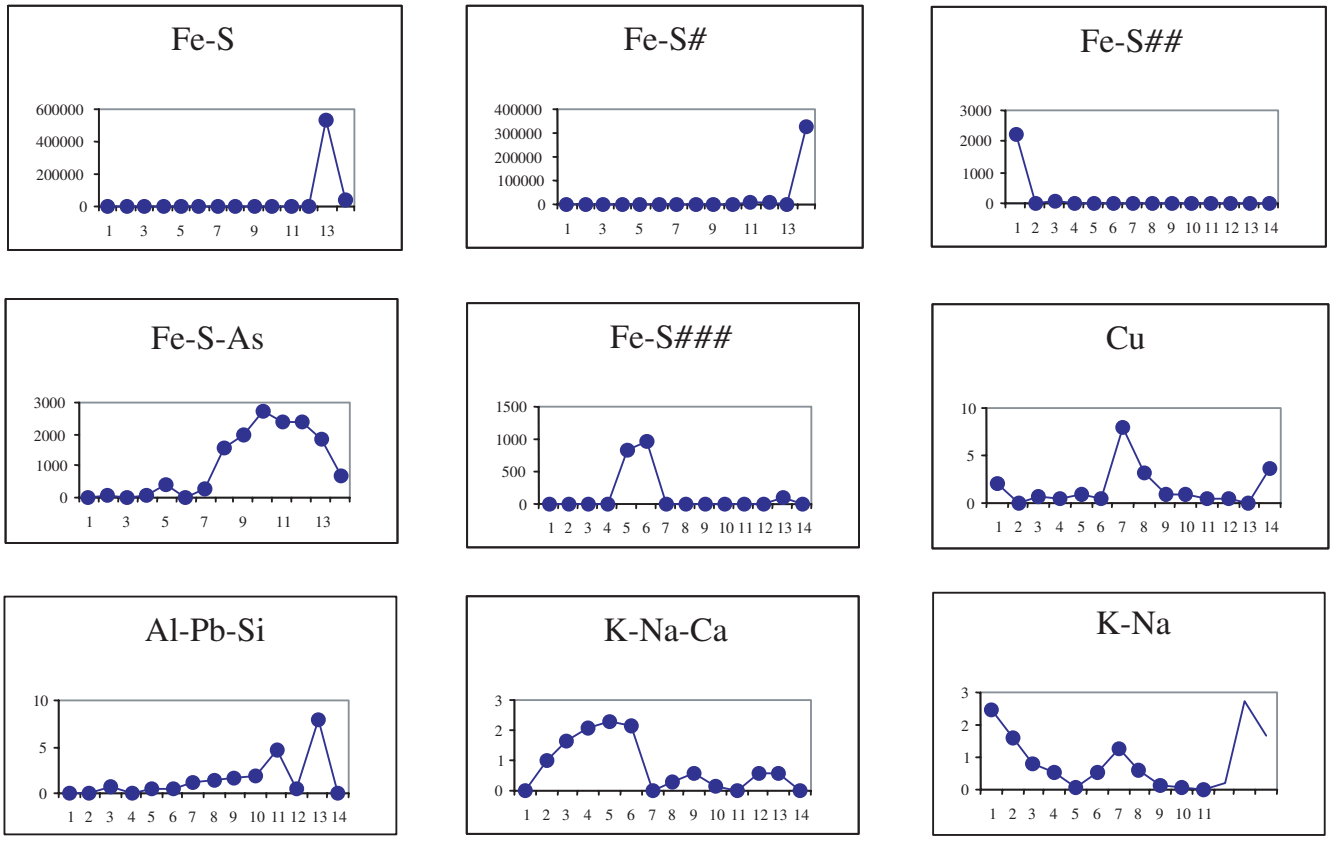

Figure 39 Extraction profiles of the 9 identified components of the reference iron sulphide (X axis: extraction steps; Y axis: total extracted solid in mg kg^{-1}).

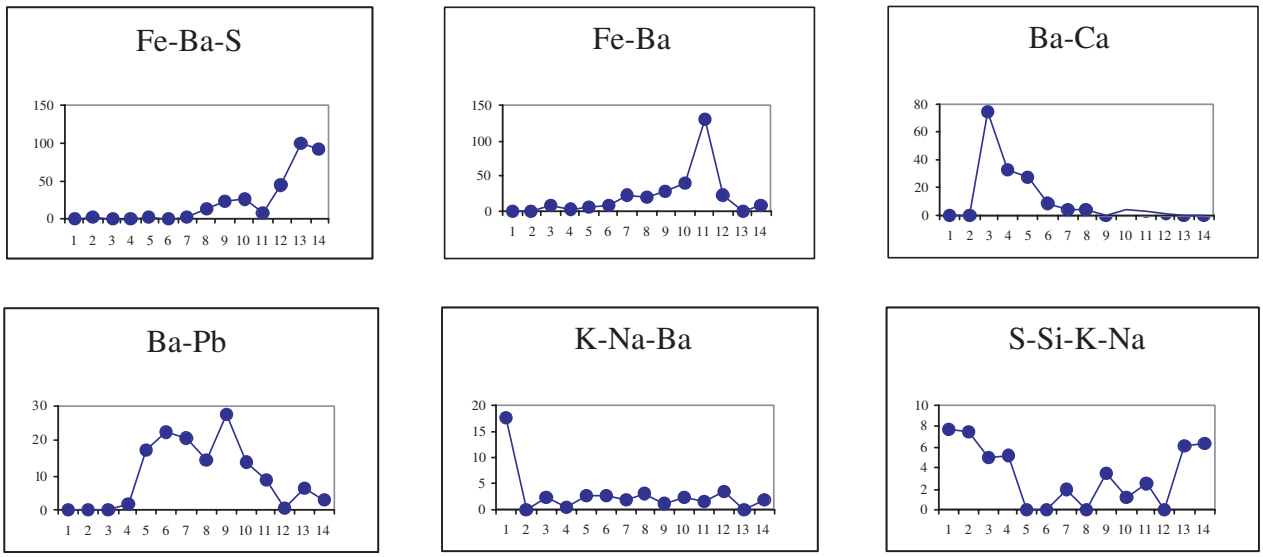

Figure 40 Extraction profiles of the 6 identified components of the reference hematite (X axis: extraction steps; Y axis: total extracted solid in mg kg^{-1}).

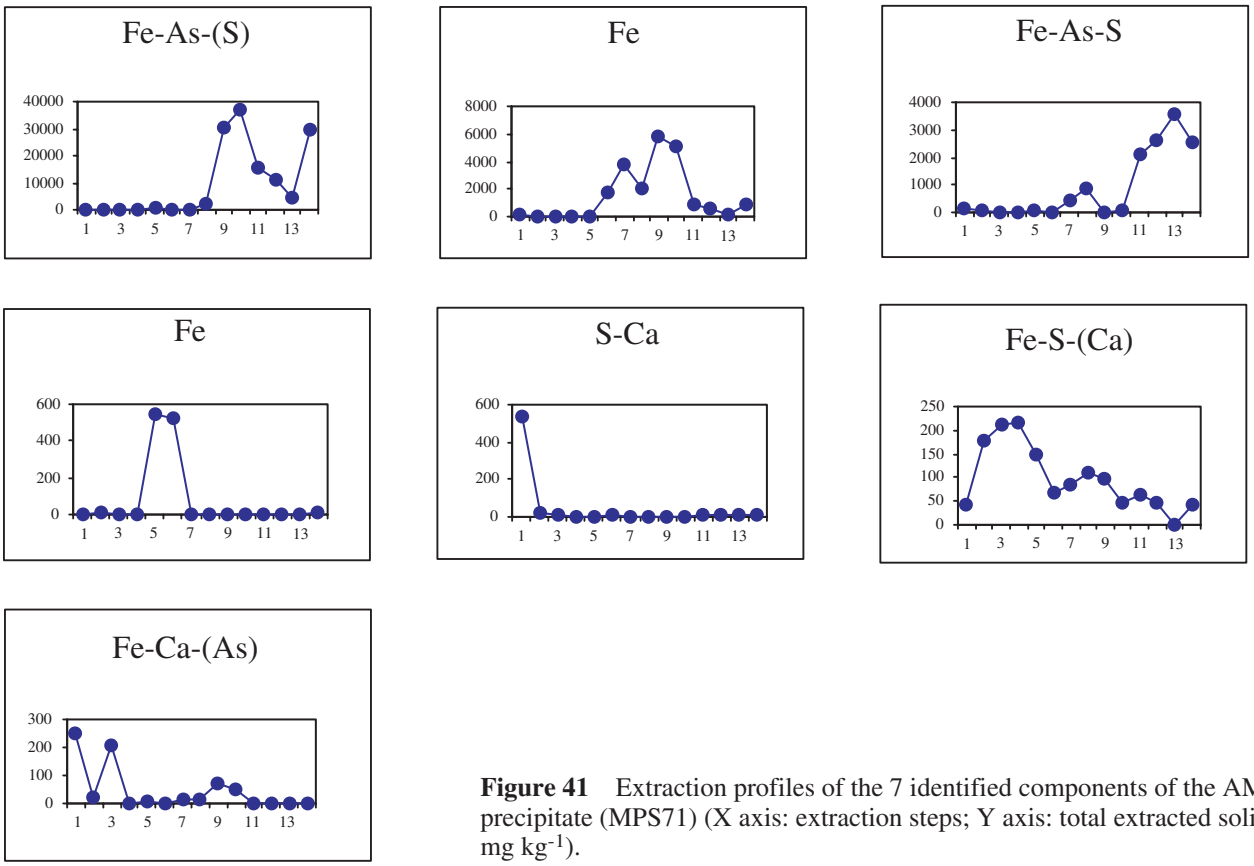

Figure 41 Extraction profiles of the 7 identified components of the AMD precipitate (MPS71) (X axis: extraction steps; Y axis: total extracted solid in mg kg^{-1}).

Figure 42 Relative distribution of arsenic in the extracted physico-chemical components for the AMD precipitate sample (MPS71).

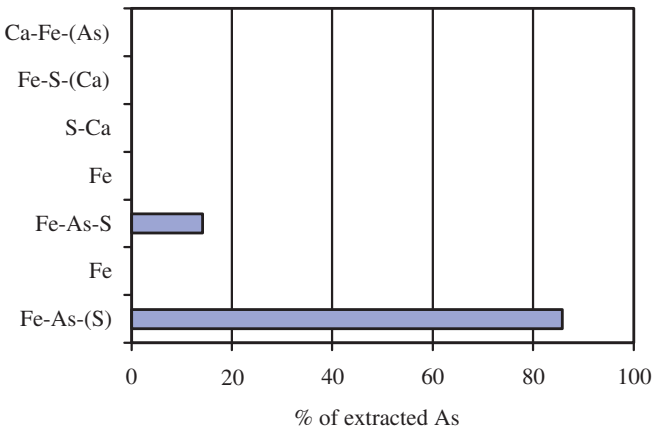

Figure 43 Comparison of total, bioaccessible and CISED extracted As in the AMD precipitate sample (MPS71).

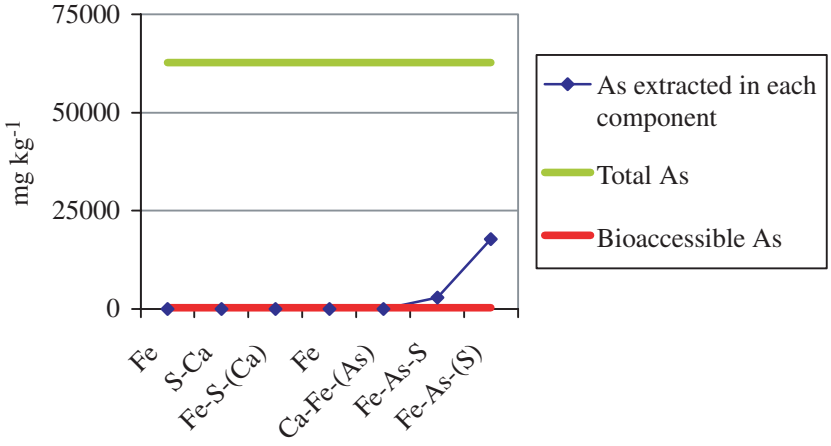

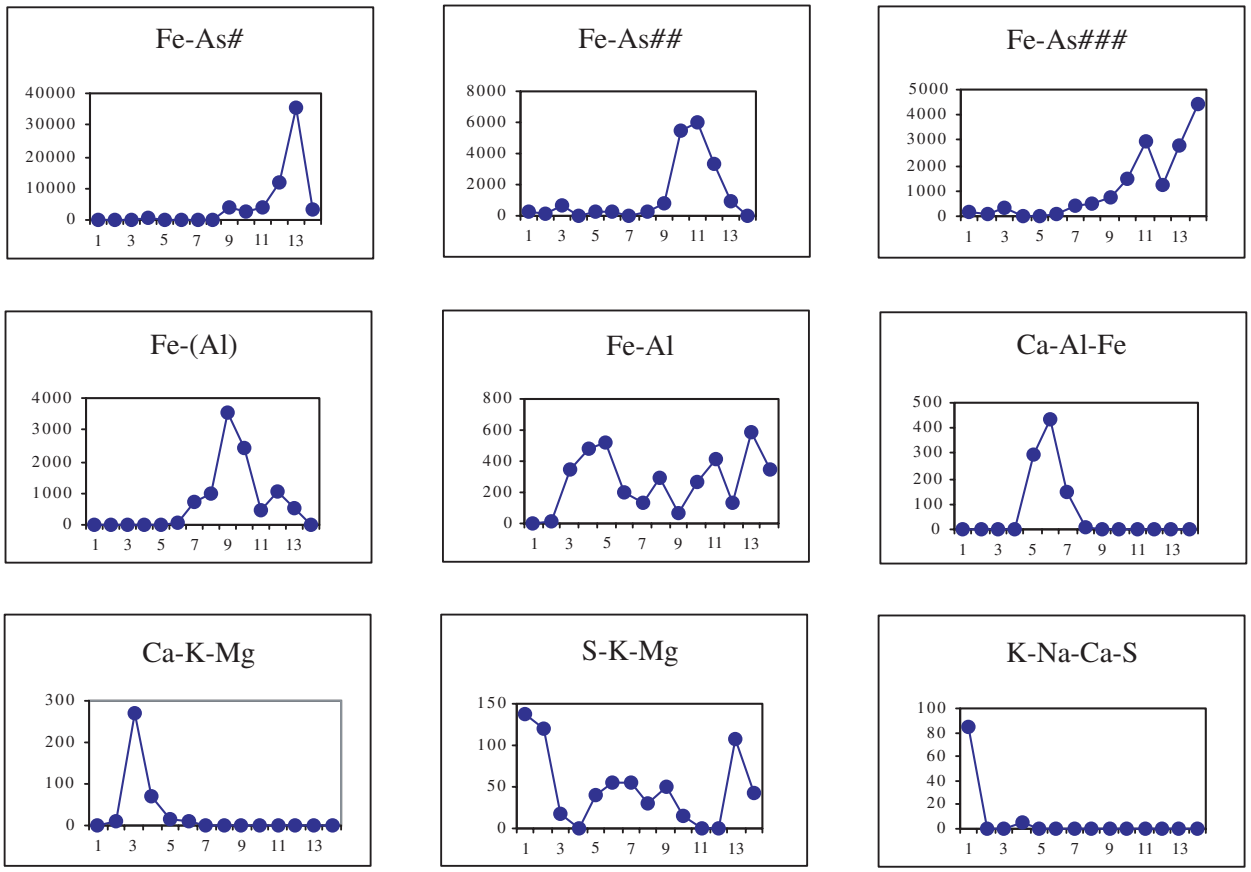

Figure 44 Extraction profiles of the 9 identified components of the soil sample MPS70 (X axis: extraction steps; Y axis: total extracted solid in mg kg^{-1}).

Figure 45 Relative distribution of arsenic in the extracted physico-chemical components for the soil sample MPS70.

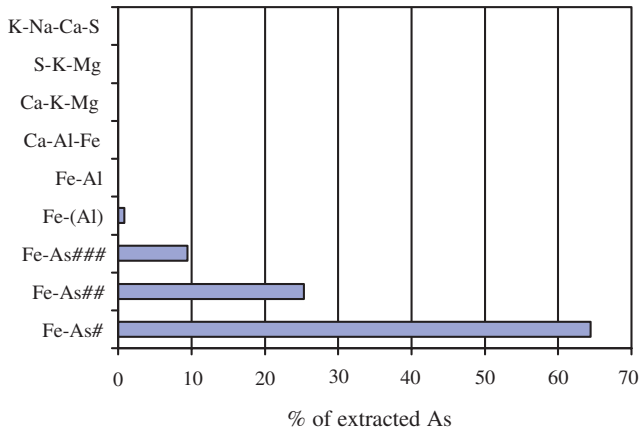

Figure 46 Comparison of total, bioaccessible and CISED extracted As in the soil sample MPS70.

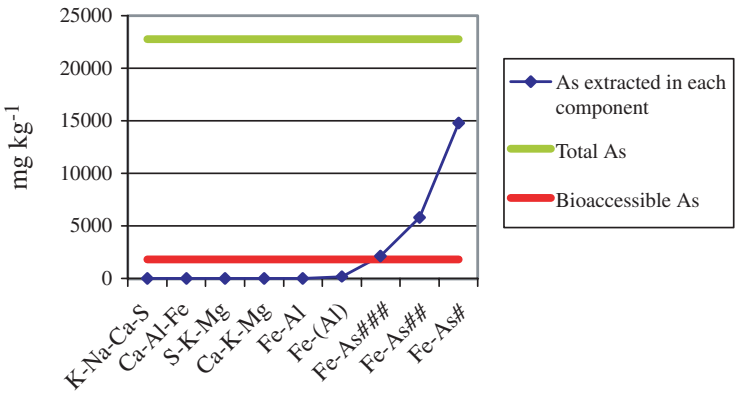

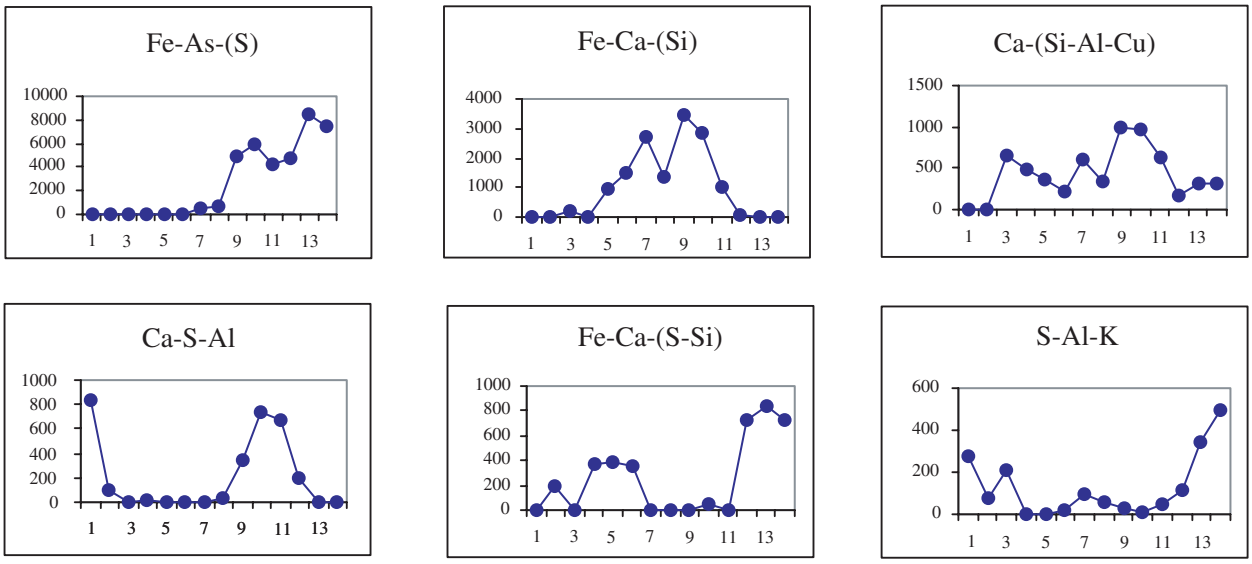

Figure 47 Extraction profiles of the 6 identified components of the sample MPS90 (X axis: extraction steps; Y axis: total extracted solid in mg kg^{-1}).

Figure 48 Relative distribution of arsenic in the extracted physico-chemical components for the sample MPS 90.

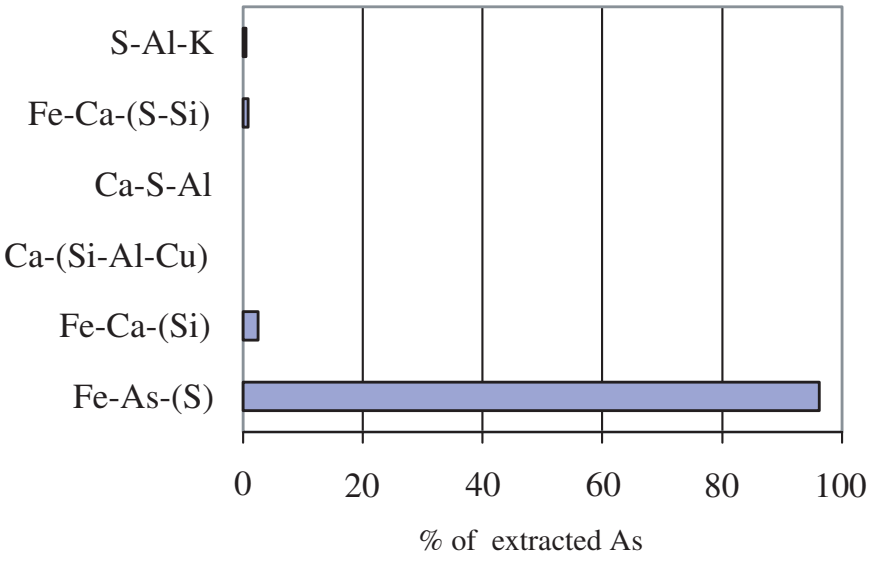

Figure 49 Comparison of total, bioaccessible and CISED extracted arsenic in the sample MPS 90.

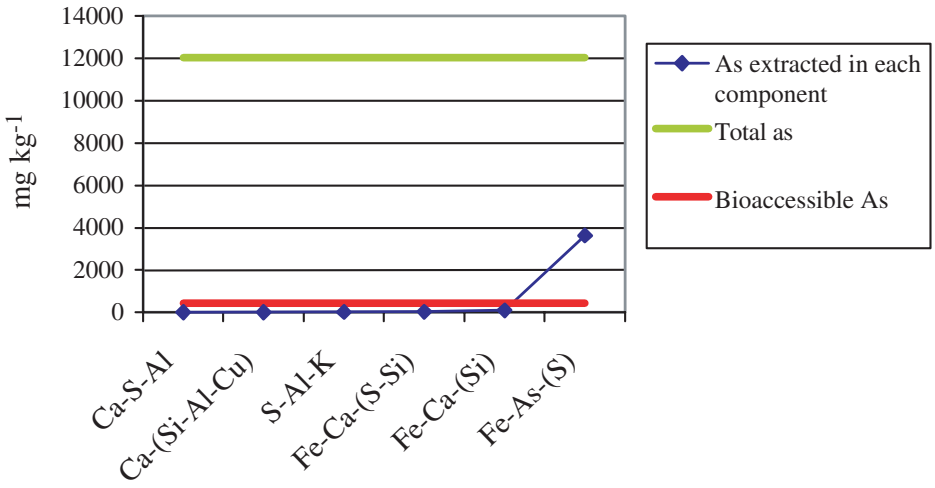

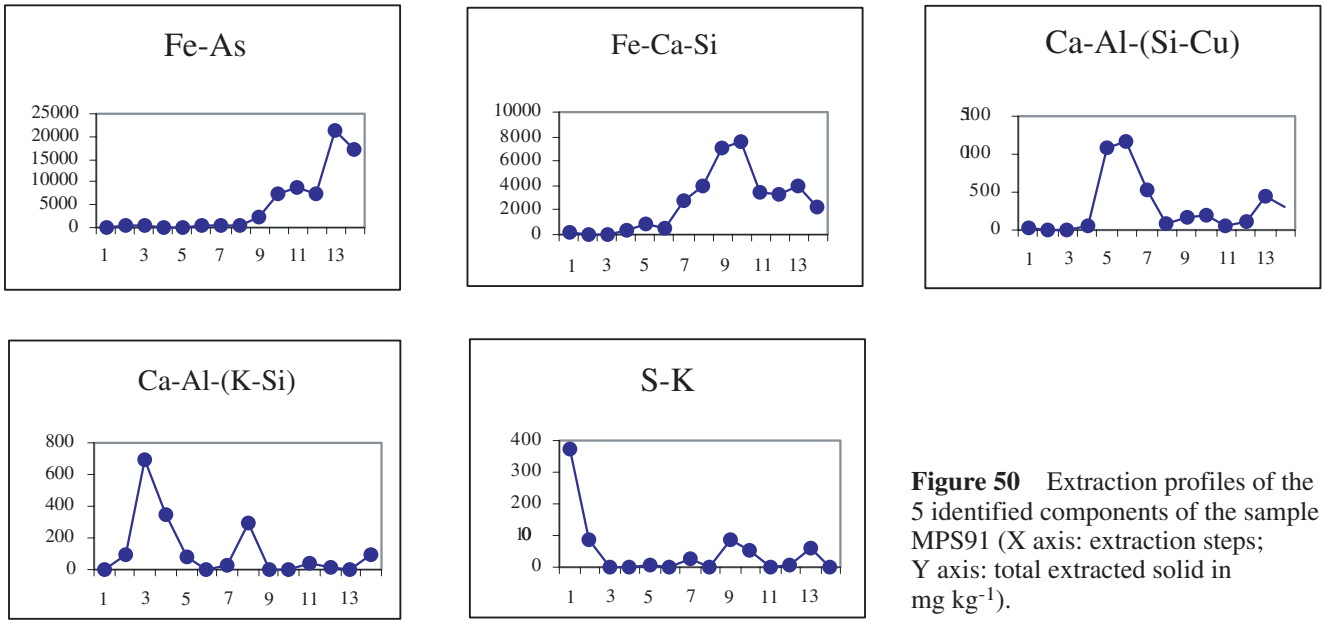

Figure 50 Extraction profiles of the 5 identified components of the sample MPS91 (X axis: extraction steps; Y axis: total extracted solid in mg kg^{-1}).

Figure 51 Relative distribution of arsenic in the extracted physico-chemical components for the sample MPS 91.

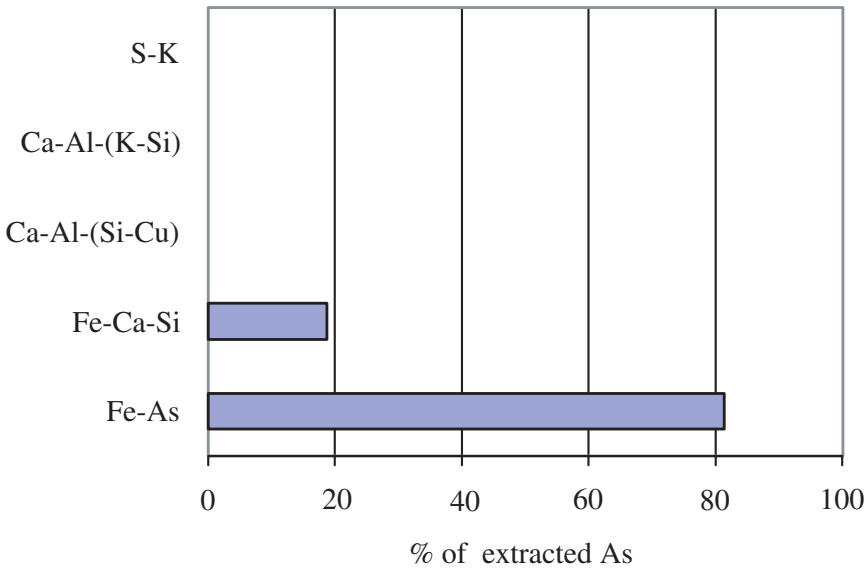

Figure 52 Comparison of total, bioaccessible and CISED extracted arsenic in sample MPS 91.

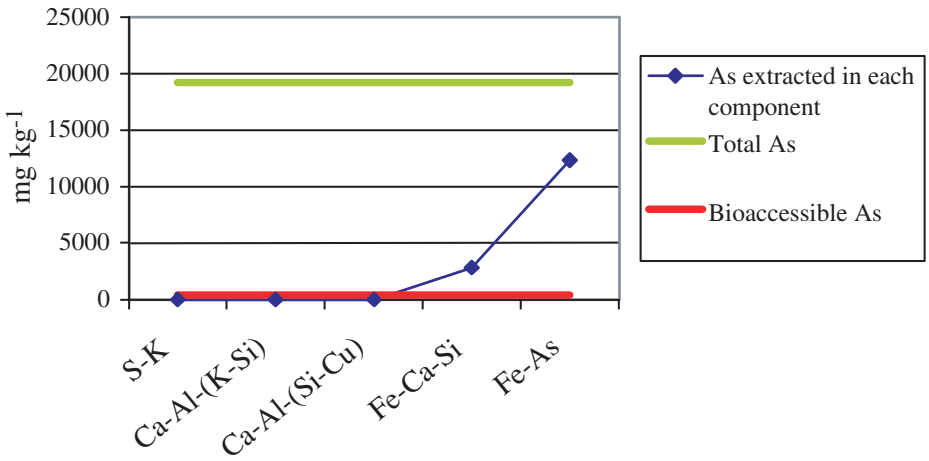

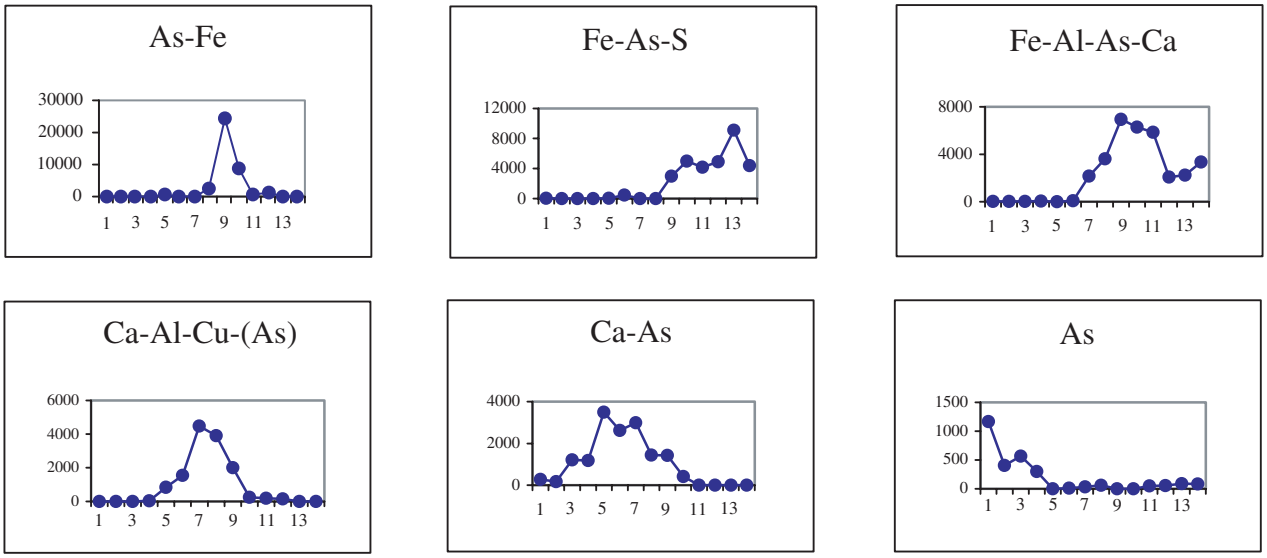

Figure 53 Extraction profiles of the 6 identified components of the sample MPS97 (X axis: extraction steps; Y axis: total extracted solid in mg kg^{-1}).

Figure 54 Relative distribution of arsenic in the extracted physico-chemical components for the sample MPS 97.

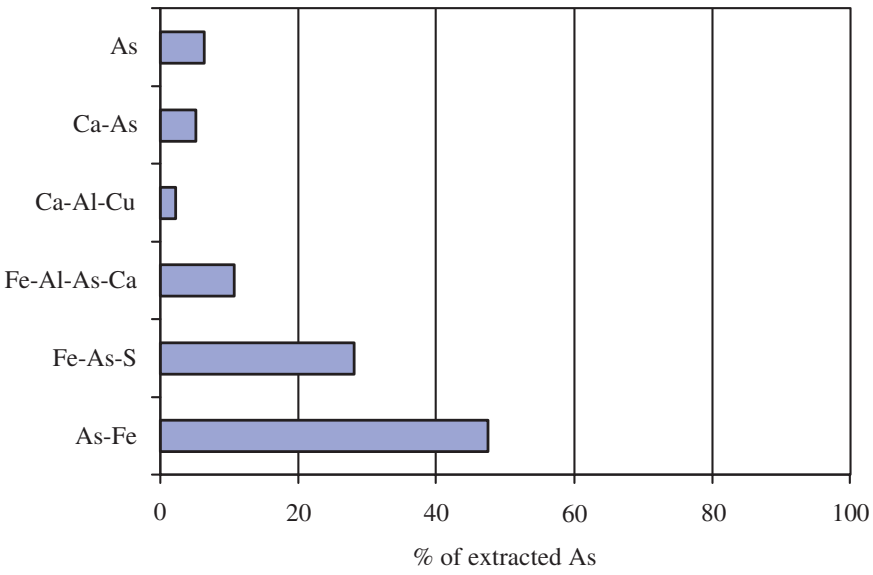

Figure 55 Comparison of total, bioaccessible and CISED extracted arsenic in sample MPS 97.

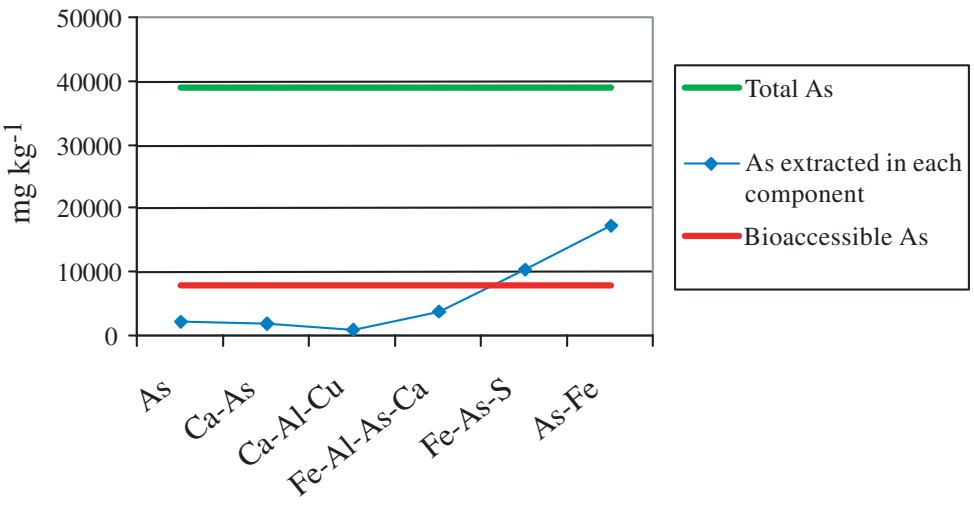

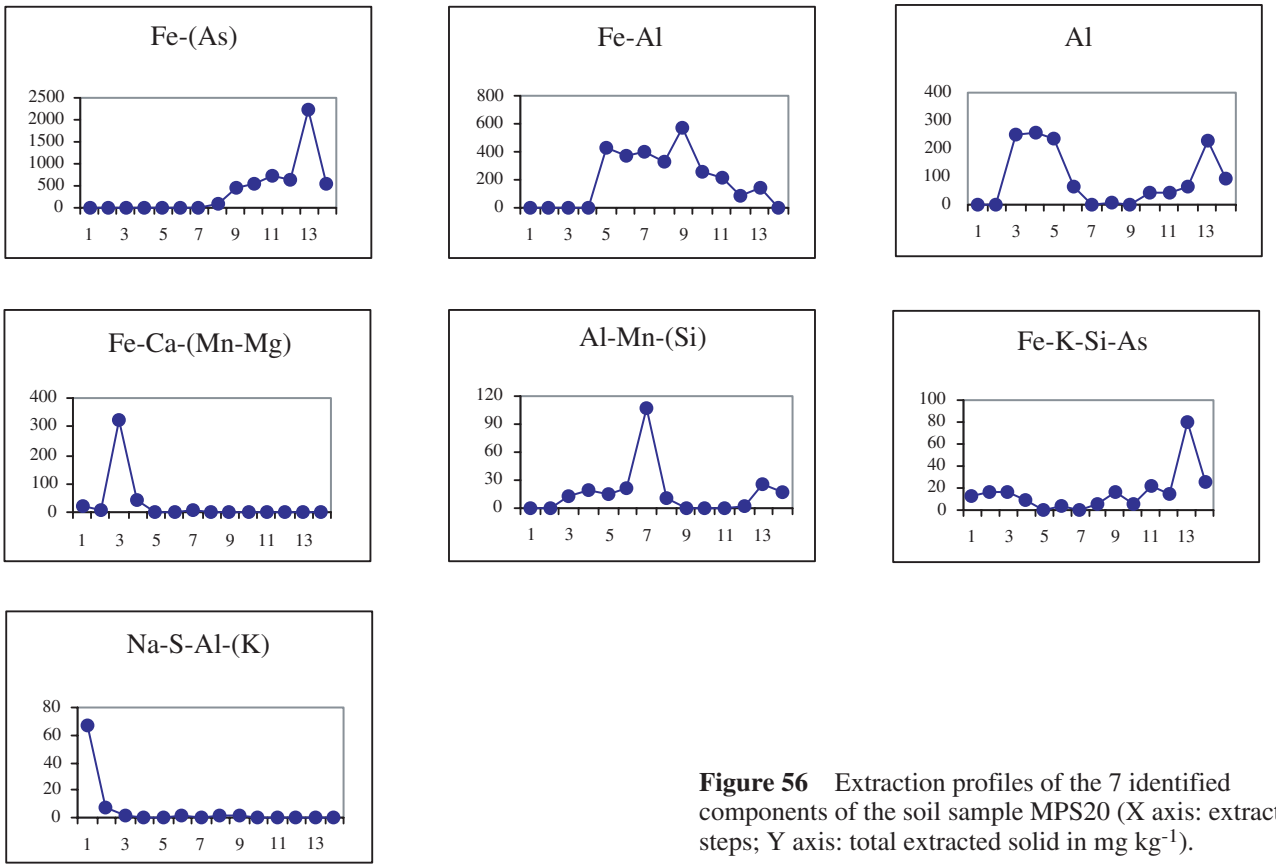

Figure 56 Extraction profiles of the 7 identified components of the soil sample MPS20 (X axis: extraction steps; Y axis: total extracted solid in mg kg^{-1}).

Figure 57 Relative distribution of arsenic in the extracted physico-chemical components for the soil sample MPS20.

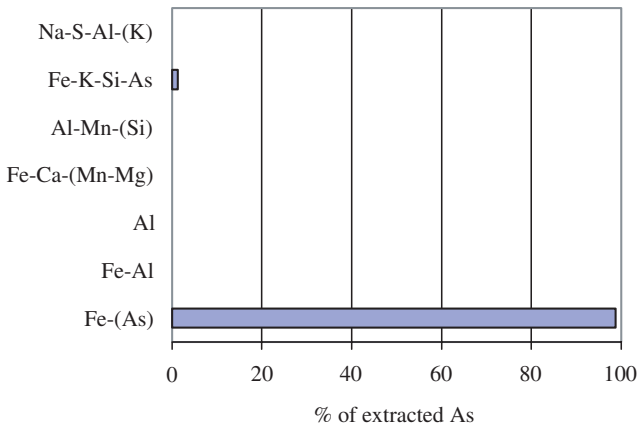

Figure 58 Comparison of total, bioaccessible and CISED extracted arsenic in soil sample MPS20.

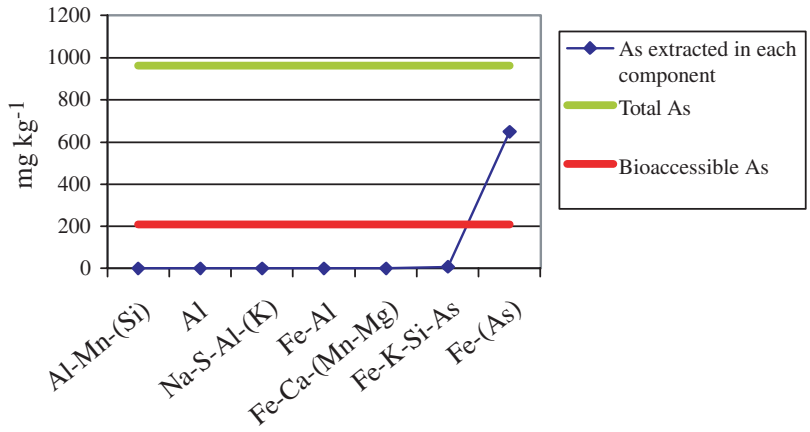

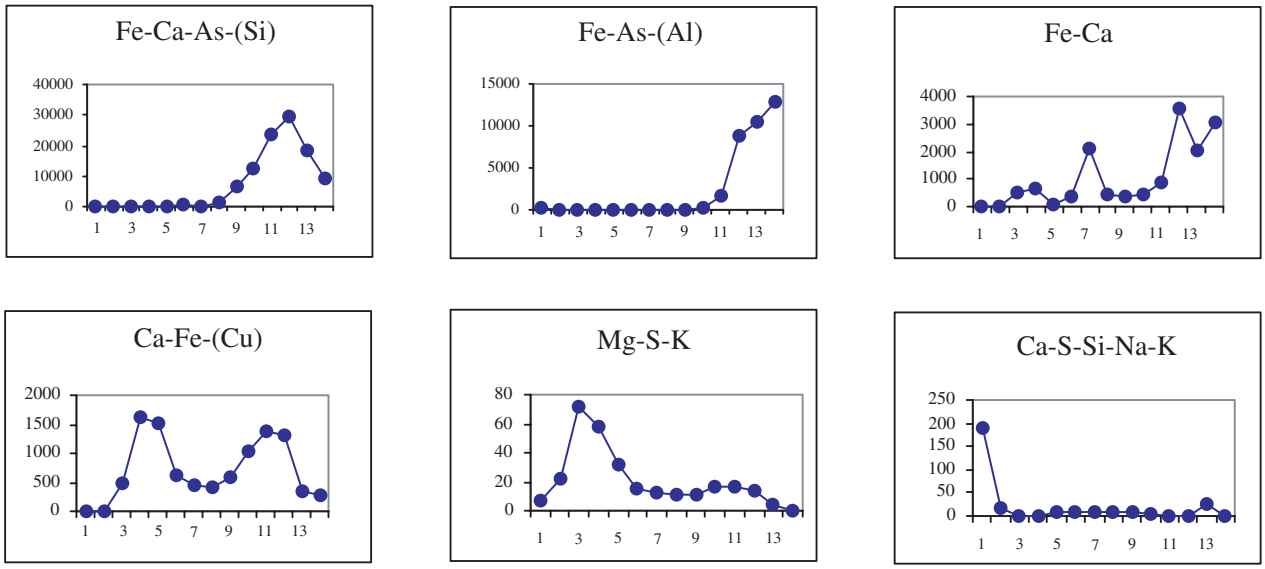

Figure 59 Extraction profiles of the 6 identified components of the soil sample MPS8 (X axis: extraction steps; Y axis: total extracted solid in mg kg^{-1}).

Figure 60 Relative distribution of arsenic in the extracted physico-chemical components for the soil sample MPS 8.

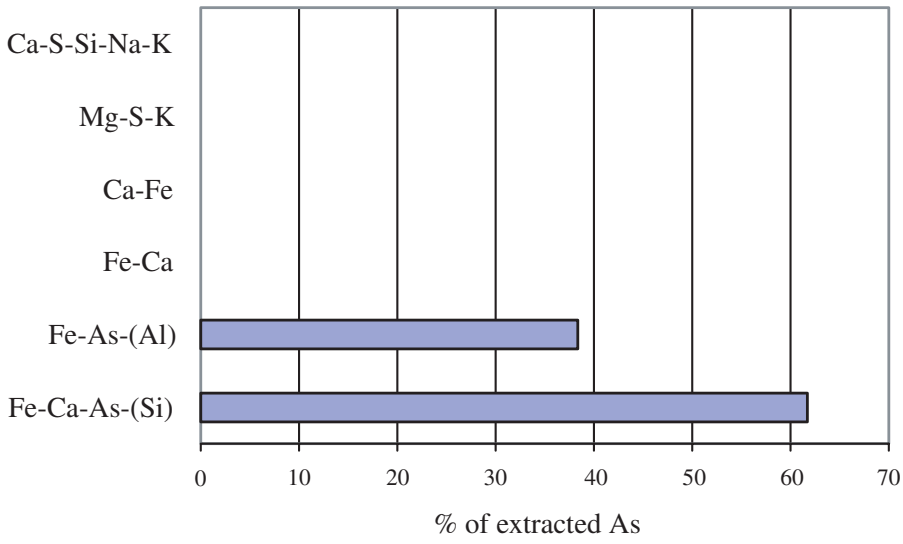

Figure 61 Comparison of total, bioaccessible and CISED extracted As in the soil sample MPS 8.

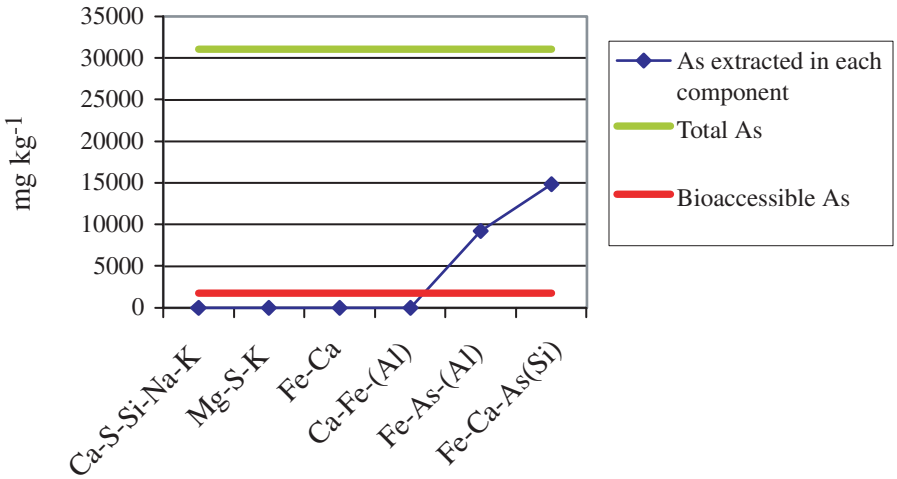

13 Arsenic speciation in solids by EXAFS spectroscopy

XANES Spectra

X-ray absorption near edge structure (XANES) spectra collected from a selection of mine waste and soil samples are shown in Figure 62. The position and shape of the spectra are all very similar and consistent with an arsenate species (As(V) tetrahedrally surrounded by 4 oxygen atoms). The compound $PbFe_3(SO_4)(AsO_4)(OH)_6$ was used as an arsenate standard and has the same shaped XANES as the samples tested.

EXAFS Spectra

Extended X-ray absorption fine structure (EXAFS) spectroscopy has been used to complement the chemical sequential extraction procedure in order to evaluate the speciation of As in the samples. EXAFS analysis of heterogeneous materials is, however, complicated by the presence of overlapping peaks, multi-atom shells, increased disorder due to the presence of poorly crystalline phases (Foster et al., 1998) and lack of sensitivity to minor forms of an element is a major obstacle using EXAFS (Isaure et al., 2002). The EXAFS signal is a weighted average of all chemical species of an element and the ability to discriminate between multiple element forms depends on their relative abundance.

Quantitative fits of EXAFS spectra using theoretical standards enable the determination of the nearest neighbour atoms and approximate coordination numbers and interatomic bond distances. The first peak in the Fourier Transforms yields information on the As-O relationship. In all cases the main contribution to the EXAFS is due to four oxygen at ca. 1.68 Å (Figures 63–64). There is no evidence in any spectrum of contributions from S or Fe at ca. 2.2–2.3 Å, which would be characteristic of arsenopyrite. There are outer shells evident in all the Fourier transforms. In most cases the EXAFS oscillations giving rise to these could be fitted using Si, As or Fe backscatterers. However, iron at ca. 2.86 Å usually gave the best fit and the fit was usually improved further by addition of a second shell of Fe at ca. 3.34 Å. These results imply either adsorption of the As onto an iron oxide/hydroxide substrate or incorporation of the As into a mixed metal oxide phase. Previous EXAFS spectroscopy studies by Foster et al. (1998), Randall et al. (2001) and Savage et al. (2000) had indicated arsenate tetrahedra sorbed onto the fine-grained iron-rich weathering products of As mine tailings. The two different As-Fe distances may reflect the presence of doubly oxo-bridged and singly oxo-bridged species. Table 14 lists the parameters of the best fits.

Table 14 Best fit parameters for the As K-edge EXAFS spectra.

Sample	Scatterer	N	r / Å	$2\sigma^2$ / Å^2	R-factor
MPS 4	O	4	1.69	0.004	19.9
	Fe	2	2.87	0.034	
	Fe	1	3.31	0.010	
MPS 12	O	4	1.69	0.004	19.4
	Fe	2	2.88	0.034	
	Fe	1	3.33	0.015	
MPS 15	O	4	1.69	0.004	21.0
	Fe	2	2.85	0.032	
	Fe	1	3.33	0.008	
MPS 20	O	4	1.69	0.005	22.2
	Fe	2	2.86	0.036	
	Fe	1	3.33	0.010	
MPM 4	O	4	1.69	0.007	26.1
	Fe	2	2.85	0.035	
	Fe	1	3.33	0.011	
MPS 71	O	4	1.69	0.005	19.1
	Fe	2	2.85	0.034	
	Fe	1	3.32	0.009	
MPS 90	O	4	1.69	0.006	23.0
	Fe	2	2.85	0.033	
	Fe	1	3.37	0.017	
MPS 91	O	4	1.69	0.006	21.6
	Fe	2	2.86	0.035	
	Fe	1	3.33	0.011	
MPS 95	O	4	1.69	0.004	23.9
	Fe	2	2.86	0.035	
	Fe	1	3.33	0.012	

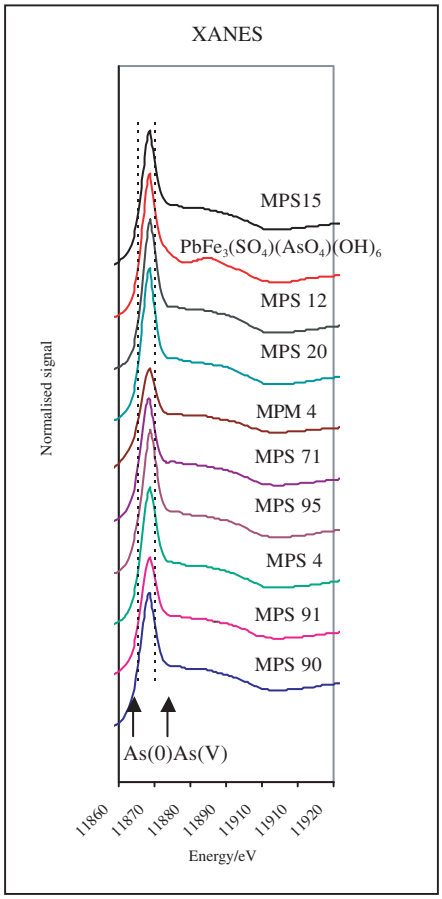

Figure 62 X-ray absorption near edge structure (XANES) spectra of mine waste and soil samples. A model compound $PbFe_3(SO_4)(AsO_4)(OH)_6$ is included. The dashed vertical lines show the theoretical absorption edge position for As(0) (11865 eV) and As(V) (11870 eV).

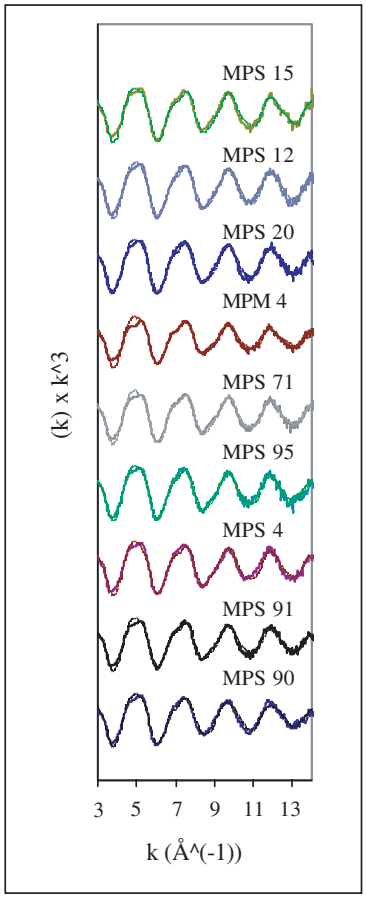

Figure 63 Normalised, K^3 — weighted EXAFS spectra for mine waste and soil samples. Solid line: experimental data, dashed line: least squares fit using parameters shown in Table 14.

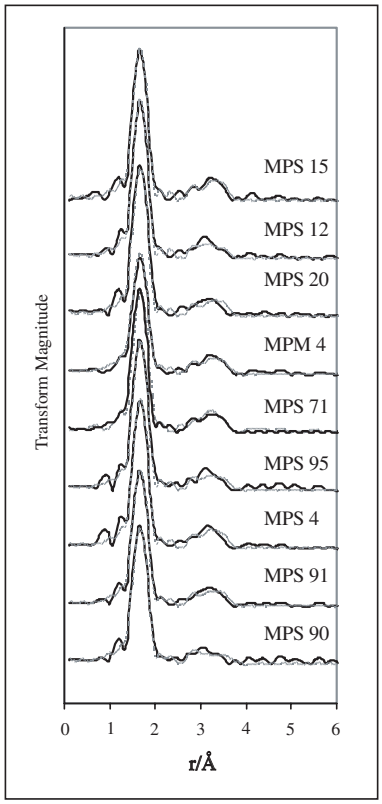

Figure 64 Radial structure functions (RSF) for mine waste and soil samples. Solid line: experimental data, dashed line: least squares fit using parameters shown in Table 14.

14 Arsenic speciation in waters and leachates

Arsenic is present predominantly as As(III) in most water samples as well as in the water leachates extracted from tailings and soils (Tables 15 to 16). Since As(III) is more toxic and mobile than As(V), processes affecting the speciation are of particular environmental concern.

The Eh-pH plot (Figure 65) suggests that the majority of the inorganic As should exist in the form of $H_2AsO_4^-$ indicating a thermodynamic disequilibrium of the As(V)–As(III) redox couple. As(III) has been observed to predominate, even if not thermodynamically favoured, in many natural systems and kinetically inhibited transformation between As(V) and As(III) has been invoked (Yan et al., 2000). Mandl et al. (1992) demonstrated the stability of As(III) in a leaching medium during spontaneous bacterial oxidation of arsenopyrite. A large proportion of the total As occurred as As(III) in the leaching medium and was not oxidised by Fe(III) in the presence of the mesophilic bacterium *Thiobacillus*

Table 15 Arsenic speciation in waters.

Sample	Description	As total µg l^{-1}	As (III) µg l^{-1}	As (V) µg l^{-1}	As(V)/As(III)
DC1	Tailings pond	40	24	15	0.64
DC2	Tailings pond	12	7	4	0.59
DC3	Seepage	3	1	2	1.31
DC4	Tailings pond	22	13	8	0.63
DC5	Tailings pond	163	142	21	0.15
DC5R	Tailings pond	613	480	133	0.28
DC6	Seepage	6577	5831	746	0.13
DC7	Adit discharge	19	10	9	0.95
DC7R	Adit discharge	90	73	17	0.23
DC8	Tailings pond	360	316	45	0.14
DC9	Spring	2	2	0	0.09
DC11	Pond	21	18	3	0.18
DC12	Stream	13	11	1	0.13
DC13	Leat	15	12	3	0.29
DC14	Leat	22	18	4	0.23

R=October sampling

Table 16 Arsenic speciation in water leachates.

Sample name	As total µg l^{-1}	As (III) µg l^{-1}	As (V) µg l^{-1}	As(V)/As(III)
MPM9 (A)	183	171	12	0.07
MPM9 (B)	149	125	24	0.19
MPS90 (A)	229	217	12	0.06
MPS90 (B)	125	103	22	0.21
MPS71 (A)	28	25	3	0.12
MPS71 (B)	20	9	11	1.17
MPS92 (A)	669	637	32	0.05
MPS92 (B)	745	629	117	0.19
MPS97 (A)	234000	232500	1500	0.01
MPS97 (B)	112500	103000	9500	0.09
MPM4 Re (A)	1055	950	106	0.11
MPM4 Re (B)	1055	928	128	0.14
MPS70 (A)	267	229	39	0.17
MPS70 (B)	244	199	46	0.23
MPS73 (A)	57500	45900	11600	0.25
MPS73 (B)	44000	34100	9900	0.29
MPS95 (A)	2842.5	2721	121.5	0.04
MPS95 (B)	1427.5	1222	205.5	0.17
MPS91 (A)	47.2	25.48	21.72	0.85
MPS91 (B)	90.05	62.9	27.15	0.43
MPR2 He (A)	2560.5	2102.5	458	0.22
MPR2 He (B)	185	157.3	27.7	0.18

ferrooxidans. The authors suggest a dependence of the type of leaching microorganisms in the leaching medium on As valency to explain the different results.

Arsenic speciation with As(III) as dominant As species in DGC water leachates from soils and tailings contrasts with the EXAFS results and with the work of Haswell et al. (1985) who found arsenate as the dominant As species in the soil-pore waters of aerobic soils from mineralised areas of south-west England. The low As(V)/As(III) ratio of the DGC water leachates could be explained by preferential leaching of As(III) compared to As(V) as a result of a much weaker interaction of As(III) and hydrous ferric oxides (HFO) than that of As(V) and HFO. This explanation is supported by the leaching experiment results of Gulens et al. (1979) who showed that As(III) is eluted five to six times faster than As(V) from the hydrous oxide surface of sand in an oxidising environment.

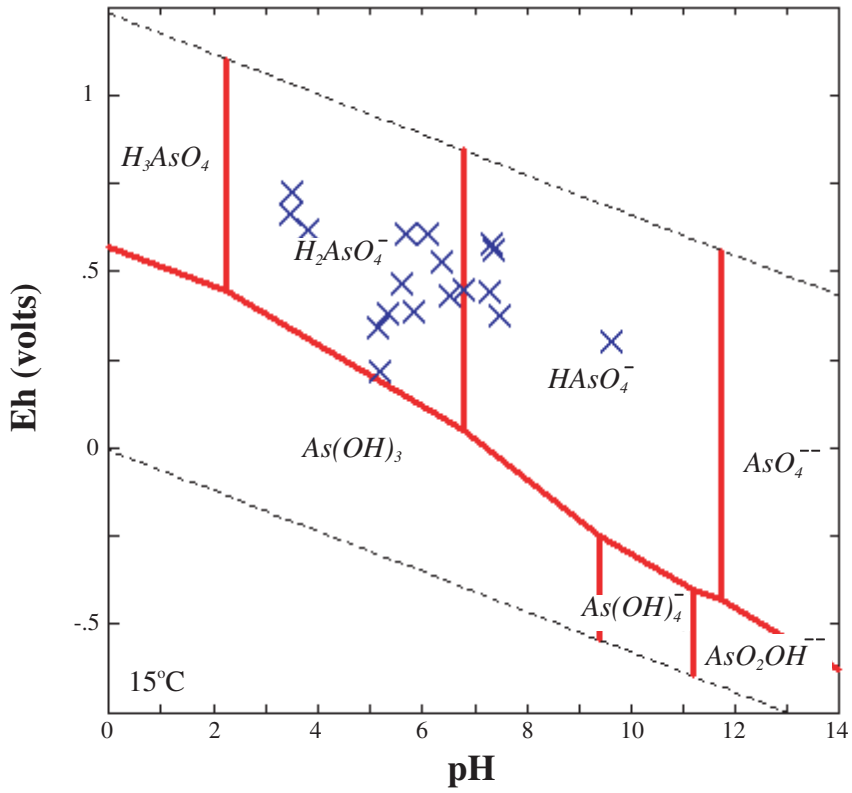

Figure 65 Eh-pH arsenic stability diagram for arsenic species.

15 Exposure assessment

The Contaminated Land Exposure Assessment (CLEA) model developed by DEFRA and Environment Agency (2002) has been used to determine the current risk of As exposure to sensitive receptors living within the mine influence and consuming homegrown vegetables. In particular, a residential scenario is addressed. The exposure pathways that are considered applicable to the residential land use are: ingestion of soil, ingestion of household dust, ingestion of contaminated vegetables and ingestion of soil attached to vegetables. Dermal and inhalation routes have been excluded because the contribution of these pathways to the overall exposure is considered to be less than 1%.

The critical receptor is set to be protective of young children (a young female child with the exposure occurring in the first six years of life), because in general they are more likely to have higher exposure to soil contaminants.

In deriving the average daily human exposure (ADE) the bioaccessible As concentrations have been used rather than the total soil As content. Soil texture, pH and organic matter parameters are based on site-derived data.

Arsenic is a non-threshold substance, i.e. it carries a risk at any level of exposure. In deriving toxicological criteria for the protection of human health for non-threshold contaminants the Index Dose (ID) defines the minimal human health risk level, with the additional requirement to keep any intake as low as reasonably practicable. By using the 95th percentile bound value of bioaccessible As in the soils around the mine site (219 mg kg^{-1}) the predicted average daily exposure (ADE) / Index Dose (ID) ratio is 11. The most important exposure pathway is the soil ingestion (71%), followed by plant uptake (22%) and attached soil (7%). The implication is that there is a toxic risk associated with the soils surrounding the mine site.

16 Conclusions

In this study the geochemical cycling of As in an environment affected by past mining activities has been investigated by using a variety of analytical methods that characterise As concentration and speciation in the soil, waste, water and vegetation. A number of features and conclusions have emerged:

- The study of the spatial distribution of As at Devon Great Consols Mine defines a widespread As contamination of local soils both within and without the mine boundaries.
- Sequential chemical extraction data have been used to help elucidate the nature of the As host minerals. In both soil and mine waste material As is primarily associated with Fe. Scanning electron microscopy (SEM) analysis equipped with an energy dispersive spectrometer (EDXA) allows one to localise the Fe-As association in iron oxyhydroxide phases coating the surface of altered waste fragments and clastic grains. The coatings show various microfabrics from colloform iron oxyhydroxide to more crystalline coatings (fine-needle-like crystals) and variable concentrations of As, typically from <0.5% to 3% As_2O_3.
- Beside the main occurrence of As adsorbed or coprecipited with amorphous iron oxyhydroxides, sequential extraction analysis supported by SEM-EDXA observation gives evidence of As also associated with Ca in the ore crusher ground, likely as amorphous calcium arsenate precipitates. Calcium and As were found associated in the form of amorphous precipitates also in the efflorescence covering extensively the brickwork of the calciner and flue remains, possibly as co-precipitated/solid solution masses with gypsum or as coatings on gypsum particles. Evidence of arsenolite is found in the ore crusher ground.
- The geochemical control of As bearing phases on dissolved As and element mobility have been also evaluated by analysing natural run-off and by carrying out a de-ionised water extraction together with thermodynamic modelling validation. By carrying out water leaching of sulphide ore and different wastes it has been shown that there is a high potential for As release from the wastes collected inside the As works, in particular the ore crusher ground material and the calciner ashes where As is found associated to Ca along with Fe and evidence of arsenolite is found. This is confirmed by the chemical analysis of the natural run-off collected at the As works containing elevated concentration of As (6577 $\mu g\ l^{-1}$). The leachates from the roasted tailings sand and the arsenopyrite ore generate less significant As concentration. Arsenic is virtually not leachable by water in the iron oxyhydroxides precipitated from the acid mine drainage waters on the site.
- Most of the waters flowing on the mine site and from tailings ponds contain elevated concentrations of As. The As distribution pattern in the waters shows a self mitigating capacity of drainage due to absorption on Fe-rich precipitates. Chemical modelling has demonstrated As sorption on iron oxyhydroxides. Acid mine drainage waters flooding surrounding alluvial soils have been pointed out to be responsible for some of the high As concentrations in the soils from the mine site.
- X-ray absorption near edge structure (XANES) analysis indicates that As(V) is the dominant oxidation state in the mine waste materials and soils. Quantitative fits of EXAFS spectra using standards indicate As(V) in tetrahedral coordination with O and second and third -neighbour Fe atoms, ruling out the presence of major arsenopyrite and confirming the results from chemical extractions and SEM. Second and third neighbour As-Fe EXAFS distances imply either adsorption of the As onto an iron oxide/hydroxide substrate or incorporation of As into a mixed metal oxide phase.
- The predominant species of As in waters and in the soil and tailings leachates is As(III), however samples plot in the arsenate stability field, indicating that waters are not in thermodynamic equilibrium. The results contradict also the findings from EXAFS and would require further investigation.
- Using the bioaccessible concentration of As in soils gives a more realistic indication of areas that are likely to pose an unacceptable risk to human health. The values for the soils in the mine area with a median value of bioaccessible As of 408 $mg\ kg^{-1}$ fall within the Soil Guideline Value of 500 $mg\ kg^{-1}$ calculated by the CLEA model for commercial/industrial use. However, high concentrations up to 624 $mg\ kg^{-1}$ of bioaccessible As measured in residential gardens and farm fields around the mine are well above the 19 $mg\ kg^{-1}$ CLEA SGV for gardens and allotments and highlight areas at highest risk in terms of source to receptor transfer. The soils from Bere Alston and Higher Todsworthy Farm are below the guideline values for gardens and allotments. If total concentration of As had been used then the sites would have failed the SGV screening criteria.
- The influence of soil chemical composition on As relative bioaccessibility has been investigated by using multivariate statistical analysis. The results suggest the presence of at least two mineralogical phases (iron sulphides and iron oxyhydroxides) affecting the bioaccessibility of As in soils. Complexity of iron oxyhydroxides phases and factors affecting As coprecipitation/adsorption processes necessitates that further studies are undertaken to better understand the influence of various soil physical and chemical properties on As bioaccessibility.
- Preliminary results on vegetation grown in highly contaminated garden soils around the mine have confirmed the health hazard represented by As uptake by vegetables in contaminated soil. The UK statutory limit of 1 $mg\ kg^{-1}$ (fresh weight) in food was exceeded in the beetroot, tomato, celery and lettuce samples with lettuce and celery being higher accumulators than fruits.

References

Most of the references listed below are held in the Library of the British Geological Survey at Keyworth, Nottingham. Copies of the references may be purchased from the Library subject to the current copyright legislation.

ABRAHAMS, P W, and THORNTON, I. 1987. Distribution and extent of land contaminated by arsenic and associated metals in mining regions of south-west England. *Transactions of the Institute of Mining and Metallurgy*, Vol. B, 1–8.

ASTON, S R, THORNTON, I, and WEBB, J S. 1975. Arsenic in stream sediments and waters of South West England. *The science of total environment*, Vol. 4, 347–358.

BALL, J W, and NORDSTROM, D K. 1991. User's manual for WATEQ4F,with revised thermodynamic data base and test cases for calculating speciation of major, trace, and redox elements in natural waters. *US Geological Survey Open-File Report*, 91–183.

BIGHAM, J M, SCHWERTMANN, U, TRAINA, S J, WINLAND, R L, and WOLF, M. 1996. Schwertmannite and the chemical modeling of iron in acid sulfate waters. *Geochemica et Cosmochimica Acta*, Vol. 60, 2111–2121.

BINSTED, N. 1998. Daresbury laboratory EXCURV98 PROGRAM.

BINSTED, N, STRANGE, R W, and HASNAIN, S S. 1992. Constrained and restrained refinement in EXAFS data analysis with curved wave theory, *Biochemistry*, Vol. 31, 12117–12125.

BLOOMFIELD, C, and COULTER, J K. 1973. Genesis and management of acid sulfate soils. *Advances in Agronomy*, Vol. 25, 265–326.

BOWELL, R J, and BRUCE, I. 1995. Geochemistry of iron ochres and mine waters from Levant Mine, Cornwall. *Applied Geochemistry*, Vol. 10, 237–250.

CAVE, M R, MILOWDOSWKI, A E, and FRIEL, H. 2004. Evaluation of a method for Identification of Host Physico-chemical Phases for Trace Metals and Measurement of their Solid-Phase Partitioning in Soil Samples by Nitric Acid Extraction and Chemometric Mixture Resolution. *Geochemistry: Exploration, Environment, Analysis*, Vol. 4, 71–86.

CHAROY, B. 1986. The genesis of the Cornubian Batholith (South-West England): the example of the Carnmenellis pluton. *Journal of Petrology*, Vol. 27, 571–604.

COLBOURN, P, ALLOWAY, B J, and THORNTON, I. 1975. Arsenic and heavy metals in soils associated with regional geochemical anomalies in south-west England. *The Science of the Total Environment*, Vol. 4, 359–363.

DAVIES, B E. 1971. Trace metal content of soils affected by base metal mining in the west of England. *Oikos*, Vol. 22, 366–372.

DEFRA, and ENVIRONMENT AGENCY. 2002. The contaminated Land Exposure Assessment Model (CLEA): technical basis and algorithms. The R & D Dissemination Centre, WRC plc, Swindon, Wilts., Report CLR10.

DINES, H G. 1956. *The Metalliferous Mining Region of South-West England* (1st edition). Memoirs of the Geological Survey of Great Britain. (London: HMSO.) ISBN 11 880066 3

DURRANCE, E M, and LAMING, D J C. 1982. *The Geology of Devon*. (Exeter: University of Exeter.) ISBN 0 85989 153 4

DZOMBAK, D A, and MOREL, F M M. 1990. *Surface complexation modeling: Hydrous Ferric Oxide*. (New York: John Wiley & Sons.)

FARAGO, M E, THORNTON, I, KAVANAGH, P, ELLIOT, P, and LEONARDI, G S. 1997. Health aspects of human exposure to high arsenic concentrations in soil in south-west England. 210–226 in *Arsenic: Exposure and Health Effects*. ABERNATHY, C O, CALDERON, R L, and CHAPPELL, W R (editors). (London: Chapman & Hall.)

FOSTER, A L, BROWN, G E, TINGLE, T N, and PARKS, G A. 1998. Quantitative arsenic speciation in mine tailings using X-ray absorption spectroscopy. *American Mineralogist*, Vol. 83, 553–568.

FUGE, R, PEARCE, M, PEARCE, N J G, and PERKINS, W T. 1994. Acid mine drainage in Wales and influence of ochre precipitation on water chemistry. 261–274 in *Environmental Geochemistry of Sulphide Oxidation*.

GASKOVA, O, AZAROUAL, M, PIANTONE, P, and LASSIN, A. 2001. Arsenic behaviour in subsurface hydrogeological systems — A critical review of thermodynamic data for arsenic minerals and aqueous species — A compilation of arsenic suface complexation reactions. *BRGM*, BRGM/RP-51356-FR.

GOLDSTEIN, J E, NEWBURY, D E, ECHLIN, P, JOY, D C, FIORI, C, and LIFSHIN, E. 1981. *Scanning Electron Microscopy and X-ray Microanalysis. A Text for Biologists, Materials Scientists, and Geologists*. (New York: Plenum Press.) ISBN 0-306-40768-X.

GULENS, J, CHAMP, D R, and JACKSON, R E. 1979. Influence of redox environments on the mobility of arsenic in ground water. 81–95 in *Chemical modeling in aqueous systems*. JENNE, E A (editor). (Washington: American Chemical Society.)

GURMAN, S J, BINSTED, N, and ROSS, I. 1984. A rapid, exact curved-wave theory for EXAFS calculations. *Journal of Physics*. C, Vol. 17, 143–151.

HALLIDAY, A N. 1980. The timing of early and main stage ore mineralisation in southwest Cornwall. *Economic Geology*, Vol. 75, 752–759.

HAMILTON, E I. 2000. Environmental variables in a holistic evaluation of land contaminated by historic mine wastes: a study of multi-element mine wastes in West Devon, England using arsenic as an element of potential concern to human health. *The Science of the Total Environment*, Vol. 249, 171–221.

HASWELL, S J, O'NEILL, P, and BANCROFT, K C C. 1985. Arsenic speciation in soil-pore waters from mineralized and unmineralized areas of south-west England. *Talanta*, Vol. 32, 69–72.

HEDIN, L, and LUNDQVIST, S. 1969. Effects of electron-electron and electron-phonon interactions on the one-electron states of solids. *Solid State Physics*, Vol. 23, 1–181.

ISAURE, M, LABOUDIGUE, A, MANCEAU, A, SARRET, G, TIFFREAU, C, TROCHELLIER, P, LAMBLE, G, HAZEMANN, J, and CHATEIGNER, D. 2002. Quantitative Zn speciation in a contaminated dredged sediment by u-Pixe, u-SXRF, EXAFS spectroscopy and principal component analysis. *Geochemica et Cosmochimica Acta*, Vol. 66, 1549–1567.

JUILLOT, F, ILDEFONSE, P, MORIN, G, CALAS, G, DE KERSABIEC, A M, and BENEDETTI, M. 1999. Remobilization of arsenic from buried wastes at an industrial site: mineralogical and geochemical control. *Applied Geochemistry*, Vol. 14, 1031–1048.

KABATA-PENDIAS, A. 2000. *Trace elements in soils and plants* (3rd edition). (Boca Raton: CRC Press.)

LE BOUTILLIER, N G. 2001. The tectonics of Variscan magmatism and mineralisation in southwest England. Unpublished PhD thesis, Cambourne School of Mines, University of Essex.

MAFF. 1982. Survey of Arsenic in food. *Food Surveilance Paper* No. 8. (London: HMSO.)

MANDL, M R M, and DOCEKALOVA, H. 1992. Migration of arsenic (III) during bacterial oxidation of arsenopyrite in chalcopyrite concentrate by *Thiobacillus ferrooxidans*. *Applied Microbiology Biotechnology*, Vol. 38, 429–431.

PARKHURST, D L. 1995. User's Guide to PHREEQC- a computer program for speciation, reactio-path, advective-transport, and inverse geochemical calculations. *US Geological Survey, Water-Resources Investigations Report*, 95–4227.

PIERCE, M L, and MOORE, C B. 1982. Adsorption of arsenite and arsenate on amorphous iron hydroxide. *Water Research*, Vol. 16, 1247–1253.

PYE, A R, and DIXON, T. 1989. The Arsenic works at Devon Great Consols mine, Tavistock. *Proceedings of the Devon Archaeology Society*, Vol. 47, 79–111.

RANDALL, S R, SHERMAN, D M, and RAGNARSDOTTIR, K V. 2001. Sorption of As(V) on green rust ($Fe_4(II)Fe_2(III)(OH)12SO_4 \cdot {}_3H_2O$) and lepidocrocite (-FeOOH): Surface complexes from EXAFS spectroscopy. *Geochemica et Cosmochimica Acta*, Vol. 65, 1015–1023.

ROSE, A W, and HAWKES, H E. 1979. *Geochemistry in mineral exploration.* (San Diego: Academic Press.)

ROSE, S, and GHAZI, A M. 1997. Experimental study of the stability of metals associated with iron oxyhydroxides precipitated in acid mine drainage. *Environmental Geology*, Vol. 36, 364–370.

RUBY, M V, DAVIS, A, SCHOOF, R, EBERLES, S, and SELLSTONE, C M. 1996. Estimation of Lead and Arsenic Bioavailability Using a Physiologically Based Extraction Test. *Environmental Science & Technology*, Vol. 30, 422–430.

RUBY, M V, SCHOOF, R, BRATTIN, W, GOLDADE, M, POST, G, HARNOIS, M, MOSBY, D E, CASTEEL, S W, BERTI, W, CARPENTER, R, EDWARDS, D, CRAGIN, D, and CHAPPELL, W R. 1999. Advances in Evaluating the Oral Bioavailability of Inorganics in Soil for Use in Human Health Risk Assessment. *Environental Science & Technology*, Vol. 33, 3697–3705.

SAVAGE, K S, TINGLE, T N, O'DAY, P A, WAYCHUNAS, G A, and BIRD, D K. 2000. Arsenic speciation in pyrite and secondary weathering phases, Mother Lode Gold District, Tuolumne Country, California. *Applied Geochemistry*, Vol. 15, 1219–1244.

SCRIVENER, R C, DARBYSHIRE, D P F, and SHEPHERD, T J. 1994. Timing and significance of crosscourse mineralization in SW England. *Journal of the Geological Society of London*, Vol. 151, 587–590.

SINGH, B, WILSON, M J, MCHARDY, W J, FRASER, A R, and MERRINGTON, G. 1999. Mineralogy and chemistry of ochre sediments from an acid mine drainage near a disused mine in Cornwall, UK. *Clay Minerals*, Vol. 34, 301–317.

THORESBY, P, and THORNTON, I. 1979. Heavy metals and As in soil, pasture herbage and barley in some mineralised areas in Britain; significance to animal and human health. in *Trace substances in Environmental Health XII*. HEMPHILL, D D (editor).

WEBSTER, J G, SWEDLUND, P J, and WEBSTER, K S. 1998. Trace metal adsorption onto acid mine drainage iron oxide. 951–954 in Water-Rock Interaction. *Proceedings of the 9th International symposium on Water–Rock Interaction*, WR1–9, Taupo, New Zealand, 30 March–3 April 1998. AREHURT, G B, and HULSTON, J R (editors). (Rotterdam: Balkema.)

WILLIS-RICHARDS, J, and JACKSON, N J. 1989. Evolution of the Cornubian Ore Field, Southwest England: Part 1. Batholith Modeling and Ore Distribution. *Economic Geology*, Vol. 84, 1078–1100.

XU, J, and THORNTON, I. 1985. Arsenic in garden soils and vegatable crops in Cornwall, England: implications for human health. *Enviromental Geochemistry and Health*, Vol. 7, 131–133.

YAN, X, KERRICH, R, and M J H. 2000. Distribution of arsenic(III), arsenic(V) and total arsenic in porewaters from a thick till and clay-rich aquitard sequence, Saskatchewan, Canada. *Geochemica et Cosmochimica Acta*, Vol. 62, 2637–2648.